SMIP92

SEMINAR ON
SEISMOLOGICAL AND ENGINEERING IMPLICATIONS
OF RECENT STRONG-MOTION DATA

Sacramento, California
May 21, 1992

PROCEEDINGS

Sponsored by

Strong Motion Instrumentation Program
Division of Mines and Geology
California Department of Conservation

Supported in Part by

California Seismic Safety Commission

The Strong Motion Instrumentation Program (SMIP) is a program within the Division of Mines and Geology of the California Department of Conservation and is advised by the Strong Motion Instrumentation Advisory Committee (SMIAC), a committee of the California Seismic Safety Commission. Current program funding is provided by an assessment on construction costs for building permits issued by cities and counties in California, with additional funding from the California Department of Transportation and other State agencies.

DISCLAIMER

SMIP92

SEMINAR ON
SEISMOLOGICAL AND ENGINEERING IMPLICATIONS
OF RECENT STRONG-MOTION DATA

Sacramento, California
May 21, 1992

PROCEEDINGS

Edited by

M.J. Huang

Sponsored by

Strong Motion Instrumentation Program
Division of Mines and Geology
California Department of Conservation

Supported in Part by

California Seismic Safety Commission

PREFACE

The Strong Motion Instrumentation Program (SMIP) in the Division of Mines and Geology of the California Department of Conservation promotes and facilitates the improvement of seismic codes through the Directed Research Project. The objective of this project is to increase the understanding of earthquake strong ground shaking and its effects on structures through interpretation and analysis studies of SMIP and other applicable strong-motion data. The ultimate goal is to accelerate the process by which lessons learned from earthquake data are incorporated into seismic code provisions and seismic design practices.

Since the establishment of SMIP in early 1970s, over 500 stations, including 120 buildings, 20 dams and 8 bridges, have been installed. Significant strong-motion records have been obtained from many of these stations. The most important set of strong-motion records is from the 1989 Loma Prieta earthquake during which strong-motion records were obtained from 53 ground-response stations and 41 extensively-instrumented structures. The most recent sets are from the Desert Hot Springs earthquake of April 22, 1992 and the Petrolia earthquake of April 25, 1992. These records have been and will be the subject of SMIP directed research projects.

The SMIP92 Seminar is the fourth in a series of annual events designed to transfer recent research findings on strong-motion data to practicing seismic design professionals and earth scientists. In both oral presentations and poster sessions, ten investigators will provide state-of-the-art data and analysis results from recent research studies of SMIP data during the past year.

The papers in this Proceedings volume represent interim results obtained by the investigators. Following this seminar the investigators will be preparing final reports with their final conclusions. These reports will be more detailed and will update the results presented here. SMIP will make these reports available after the completion of the studies.

TABLE OF CONTENTS

SMIP92 SEMINAR ON

SEISMOLOGICAL AND ENGINEERING IMPLICATIONS

OF RECENT STRONG MOTION DATA

Hilton Inn, Sacramento, California
May 21, 1992

PROGRAM

8:00-9:00	**Registration**
9:00-9:10	**Welcoming Remarks** *Bill Guerard*, Acting Assistant Director for Mining and Geology, and *LeRoy Crandall*, Seismic Safety Commission, and Chair, Strong Motion Instrumentation Advisory Committee (SMIAC)
9:10-9:30	**Introductory Remarks and Comments on Strong-motion Data from Petrolia Earthquake** *Anthony Shakal*, Manager, Strong Motion Instrumentation Program
SESSION I	**GROUND RESPONSE** **Moderator:** *Bruce Bolt*, UC Berkeley/Seismic Safety Commission Chair, SMIAC Ground-Response Subcommittee
9:30-9:55	**The Site Response of Two Rock and Soil Station Pairs to Strong and Weak Ground Motion** *R. Darragh and A. Shakal*, SMIP
9:55-10:20	**Quantification of Long Period Strong Ground Motion Attenuation for Engineering Design** *W. Silva and N. Abrahamson*, Pacific Engineering & Analysis El Cerrito
10:20-10:45	**Comparison of Strong Motion and Weak Motion Recordings of the Loma Prieta Sequence** *O. Bonamassa, H. Houston and J. Vidale*, UC Santa Cruz
10:45-11:10	Break
SESSION II	**BUILDING RESPONSE 1** **Moderator:** *Wilferd Peak*, Consulting Engineering Geologist Chair, SMIAC Directed Research Subcommittee
11:10-11:35	**Evaluation of Code-Accidental Torsion Provisions Using Strong-Motion Records from Three Symmetric-Plan Buildings** *J. De la Llera and A. Chopra*, UC Berkeley
11:35-12:00	**Evaluation of Displacement Amplification Factor for Seismic Design Codes** *C.-M. Uang and A. Maarouf*, Northeastern University, Boston
12:00-12:30	**Poster Session for Sessions I & II**

12:30-1:50 **Lunch**
Luncheon Speaker: *George Housner*, EERI Distinguished Lecturer

SESSION III **BUILDING RESPONSE 2**
Moderator: *Robert Thacker*, Office of the State Architect
SMIAC Building Subcommittee

2:00-2:25 **Analysis of Strong-Motion Records from Buildings to Verify or Improve Uniform Building Code Formulas for Calculating Periods of Buildings**
E. Cole, C. Tokas and J. Meehan, Cole/Yee/Schubert and Associates Sacramento

2:25-2:50 **Effects of Duration on Structural Response Factors and on Ground Motion Damageability**
R. Sewell, Risk Engineering, Golden, Colorado

2:50-3:15 **Verification of a Method for Estimating Overturning Moment of Tall Buildings**
M.-C. Chen, Collaborative Engineering Service, Cupertino

3:15-3:40 Break

SESSION IV **LIFELINE STRUCTURE RESPONSE**
Moderator: *Vern Persson*, Division of Safety of Dams, DWR
Chair, SMIAC Lifelines Subcommittee

3:40-4:05 **Effect of Relative Displacements Between Adjacent Bridge Segments**
K. Kasai, W. Liu and V. Jeng, Illinois Institute of Technology, Chicago

4:05-4:30 **Nonlinear Analysis of Seismic Response of Lexington Dam**
L. Mejia, J. Sun, S. Salah-mars, Y. Moriwaki and M. Beikae Woodward-Clyde Consultants, Oakland

4:30-5:00 **Poster Session for Sessions III & IV**

THE SITE RESPONSE OF TWO ROCK AND SOIL STATION PAIRS TO STRONG AND WEAK GROUND MOTION

R. B. Darragh and A. F. Shakal

California Department of Conservation
Division of Mines and Geology
Strong Motion Instrumentation Program

ABSTRACT

The site response to strong and weak ground motion depends largely on the subsurface conditions at the soil site for the two rock-soil station pairs studied. The first station pair consists of a soft-soil site and a sandstone/shale site (Treasure Island and Yerba Buena Island). For strong motion, the soft-soil site is amplified by a factor of about 3 over the rock site from 0.5 to 2.0 Hz. The amplification is much higher for weak motion and suggests a dependence on signal amplitude.

A second station pair near Gilroy consisting of a stiff-soil site and a sandstone site was studied with contrasting results. Unlike the results for the soft-soil study above, the estimated stiff-soil site response is not significantly different for strong and weak motion from 0.5 to 2.0 Hz.

INTRODUCTION

A dependence of ground motion on site conditions is clearly seen in the Loma Prieta damage pattern (e.g., EERI, 1990) and the strong motion records (Shakal et al., 1989; Maley et al., 1989). In general, the effect of site conditions is shown in the strong motion accelerograms by smaller amplitudes recorded at rock sites than at soil sites located at comparable distances and azimuths from the mainshock. For example, rock and soil sites in the San Francisco - Oakland area have peak ground accelerations of approximately 0.08 and 0.20 g, respectively (Shakal et al., 1989: Maley et al., 1989)

In this study, two rock and soil station pairs are chosen for analysis because of their proximity, the availability and quality of strong and weak ground motion recordings, and the differing subsurface conditions at the soil sites. The soil site for the first pair is a soft-soil site, while it is a stiff-soil site for the second pair. An analysis using Fourier spectral ratios allows the isolation of the soil site response from the effects of the source and the path. Also, a comparison of the site response estimated from weak and strong ground motions further defines the range of subsurface conditions and levels of ground motion for which techniques that estimate the ground motions of large earthquakes from the recordings of more frequent smaller earthquakes are applicable (e.g., Tucker and King, 1984).

THE STATION PAIRS

Soft-soil. Yerba Buena Island and Treasure Island form a rock and soil station pair located in San Francisco Bay, approximately 100 km from the Loma Prieta epicenter and 2.5 km from each other. The station at Yerba Buena Island is located on an outcrop of Franciscan sandstone and shale. Treasure Island is a manmade island created in the 1930s. According to Gibbs et al. (1992), the

station is located on 14 m of hydraulic fill over sand and bay mud (soft clay sediments). The depth to basement, consisting of shale and sandstone, is 88 m at this site. The site geology and the P- and S-wave velocities are given in Gibbs et al. (1992). After the Loma Prieta earthquake sand boils provided evidence of liquefaction near the station on Treasure Island (Shakal et al., 1989; EERI, 1990).

This pair of stations was installed over 15 years ago by California's Strong Motion Instrumentation Program (CSMIP) specifically to record strong ground motion on these very different site conditions. This station pair triggered for the first time during the Loma Prieta earthquake. Because of the important characteristics of the mainshock accelerograms (Shakal et al., 1989) CSMIP recommended these sites to Lawrence Livermore National Laboratory (LLNL) as good candidate sites at which to locate high-gain instruments LLNL planned to deploy. As described in Jarpe et al. (1989) high-gain seismometers were co-located by LLNL at these sites for several weeks to record the weak ground motion from aftershocks. The instrumentation at each site consisted of a 16-bit fixed-gain recorder and a three component seismometer with a 1 Hz free period and a recording bandwidth (flat in velocity) from 0.2 to 100 Hz. A total of nine Loma Prieta aftershocks were recorded on both horizontal components at the two stations (Jarpe et al., 1989). From these nine aftershocks recordings, four were selected for this study that had the broadest useable bandwidth based on a signal-to-noise ratio analysis (see Darragh and Shakal, 1991). Table I summarizes various parameters of the set of five Loma Prieta events studied at this pair of stations.

Previous investigators using the data recorded at this station pair have analyzed the effect of soft-soils on strong and weak ground shaking from the Loma Prieta earthquake sequence (Jarpe et al., 1989; Shakal et al., 1990). These studies showed amplification of ground motion at the soft-soil site relative to the rock site for frequencies from approximately 0.5 to 5 Hz, and the level of amplification was greater for weak ground motion than for strong ground motion. This research extends these earlier studies by including a signal-to-noise analysis for the aftershocks (see Darragh and Shakal, 1991), a consideration of the dependence of amplification on signal amplitude, and a discussion of a similar analysis at a stiff-soil and rock station pair.

Stiff-soil. The second pair of stations is part of the Gilroy array, approximately 30 km east of the Loma Prieta epicenter. The Gilroy array is an alignment of six stations extending from sandstone on the east, across the alluvial Santa Clara Valley, to sandstone on the west. This array is a cooperative effort of CSMIP and the U.S. Geological Survey and is currently instrumented and maintained by CSMIP.

The array provides an opportunity to study the response of rock and deep soil sites to strong and weak ground motion. For this analysis, only the records from Gilroy #1 and #2, the closest rock and soil pair, are used. These stations are located 2 km from each other. The site geology and the P- and S-wave velocities at these stations are given in Fumal et al. (1982), Joyner et al. (1981) and Gibbs et al. (1992). Gilroy #1 is underlain by moderately weathered sandstone at the surface, with thin beds of shale at depth, while Gilroy #2 is underlain by alluvium (stiff-soil) to a depth of 167 m. Sandstone, siltstone and shale are encountered below this depth.

Previous investigators using data recorded at the Gilroy array have analyzed

the effect of the stiff-soils on strong ground shaking recorded from the 1979 Coyote Lake earthquake (Joyner et al., 1981; Silva et al., 1986) and the 1984 Morgan Hill earthquake (Silva et al., 1986). Joyner et al. (1981), using a linear plane-layered model, showed that there is no clear evidence of nonlinear response at the stiff-soil site. Silva et al. (1986) concluded that the stiff-soil site response estimated from strong (direct S-wave window) and weak ground motions (S-wave coda window) were not significantly different for peak accelerations and velocities less than 0.25 g and 32 cm/sec, respectively.

This study extends these previous analyses by incorporating the ground-motion data from the Loma Prieta mainshock and thirteen aftershocks that CSMIP recorded on analog and high-gain digital accelerographs. The record from the mainshock increases the largest peak acceleration and velocity recorded at the stiff-soil site to 0.35 g and 39 cm/sec, respectively (Table II). The records from the aftershocks, ranging in local magnitude from 4.1 to 5.4, provide many records of weak ground motion at the sites (Table II).

METHOD

In this study, an estimate of the response of a soil site is obtained by calculating the ratio of the smoothed Fourier amplitude spectra at the soil site and a nearby rock site. This method is similar to that described in Tucker and King (1984), Silva et al. (1986) and Jarpe et al. (1988). For soil and rock sites located at similar distances and azimuths from the earthquake, the spectral-ratio method isolates the site response from the effects of the source and the path.

The method used in this study consists of the following principal steps. First, for each horizontal accelerogram, a time window of approximately 10 seconds duration containing the direct S-wave arrival is selected and the mean removed. Next, the start and the end of the record are tapered with a five percent Hanning window. The Fourier spectrum is then estimated from the time history using a standard fast Fourier transform algorithm. The average horizontal spectrum is computed by adding the squared moduli of the horizontal spectra together, dividing by two, and taking the square root. The resulting spectrum is then smoothed with a running-mean filter with a bandwidth of approximately 1 Hz. The ratio obtained by dividing the smoothed average horizontal spectrum at the soil site by the corresponding rock site spectrum is an estimate of the soil-site response. These ratios are discussed in the following sections.

SOFT-SOIL SITE RESPONSE

The soft-soil site response estimated from the smoothed Fourier spectral ratios for Treasure and Yerba Buena islands are shown in Figure 1 for earthquakes with local magnitudes of 7.0, 4.3, 4.1, 3.5, and 3.3. In this figure, amplification of ground motion at the soft-soil site relative to the rock site is observed for both strong and weak ground motions in the frequency range from approximately 0.5 to 7 Hz.

For the Loma Prieta mainshock, Figure 1 shows that the motion at the soft-soil site is amplified over the rock site by a factor of about 4 over a broad frequency range. In contrast, for weak ground motion from Loma Prieta aftershocks, the motion at the soil site is amplified over the rock site by a factor of 12 to 25 near 1 Hz. For these five earthquakes, the level of

amplification near 1 Hz appears to vary with the earthquake magnitude, dependent on the level of input motion (peak ground velocity) at the rock site. The maximum amplification is approximately 25, 19, 17, 12, and 4 for earthquakes with local magnitude 3.3, 3.5, 4.1, 4.3, and 7.0, respectively. Correspondingly, as the peak rock velocity increases from 0.005 to 0.007, 0.015, 0.099, and 14.7 cm/sec, the maximum amplification decreases from 25 to 19, 17, 12, and 4, respectively. However, note that the factor-of-two difference in weak motion amplification from 12 to 25 is within the normal range of scatter (Tucker and King, 1984). Also, the local magnitude 3.3 and 3.5 earthquakes have quite similar peak rock velocities of 0.005 and 0.007 cm/sec, respectively, but they have different maximum amplifications of 25 and 19, respectively. Thus, it will be important to record future earthquakes at these sites to understand this provocative, albeit preliminary, trend in the soft-soil site response.

The shape, or frequency dependence, of the spectral ratios also varies with local magnitude. Figure 1 shows that the soft-soil site response for the aftershocks has strong peaks near 1 and 2 Hz. However, the site response estimated for the mainshock is nearly flat over the same frequency range.

These soft-site soil-response differences, in both amplitude and frequency dependence, demonstrate that caution must be exercised in using weak-motion studies to infer soft-soil site response during strong shaking for seismic hazard estimation and zonation. Weak ground motion may be amplified to a greater extent than strong ground motion, especially at sites similar to Treasure Island where nonlinear effects are observed at peak acceleration and velocity levels as low as 0.16 g and 33 cm/sec, respectively. The corresponding rock motion near this soft-soil site is only 0.07 g and 15 cm/sec.

STIFF-SOIL SITE RESPONSE

The stiff-soil site response, as estimated from smoothed Fourier spectral ratios for Gilroy #1 and Gilroy #2, are shown for three mainshocks and selected Loma Prieta aftershocks in Figures 2 and 3, respectively. The figures show that significant amplification of ground motion occurred at the stiff-soil site relative to the rock site for earthquakes with local magnitudes from 4.1 to 7.0, and for frequencies from approximately 0.5 to 2 Hz. Amplification at the soil site is about 3, similar to the soft-soil site response and previous work (e.g. King and Tucker, 1984; Tucker and King, 1984). However, in contrast to the behavior of the soft-soil site response discussed above, the stiff-soil site response is similar for strong and weak ground motions over the frequency range of 0.5 to 2 Hz, as discussed below.

The motion at the stiff-soil site is amplified over the rock site by a factor of about 2 for the Loma Prieta mainshock from 0.5 to 2 Hz (Figure 2). The amplification factor is approximately 4 over the same frequency range for the Coyote Lake and the Morgan Hill mainshocks, approximately double that estimated for the Loma Prieta mainshock. From 2 to 10 Hz, the amplification factor is generally less than 1 for the Loma Prieta mainshock, and generally greater than 1 for the other two mainshocks. These differences are not large and may be interpreted as the statistical variability in the site response produced by differences in azimuth, angle of incidence or path attenuation or other effects.

Though highly variable, the motion at the stiff-soil site is again amplified over the rock site by a factor of approximately 2 in the same frequency range for the ground motion recorded during the Loma Prieta aftershocks (Figure 3). This

is in agreement with the results of Tucker and King (1984) who determined the average site responses for three sediment-filled valleys and found that they were within $\pm$0.25 log units (factor of 1.8).

Considering higher frequencies, the stiff-soil spectral ratio peaks near 2.5 Hz for weak motion (Figure 3) and for one of the three mainshocks -- Coyote Lake (Figure 2). Near this 2.5 Hz peak the smoothed spectra at both Gilroy #1 and Gilroy #2 have similarly shaped troughs for the Coyote Lake mainshock (see Darragh and Shakal, 1991). For these earthquakes, the amplitude of the spectral ratio ranges from about 2.5 to 6.5, with an average near 3.5. However, the site response estimated from the Loma Prieta mainshock is below unity in this range (Figure 2). In this frequency band, a factor of approximately 6 is observed in the stiff-site soil response between weak and the strongest ground motion. Compared to the soft-soil results, these amplification ratios are smaller and more variable, and suggest that any signal-dependence, if present, is comparable to the intrinsic variability.

SUMMARY AND CONCLUSIONS

The analysis of spectral ratios for two rock-soil station pairs clearly shows the amplification of the ground motion recorded at the soil site relative to the rock site in both strong and weak shaking. At the soil sites, Treasure Island and Gilroy #2, the ground motion is amplified by a factor near 3 for frequencies between 0.5 and 2 Hz during the Loma Prieta mainshock.

At the soft-soil site (Treasure Island), the amplification factor ranges from 12 to 25 near 1 Hz for four Loma Prieta aftershocks. This is approximately 3 to 8 times greater than the amplification of 4 estimated for the mainshock recordings. This difference may be explained by nonlinear response of the soils at Treasure Island during the mainshock for peak acceleration and velocity levels as low as 0.16 g and 33 cm/sec, respectively. This explanation is supported by observations of liquefaction within 100m of the Treasure Island station after the Loma Prieta mainshock (Shakal et al., 1989; EERI, 1990). Also, the effects of liquefaction are observable in the Treasure Island accelerogram. Approximately 15 seconds into the record, at the inferred onset of liquefaction, short period ground motions decrease abruptly from above 0.15 g to low amplitude, long period motion comparable to the motion at Yerba Buena Island (CSMIP, 1989; Shakal et al., 1990). The effect of liquefaction on the smoothed spectra calculated from the Treasure Island accelerograms is discussed in Darragh and Shakal (1991).

In contrast, at the stiff-soil site (Gilroy #2 site), the amplification estimated from aftershocks is generally within the scatter observed for the three mainshocks for 0.5 to 2 Hz. Any effects of nonlinear soil response at this stiff-soil site are difficult to detect from the data and the means of analysis used in this study.

These results document the effects of two contrasting soil profiles on strong and weak ground shaking. They emphasize that the nonlinear effects of soils need to be considered when using weak ground motion data to infer the site response under stronger levels of shaking, especially at soft-soil sites.

ACKNOWLEDGEMENTS

The California Strong Motion Instrumentation Program extends its appreciation to the individuals and organizations that have permitted and cooperated with the

installation of seismic strong-motion equipment on their property. The authors would also like to recognize the CSMIP technicians for their diligence and care in installing and maintaining the instruments, and recovering the records. Also, the authors thank Steve Jarpe and Larry Hutchings and their colleagues at LLNL for the aftershock data collected after the Loma Prieta mainshock at Treasure and Yerba Buena islands. The manuscript was significantly improved by reviews of M. C. Andrews, Jack Boatwright, Dave Boore.

REFERENCES

Aki, K. (1988). Local site effects of strong ground motion, in Proceedings of Earthquake Engineering and Soil Dynamics II, Geotechnical Division ASCE, Park City Utah, June 27-30, 103-155.

CSMIP (1989). Plots of the processed data for the interim set of 14 records from the Santa Cruz Mountains (Loma Prieta) earthquake of 17 October 1989, California Division of Mines and Geology, Office of Strong Motion Studies Report, 141 pp.

Darragh, R. B. and A. F. Shakal (1991). The site response of two rock and soil station pairs to strong and weak ground motion, Bull. Seism. Soc. Am. 81, 1885-1899.

EERI (1990). Loma Prieta earthquake reconnaissance report, Earthquake Spectra, 6, (supplement), 448 pp.

Fumal, T. E., J. F. Gibbs, and E. F. Roth (1982). In-situ measurements of seismic velocity at 10 strong motion accelerograph stations in Central California, U.S. Geological Survey, Open-File Report 82-407, 76 pp.

Gibbs, J. F., T. E. Fumal, D. M. Boore and W. B. Joyner (1992). Seismic velocity and geologic logs from borehole measurements at seven strong-motion stations that recorded the 1989 Loma Prieta earthquake, U.S. Geological Survey, Open-File Report 92-287, 139 pp.

Huang, M. J., T. Q. Cao, U. R. Vetter and A. F. Shakal (1990). Second interim set of CSMIP from the Santa Cruz Mountains (Loma Prieta) earthquake of 17 October 1989, California Division of Mines and Geology, Office of Strong Motion Studies, Report OSMS 90-01, 188 pp.

Jarpe, S. P., C. H. Cramer, B. E. Tucker, and A. F. Shakal (1988). A comparison of observations of ground response to weak and strong ground motion at Coalinga, California, Bull. Seism. Soc. Am. 78, 421-435.

Jarpe, S. P., L. J. Hutchings, T. F. Hauk, and A. F. Shakal (1989). Selected strong- and weak-motion data from the Loma Prieta sequence, Seism. Res. Ltrs. 60, 167-176.

Joyner, W. B., R. E. Warrick , and T. E. Fumal (1981). The effect of Quaternary alluvium on strong ground motion in the Coyote Lake, California earthquake of 1979, Bull. Seism. Soc. Am. 71, 1333-1349.

King, J. L. and B. E. Tucker (1984). Observed variations of earthquake motion across a sediment-filled valley, Bull. Seism. Soc. Am. 74, 137-151.

Maley, R., A. Acosta, F. Ellis, E. Etheredge, L. Foote, D. Johnson, R. Porcella, M. Salsman, and J. Switzer (1989). U.S. Geological Survey strong -motion records from Northern California (Loma Prieta) earthquake of October 17, 1989, U.S. Geological Survey, Open-File Report 89-568, 85 pp.

Shakal, A., M. Huang, M. Reichle, C. Ventura, T. Cao, R. Sherburne, M. Savage, R. Darragh, and C. Petersen (1989). CSMIP strong-motion records from the Santa Cruz Mountains (Loma Prieta), California earthquake of 17 October 1989, California Division of Mines and Geology, Office of Strong Motion Studies Report, OSMS 89-06, 196 pp.

Shakal, A., R. Darragh, S. Jarpe, and L. Hutchings (1990). Site amplification during strong and weak motion: Records from a rock-soil station pair near San Francisco during the Loma Prieta mainshock and aftershocks, Seism. Res. Ltrs. 61, 50.

Silva, W., T. Turcotte, J. King, and Y. Moriwaki (1986). Soil response to earthquake ground motion, Electric Power Research Institute Report RP2556-07, 278 pp.

Tucker, B. E., and J. L. King (1984). Dependence of sediment-filled valley response on input amplitude and valley properties, Bull. Seism. Soc. Am. 74, 153-165.

TABLE I

Records From the Loma Prieta Sequence at Treasure and Yerba Buena Islands

DATE (UTC) (Mn/Day/Year) (Hr:Min:Sec)	ML (UCB)	PEAK PARAMETERS * Treasure Island			Yerba Buena Island		
		Apk (g)	Vpk (cm/sec)	Dpk (cm)	Apk (g)	Vpk (cm/sec)	Dpk (cm)
10/18/89 00:04:15	7.0	0.16	33.4	12.2	0.07	14.7	4.1
10/28/89 21:27:49	3.5	0.0004	0.03	-	0.00009	0.007	-
10/29/89 13:10:57	3.3	0.0005	0.04	-	0.00006	0.005	-
10/30/89 11:17:13	4.1	0.0010	0.08	-	0.00019	0.015	-
11/07/89 23:42:37	4.3	0.0059	0.46	-	0.0013	0.099	-

The peak parameters tabulated, acceleration (Apk), velocity (Vpk) and displacement (Dpk), are from the Volume 2 processed records for the Loma Prieta mainshock (CSMIP, 1989). For the aftershocks the corrected peak ground velocities (Jarpe et al., 1989) are listed. For comparison purposes, the estimated peak ground accelerations estimated using Apk=4(π)Vpk from a sinusoidal approximation for the waveform are also listed.

TABLE II

Earthquake Records at Gilroy #2 and Gilroy #1

DATE (UTC) (Mn/Day/Year) (Hr:Min:Sec)	ML (UCB)	PEAK PARAMETERS * Gilroy #2 Apk (g)	Gilroy #2 Vpk (cm/sec)	Gilroy #2 Dpk (cm)	Gilroy #1 Apk (g)	Gilroy #1 Vpk (cm/sec)	Gilroy #1 Dpk (cm)
		Mainshocks					
Coyote Lake 08/06/79 17:05:22	5.9	0.25	31.9	5.3	0.11	10.3	1.7
Morgan Hill 04/24/84 21:27:49	6.1	0.21	12.5	2.0	0.10	2.7	0.5
Loma Prieta 10/18/89 00:04:15	7.0	0.35	39.2	10.9	0.44	33.8	6.5
		Loma Prieta Aftershocks					
10/18/89 00:05:41	in coda	0.04	2.2	0.2	0.08	2.7	0.1
10/18/89 06:39:12	4.3	0.16	4.0	0.2	0.10	2.1	0.1
11/02/89 05:50:10	4.9	0.01	-	-	0.02	-	-
11/05/89 01:30:42	4.2	0.002	-	-	0.006	-	-
11/05/89 13:37:33	4.5	0.003	-	-	0.006	-	-
04/07/90 20:08:36	4.2	0.007	-	-	0.02	-	-
04/18/90 13:41:13	5.0	0.02	-	-	0.02	-	-
04/18/90 13:53:44	5.4	0.12	-	-	0.07	-	-
04/18/90 14:45:58	4.3	0.02	-	-	0.04	-	-
04/18/90 15:27:50	4.7	0.02	-	-	0.03	-	-
04/18/90 15:36:26	4.2	0.02	-	-	0.02	-	-
04/18/90 15:45:38	5.2	0.07	-	-	0.12	-	-
04/18/90 16:18:47	4.1	0.02	-	-	0.02	-	-

* The peak parameters tabulated, acceleration (Apk), velocity (Vpk) and displacement (Dpk), are from the Volume 2 records (Huang, et al., 1990) except for eleven later Loma Prieta aftershocks (11/02/89 and later). For these eleven aftershocks only the unprocessed peak ground accelerations are listed.

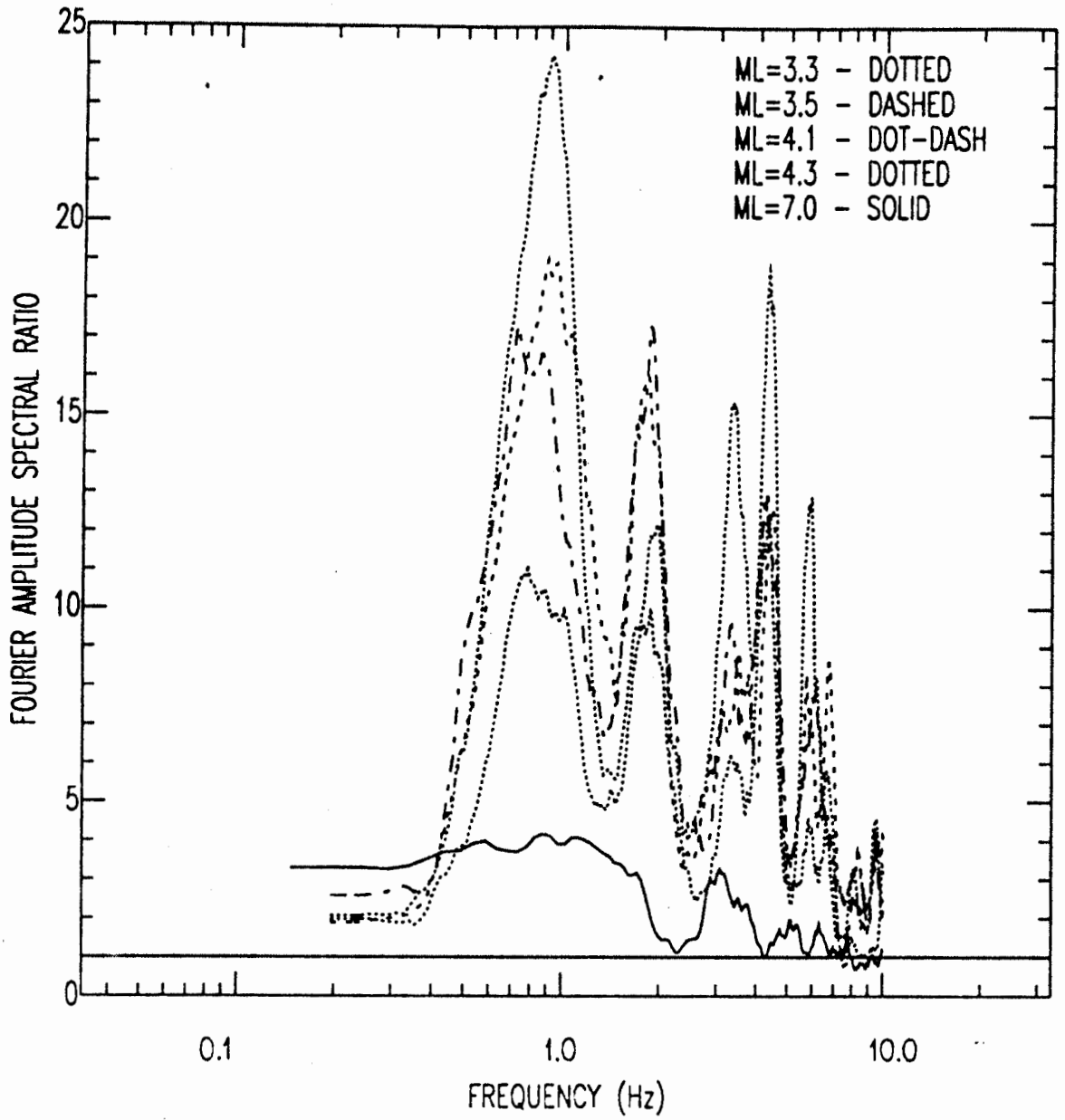

Figure 1: Amplification ratio at the soft-soil Treasure Island site relative to the nearby rock site on Yerba Buena Island for the Loma Prieta mainshock and aftershocks. The smoothed Fourier spectral ratios for the Treasure Island and Yerba Buena Island sites for the local magnitude 7.0, 4.3, 4.1, 3.5, and 3.1 Loma Prieta sequence earthquakes for a 10 second time window containing the direct S-wave arrival. For reference, a line showing no amplification (ratio of 1) is also shown. The bandwidth displayed for the mainshock is from the mid-frequency of the high-pass filter used in the standard CSMIP processing to 10 Hz. For the aftershocks, the bandwidth displayed is from 0.2 to 10 Hz. The upper frequency limit of 10 Hz was chosen to highlight the differences in the spectral ratios below this frequency.

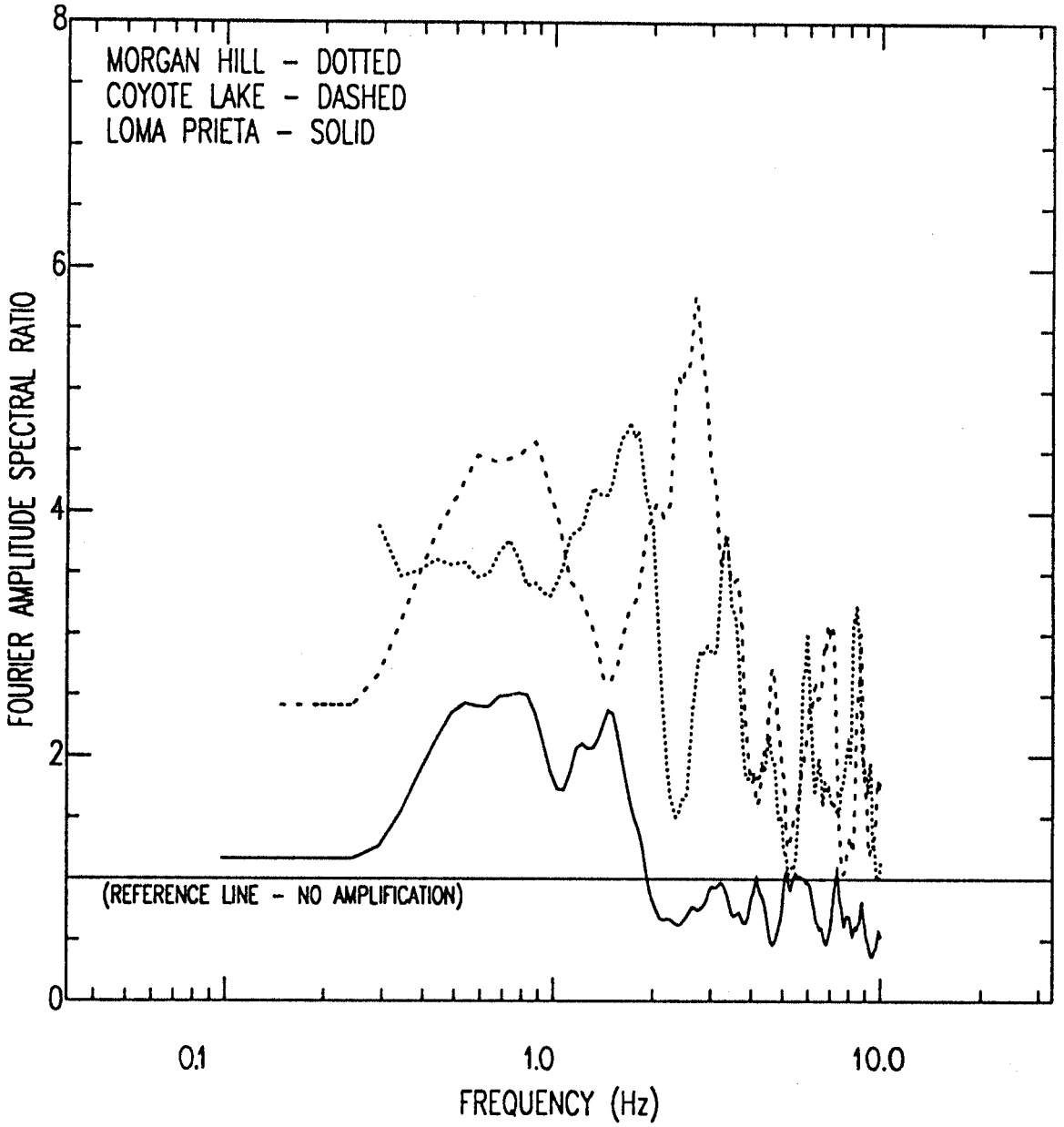

Figure 2: Amplification ratio at the stiff-soil Gilroy #2 site relative to the Gilroy #1 rock site. The amplification ratios are the smoothed Fourier spectral ratio for the Gilroy #2 and Gilroy #1 sites for the local magnitude 7.0 Loma Prieta, 6.1 Morgan Hill and 5.9 Coyote Lake mainshocks for an approximately 10 second time window containing the direct S-wave arrival. A reference line showing no amplification is also shown. The bandwidth displayed is from the mid-frequency of the high-pass filter used in the standard CSMIP processing to 10 Hz.

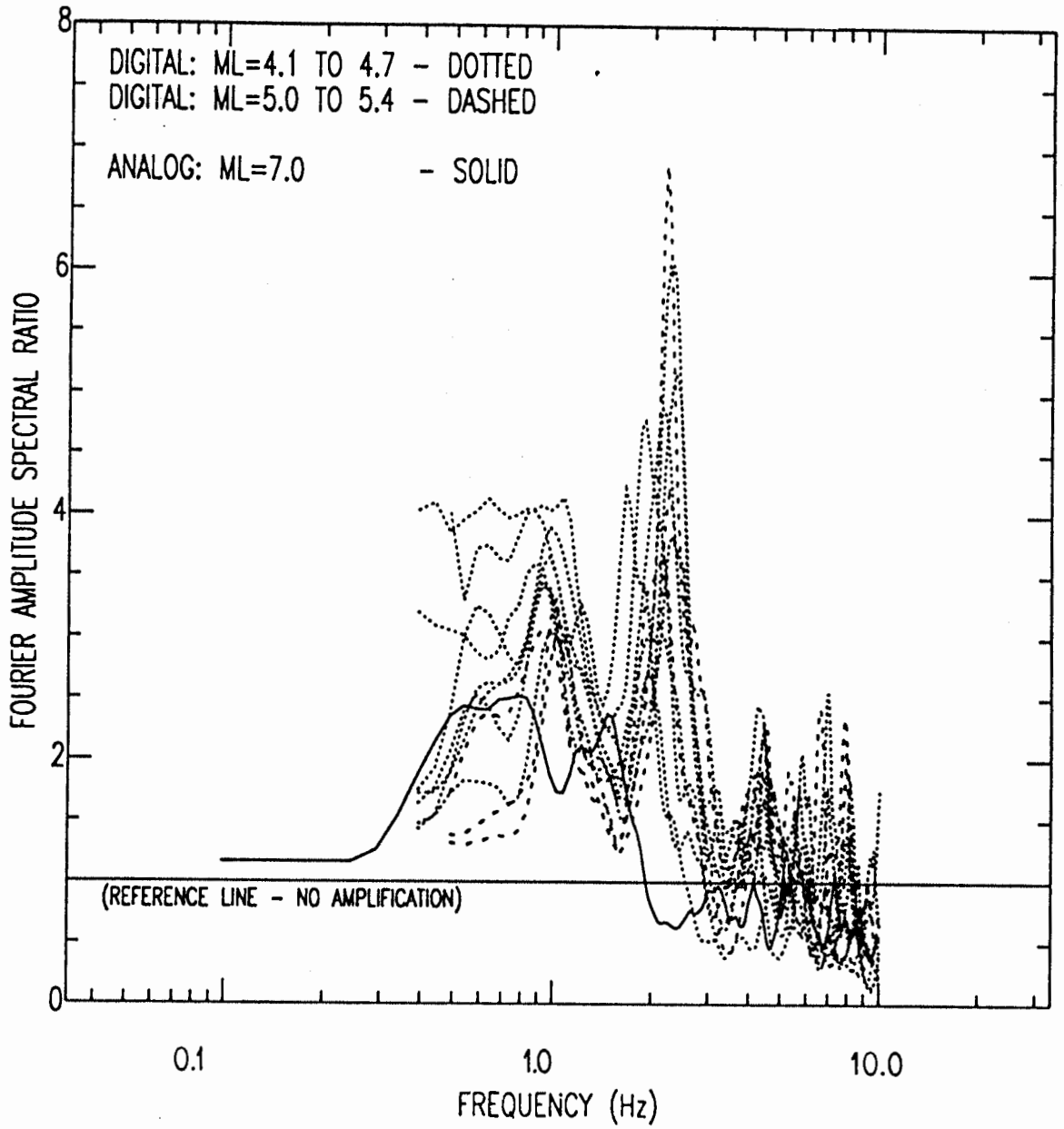

Figure 3: The smoothed Fourier spectral ratio for Gilroy #2 (stiff-soil) and Gilroy #1 (rock) for eleven aftershocks of the Loma Prieta mainshock for a time window containing the direct S-wave arrival. The corresponding spectral ratio for the Loma Prieta mainshock is shown for reference. A reference line showing no amplification is also shown. The mainshock was recorded on analog instruments, and the bandwidth displayed is from the mid-frequency of the high-pass filter used in the standard CSMIP processing to 10 Hz. For the eleven aftershocks, all recorded on digital instruments, the bandwidth displayed is from 0.4 or 0.5 to 10 Hz. The smoothed Fourier spectral ratio for two aftershocks recorded on analog instruments on 10/18/89 (Table II) are similar, and are shown in Darragh and Shakal (1991).

QUANTIFICATION OF LONG PERIOD STRONG GROUND MOTION ATTENUATION FOR ENGINEERING DESIGN

W. Silva and N. A. Abrahamson

Pacific Engineering and Analysis, El Cerrito, CA 94530

ABSTRACT

Empirical strong motion recordings from large magnitude (M≥6) events are reprocessed with an emphasis toward preserving the long period motions. A preliminary empirical attenuation relationship for response spectral values is derived for the period range 1-20 seconds.

INTRODUCTION

The major difficulty in estimating long period spectral attenuation relations from empirical data is that much of the processed data are near or below the noise level at periods greater than several seconds. To address this problem, we have reprocessed the recordings from large magnitude events using a procedure that is directed at recovering the long period motion. In addition, we have applied a new procedure for evaluating the noise level for long period motions.

Based on our analysis, at periods greater than 10 seconds, very few of the accelerograms contain energy above the noise level. We used numerical modeling to guide the extension of the attenuation relations to periods up to 20 seconds.

This paper describes the preliminary long period attenuation relations derived using recordings from the larger magnitude events. The final attenuation relations will include a larger set of data.

DATA BASE

The events used in the initial analysis are listed in Table 1. Based upon site response analyses using provincial categories and generic site profiles (Silva, 1991) the sites were initially classified as rock, shallow soil (<250 ft), intermediate depth soil (250-1000 ft), deep soil (>1000 ft), and alluvium of unknown depth. There are insufficient recordings in the shallow and intermediate categories to evaluate these categories separately. Therefore, we combined the data into two groups: soil < 250 ft and soil > 250 ft. The "alluvium of unknown depth" was put into the soil > 250 ft group. The distribution of recordings in magnitude and distance is shown in Figure 1. Distance is defined as closest distance to the seismogenic zone (Campbell, 1991) and magnitude is moment magnitude.

CORRECTION PROCEDURE

In order to extend the strong motion data base to as long of periods as possible, all records were reprocessed. The correction procedure used involves a series of five steps: 1) interpolation of uncorrected unevenly sampled records to 400 samples/sec, 2) frequency domain low-pass filtering using a causal 5-pole Buterworth filter with corner frequencies selected for each record based upon visual examination of the Fourier amplitude spectrum, 3) removing the instrument response, 4) decimating to 100 or 200 samples/sec depending upon the low-pass filter corner frequencies, and 5) applying a time domain baseline correction procedure and a final high-pass

filter. The baseline correction procedure uses polynomials in degree from 0-10 depending upon initial integrated displacements. The characteristic of the high-pass filter is that of an overdamped oscillator (Grazer, 1979). It is flat about its corner frequency and falls off proportional to frequency on either side. The filter is applied in the time domain twice, forward and reverse, resulting in a zero phase shift processed record. As with the polynomial baseline correction, the high-pass filter parameters are based upon visual examination of the filtered integrated displacements for a suite of parameter values. The response spectral values are only used in the regression if the frequency is greater than 1.25 times the high-pass filter corner frequency. This insures that the filter will not have a significant effect on the spectral values.

The visual examination of the displacements and the judgment as to the appropriate filter is based on the consistency of the amplitudes and timing of the long period energy with that of the higher frequency motion. One way to quantify the consistency of the timing of the long period motions is by examining the phase spectrum. The phase spectrum controls the timing and shape of the waveform. Seismic ground motion are expected to have a consistent phase structure at long periods whereas noise will have random phase.

Specifically, we examine the analytical derivative of the phase with respect to frequency (Tribolet, 1977). Examples of the phase derivative are shown in Figures 2a and b. Figure 2a shows a case where the phase derivative is well behaved to periods of 20 seconds. In contrast, Figure 2b shows a case where the phase derivative becomes much more random at a period of about 1.5 seconds. The final corrected acceleration time histories are evaluated for long period noise contamination by examining the analytic phase derivative. Response spectra values are only used in the regression analyses for periods at which the phase derivatives are well behaved.

REGRESSION ANALYSES

The regression analyses use the random effects model following the algorithm of Abrahamson and Youngs (1992). The random effects model explicitly models the correlation between recordings from the same earthquake. It handles uneven sampling of the earthquakes in a statistically optimal manner. This method partitions the variance into inter-event (τ^2) and intra-event (σ^2) terms.

The regression is performed for peak acceleration (pga) and response spectral values. The regression for response spectral values uses the normalized spectral shape (Sa/pga) because the data set is too small to allow stable regression on the absolute spectral values. The final response spectral attenuation is found by combining the spectra shape model with the pga model.

The peak acceleration is modeled by the following functional form:

$$\ln \text{pga(g)} = c_1 + c_2 M + c_3 \ln(r+20) + c_4 F \qquad (1)$$

where r is the distance in km and F is the fault type (F=0 for SS, and F=1 for reverse or oblique). Because the subset of the data used in this preliminary analysis has a limited range of magnitudes, the magnitude dependence is not well constrained by the data. Similarly, for the small number of events, the fault type dependence is also not well constrained. Therefore, the c_2 and c_4 parameters were fixed based on previous studies of larger data sets: c_2=1.2, c_4=0.25 (Campbell, 1991; PG&E, 1990).

The estimated coefficients for pga are listed in Table 2. The residuals are plotted in Figure 3. The residuals show a slight increase at distances of 70 to 100 km. To test if the attenuation is flat over this range (as the result of the Moho bounce), the regression was repeated using a flat attenuation from 70 to 90 km. The resulting solution produced a smaller likelihood than the

initial solution without flattening. This data set does not support a significant flattening of the pga attenuation for distances less than 100 km.

The functional form for the spectral shape was guided by results from numerical simulations and previous empirical studies. Depending on the assumptions regarding the seismic source parameter values, simulations suggest that strike-slip events maybe more likely to show near-field directivity effects at long periods than reverse events . The functional form is selected so that it can accommodate this effect. The normalized spectrum is model by

$$\ln\left(\frac{Sa}{pga}\right) = c_1 + c_3 r + c_4(1-\tanh\{(r^{1.1} - 10)/3\})(1-F) \qquad (2)$$

The last term accommodates the near-field effect for strike-slip events. As with the pga, the magnitude dependence of the spectral shape cannot be reliably determined from this data set. Therefore, the magnitude dependence is not modeled in this preliminary regression.

The coefficients computed for the rock/shallow soil and deep soil site conditions are listed in Table 3. The near-field term, c_4, corresponds to a 35% difference in long period spectral shape at short distances. The empirical data could only be used for periods up to 7.5 seconds because there were not enough records with reliable long periods to justify a high-pass corner frequency lower than 0.1 Hz. Based on numerical simulations, the response spectrum is approximately flat to spectral displacement at periods greater than 8 seconds for magnitudes less than 7.5. The spectral attenuation relations were extended to 20 seconds assuming constant spectral displacement. For magnitudes larger than 7.5, this extension my not be appropriate.

This data set shows a strong distance dependence of the spectral shape. This effect is dominated by the recordings from the Loma Prieta earthquake. The Loma Prieta Earthquake is a major portion of the data set and the distance dependence of the spectral shape may be reduced when the full data set is used.

The spectral attenuation relation for a magnitude 7.0 strike-slip event at deep soil and rock/shallow soil sites are shown in Figures 4a and 4b, respectively. In Figure 5a and 5b, the deep soil attenuation relation is compared to the Joyner and Boore (1982) and Sadigh (1987) attenuation relations for soil for distances of 10 and 50 km. The attenuation relation from this study is significantly lower than the Sadigh and Joyner and Boore relations at 10 km, but it is similar at 50 km. This is due to the strong distance dependence of the spectral shape discussed earlier. A similar comparison for the rock/shallow soil site model is shown in Figures 6a and 6b.

REFERENCES

Abrahamson, N.A. and R.P. Youngs (1992). A stable algorithm for regression analyses using the random effects model, Bull. Seism. Soc. Am., 505-510.

Campbell, K. W. (1991). A random-effects analysis of near-source ground motion for the Diablo Canyon Power Plant site, San Luis Obispo County, California, Report prepared for LLNL.

Grazier, V. M. (1979). Determination of the true ground displacement by using strong motion records, Phys. Solid Earth, Izv. Acad. Sc. USSR. English edition published by Am. Geophys. Union, 15:(12) 875-885.

Joyner, W. B. and D. M. Boore (1982). Prediction of earthquake response spectra, U.S. Geol.Surv. OFR 82-977.

PG&E (1990). Response to workshop question 4, NRC Docket Nos. 50-275 and 50-323, August 1990.

Silva, W. (1991). Site geometry and global characteristics, Proc. NSF/EPRI Workshop on Dynamic Soil Properties and Site Characterization, Palo Alto, CA.

Tribolet, S.M. (1977). A new phase unwrapping algorithm, IEEE Trans, ASSP-25, 170-177.

Table 1. List of Earthquakes Used in Preliminary Analysis

Event	Mw	R	S	I	D	A	Total
1940 El Centro	7.0				1		1
1952 Kern County	7.4				3	1	4
1966 Parkfield	6.1	2			4		6
1968 Borrego Mtn.	6.6				1		1
1971 San Fernando	6.6	11	1	1	6	1	20
1976 Gazli	6.8				1		1
1978 Tabas	7.4				2		2
1979 Imperial Valley	6.5				19		19
1983 Coalinga	6.5	21			1	3	25
1985 Nahanni	6.8	3					3
1988 Spitak	7.0	1					1
1989 Loma Prieta	7.0	28	5	2	13	5	53
Total		66	6	3	51	10	136

R=rock, S=shallow soil, I=intermediate depth soil, D=deep soil, A=alluvium of unknown depth.

Table 2. Estimated Coefficients for PGA Model for the Average Horizontal Component

Coeff	Deep Soil	Rock/Shallow Soil
c_1	-3.27	-3.56
c_2	1.2	1.2
c_3	-1.79	-1.67
c_4	0.25	0.25
σ_{Total}	0.46	0.46

Table 3. Estimated Coefficients for Spectral Shape for the Average Horizontal Component

Period	Deep Soil c_1	Rock c_1	c_3	c_4	σ_{Total}	σ	τ
1.0	-0.224	-0.525	0.011	0.15	0.54	0.45	0.30
1.5	-0.587	-1.056	0.010	0.15	0.57	0.49	0.28
2.0	-0.965	-1.380	0.010	0.15	0.59	0.55	0.23
3.0	-1.453	-1.861	0.008	0.15	0.63	0.62	0.13
4.0	-1.920	-2.315	0.008	0.15	0.62	0.60	0.18
5.0	-2.009	-2.565	0.007	0.15	0.67	0.67	0.00
7.7	-2.965	-3.442	0.014	0.15	0.80	0.80	0.00
10.0	-3.49	-3.96	0.014	0.15	0.80	0.80	0.00
15.0	-4.30	-4.78	0.014	0.15	0.80	0.80	0.00
20.0	-4.87	-5.35	0.014	0.15	0.80	0.80	0.00

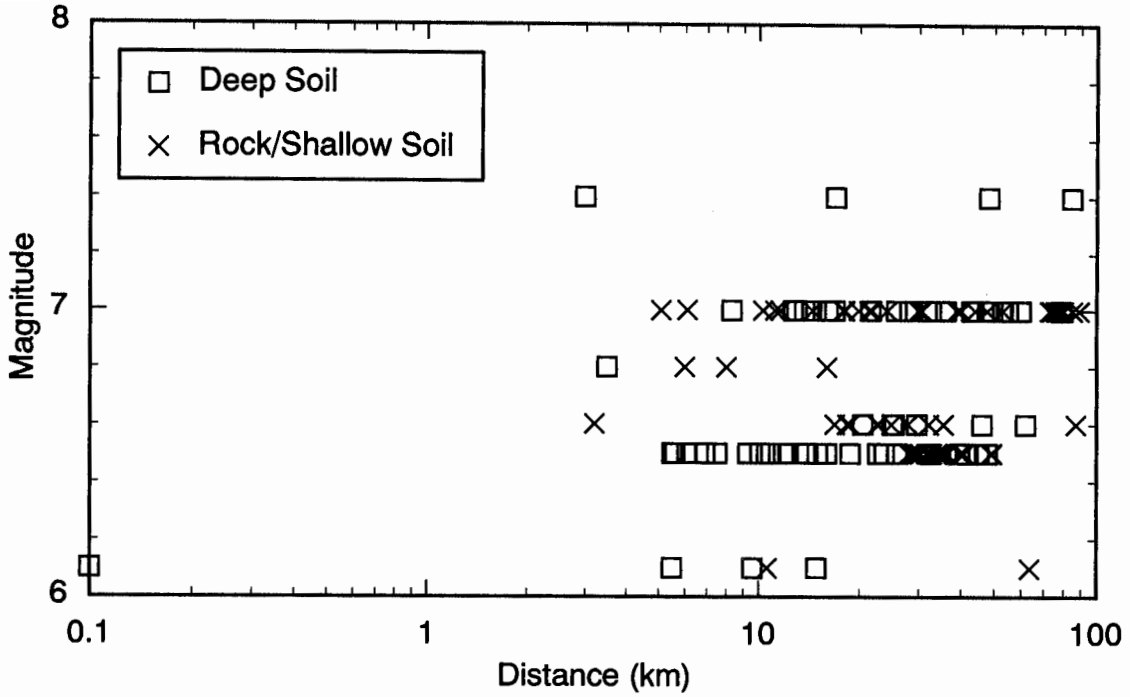

Figure 1. Data set used in the preliminary analysis.

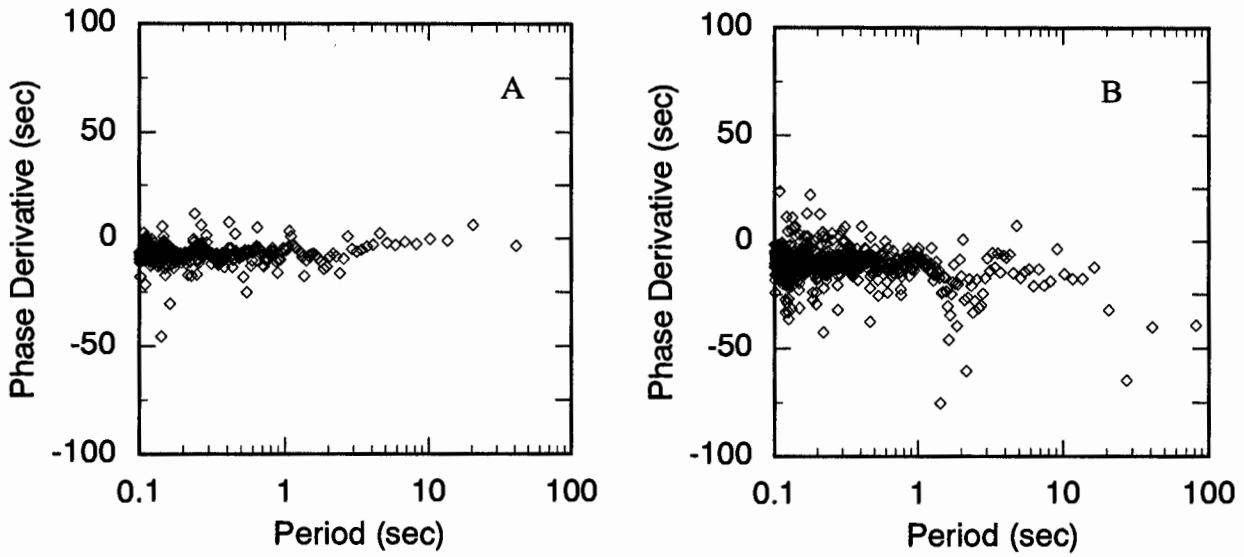

Figure 2. Sample analytical phase derivatives. Panel A shows a case in which the phase derivative is well behaved for periods up to 30 seconds. Panel B shows a case in which the phase derivative becomes more random at a period of about 1.5 seconds.

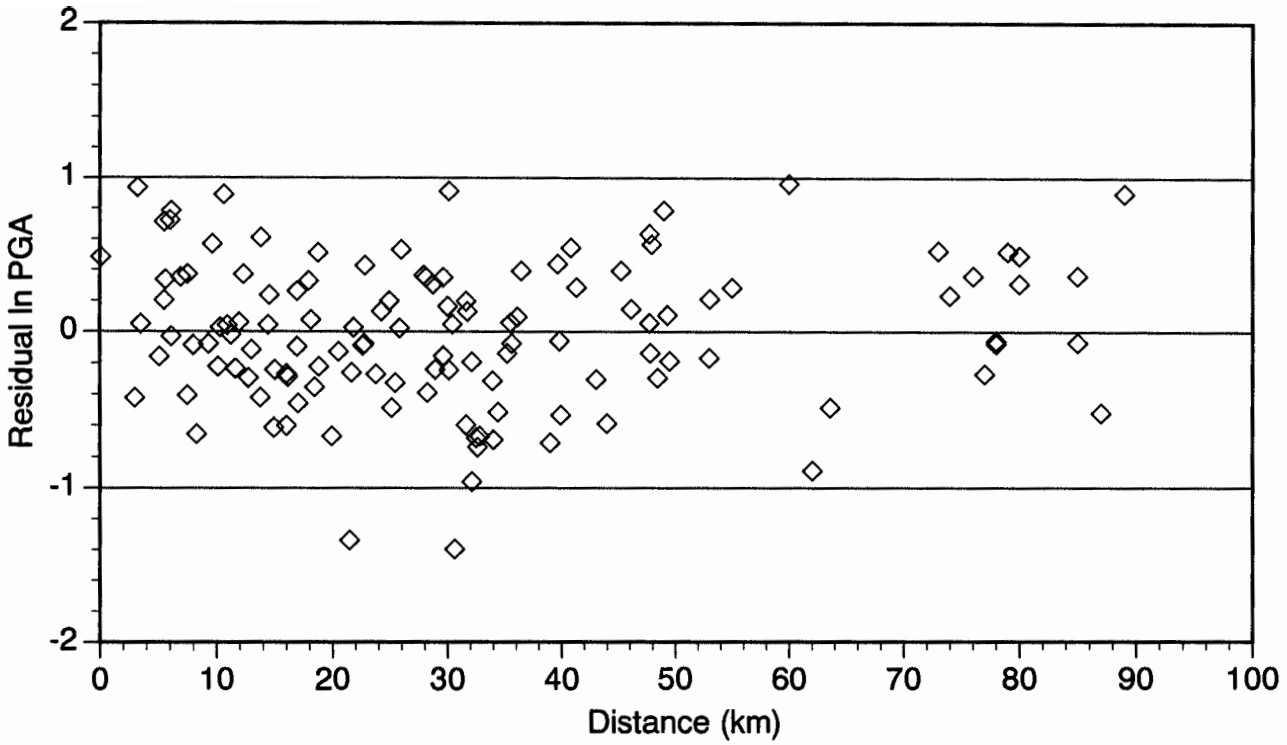

Figure 3. Peak acceleration residuals (intra-event) from Eq. 1. The residuals do not indicate that there is a significnat flattening in the attenuation for distances less than 100 km.

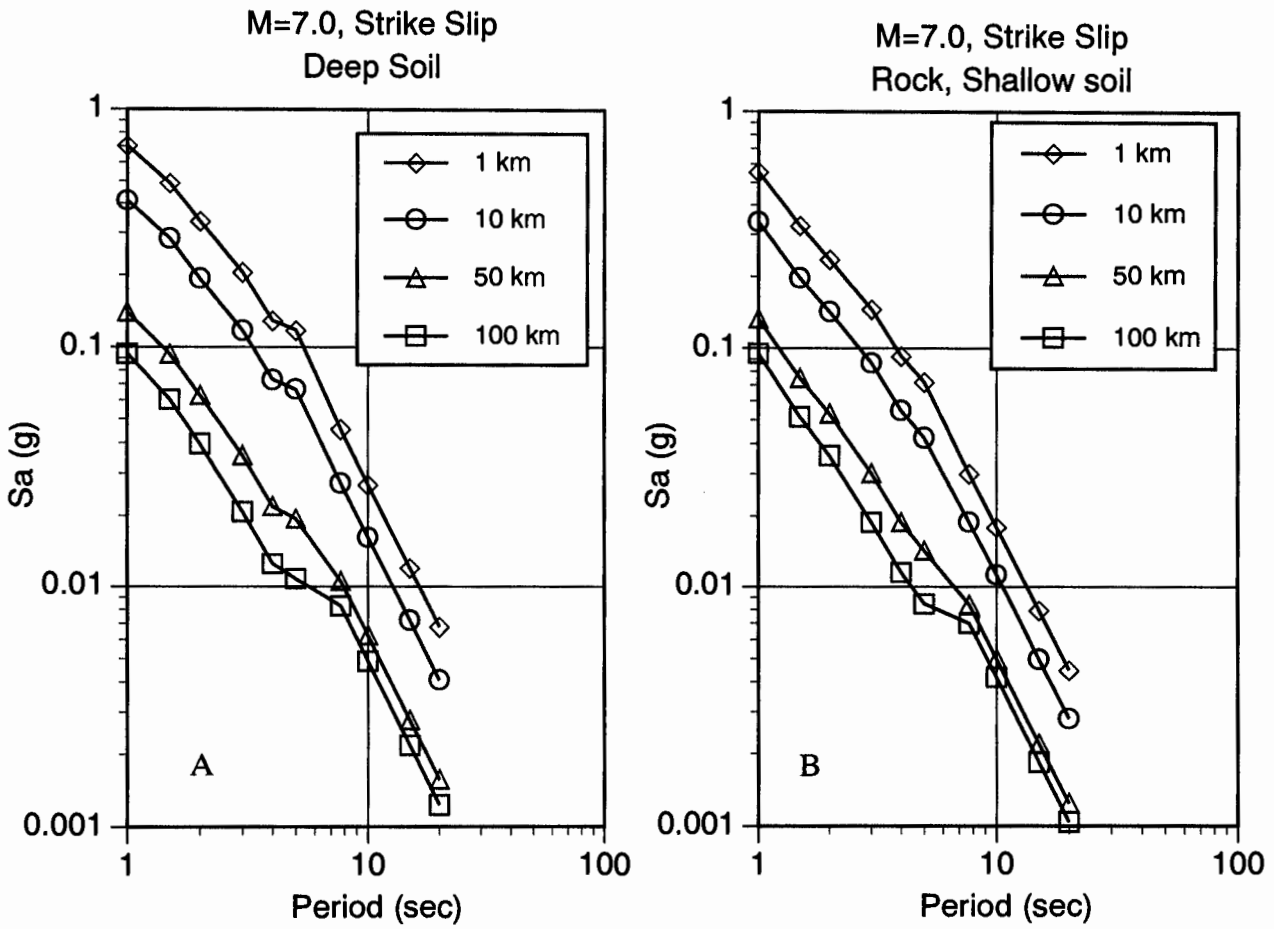

Figure 4. Attenuation of Long period spectral acceleration from Eq. 2 for a magnitude 7.0 strike-slip event. The coefficients are not smoothed. (A) Deep soil sites. (B) Rock / shallow soil sites.

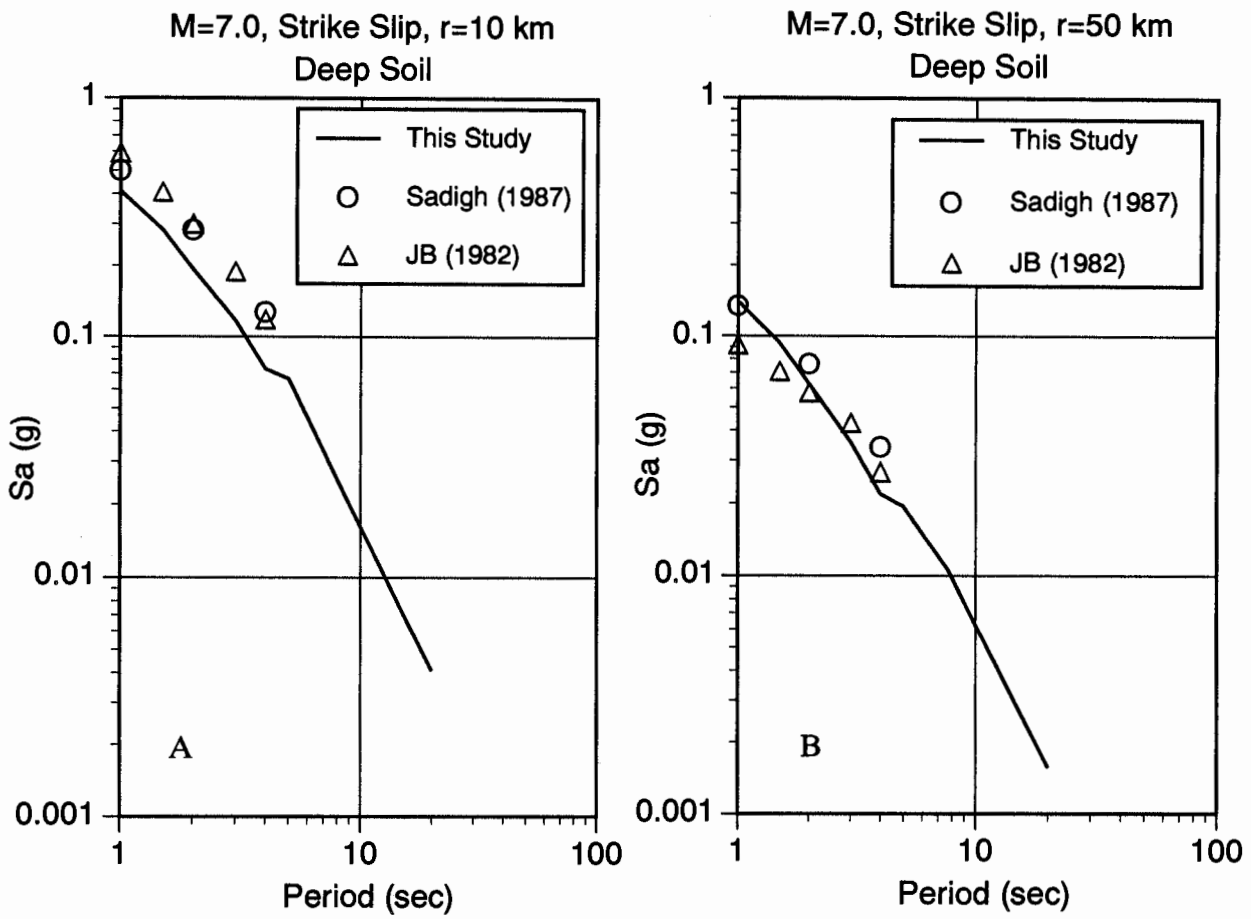

Figure 5. Comparison of the long period spectral acceleration from Eq. 2 for a magnitude 7.0 strike-slip event at deep soil sites with previously published empirical models. The relation from this study shows a much strong distance dependent spectral shape which accounts for the large differences seen in panel A. Since the distance dependence is dominated by the Loma Prieta earthquake, it is expected to be reduced when the larger data set is analyzed.

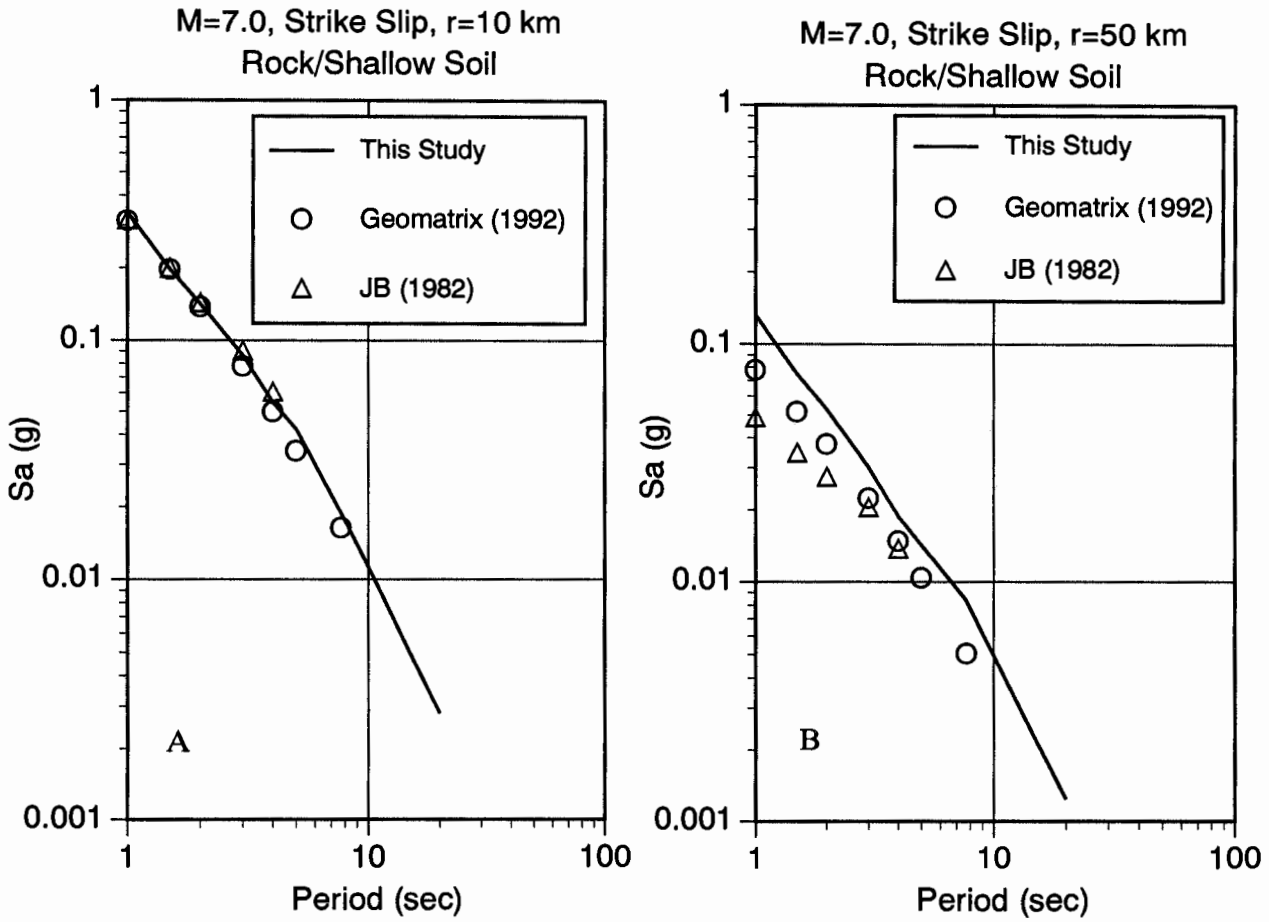

Figure 6. Comparison of the long period spectral acceleration from Eq. 2 for a magnitude 7.0 strike-slip event at rock/shallow soil sites with previously published empirical models for rock. As in Figure 5, the relation from this study shows a much strong distance dependent spectral shape which accounts for the large differences seen in panel B.

COMPARISON OF STRONG MOTION AND WEAK MOTION RECORDINGS OF THE LOMA PRIETA SEQUENCE

O. Bonamassa, H. Houston, & J.E. Vidale

Earth Sciences Board
University of California
Santa Cruz, CA 95064

ABSTRACT

The Loma Prieta earthquake sequence has provided the opportunity to compare ground motion recorded both during an magnitude 7 mainshock and numerous magnitude 2.5 to 4.5 aftershocks at 14 sites. We find two results, (1) weak motion recordings of aftershocks have predictive power to indicate the directionality of the shaking in the mainshock, and (2) non-linearity during mainshock strong motions is suggested at the sites that suffered the largest accelerations in the mainshock.

INTRODUCTION

The Loma Prieta earthquake of 18 October 1989 was the largest to strike the San Francisco Bay area since 1906. It caused considerable damage and loss of life. On the positive side, this earthquake was captured by more than a hundred strong motion seismometers, producing an unprecedented opportunity to investigate details of the earthquake and earthquake hazards in general.

The earthquake resulted in thousands of aftershocks in the following months. Fourteen strong motion recording sites (shown in Figure 1) were provided with weak motion seismometers for various time intervals (Mueller and Glassmoyer, 1990). The combination of weak and strong motions allows us to test whether site characteristics estimated from the weak motions persist during damaging strong motions.

The motion that an earthquake causes at the surface of the Earth is a combination of the details of the faulting at depth and the complications due to propagation through structures within the Earth of the seismic energy released by the faulting. Various ways of measuring the seismic source and propagational complications have been described. There exists considerable literature that documents the usefulness of the concept of a *site response*, where a particular site has a fixed set of frequencies which are amplified at that site no matter how the how the ground motion is induced (Joyner et al., 1976, Rogers et al., 1984, Borcherdt, 1970, Joyner et al., 1981). Seismic wave interaction with large-scale structures such as major sedimentary basins can be described deterministically; these structures have been shown to distort seismic waves in a fairly predictable way (Vidale and Helmberger, 1988, Kawase and Aki, 1989, Kagami et al., 1986). Bridging the gap between well-understood large structures and small structures (for which only the amplitude versus frequency behavior has been studied) is the goal of considerable recent research.

We have suggested that the direction of shaking is sometimes a feature of the recording site rather than the earthquake (Vidale et al., 1991, Bonamassa et al., 1991, Bonamassa and Vidale, 1991, Vidale and Bonamassa, 1992). These and other observations of horizontal ground motion above one Hz frequency (Dietel et al., 1989, Abrahamson et al., 1989) show very small lateral

correlation distances, less than 10's of meters for frequencies above a few Hz. Also, comparisons of seismograms written by surface and borehole instruments have shown that propagation through the shallowest 10's of meters of the Earth can severely distort seismic pulses (Haukkson et al., 1987, Malin et al., 1988, Aster and Shearer, 1991).

This report concentrates on quantifying empirically the distortion to the direction of strongest shaking and non-linearity caused by shallow earth structures.

DIRECTIONAL RESONANCES

For this presentation, we chose two stations that recorded many aftershocks with low noise. Our selection of the best-recorded aftershocks for each event, which are distributed over a wide area, as well as the station locations, are shown in Figure 2. 22 aftershocks were selected for station 378/AP7 and 25 were selected for station 006/GA2. 2 to 6 sec of the S wave, containing the largest accelerations, were windowed from the two horizontal components of each recording for the polarization analysis. The covariance matrix and its eigenvalues and eigenvectors were computed for each window. The direction of the eigenvector associated with the largest eigenvalue is the direction of the strongest shaking, and the ratio of the larger to the smaller eigenvalue is a measure of the signal linearity (Vidale, 1986).

Time domain information has been suppressed in this presentation, so it remains possible that the initial S-wave arrivals exhibit the polarization direction expected from the focal mechanism even at high frequencies, as has been observed by Bonamassa and Vidale (1991) and has also been observed for P waves by Menke and Lerner-Lam (1991).

Figure 3 shows the particle motion data for the two stations. The directions of shaking are evaluated in the frequency ranges from 0 to 1, 1 to 2, ... , and 9 to 10 Hz for each of the aftershocks and plotted as open circles. Though the pattern is more clear in the summary figures below, the tendency for some frequencies to vibrate in fixed directions at station 378/AP7 is apparent in Figure 3a. The highest frequency passband clusters strongly about NW-SE. There is also a concentration of points near E-W for the 1.5 Hz band. These clusters reveal directional resonances, where the site is most susceptible to vibrate in a fixed direction a some frequencies. We attribute this effect to local geology rather than a source effect since our previous works (Bonamassa and Vidale, 1991, and Vidale and Bonamassa, 1992 and others) show that there is generally little correlation between the particle motion predicted from the earthquake focal mechanism and the motion observed at these frequencies, and these resonance directions change between nearby stations. Station 006/GA2, in contrast, shows less clustering of the directions of strongest shaking in Figure 3b.

The overall coherence of the directional resonances is shown in Figure 4, which shows the *difference* between each aftershock polarization direction and the mainshock polarization at the same frequency. The mainshock direction is indicated by filled triangles in Figure 3. There is a strong central peak for station 378/AP7 in Figure 4a. Therefore the directions of motion in the mainshock correlate well with the directions in the aftershocks. Figure 4b, in contrast, shows that for station 006/GA2, there is little correlation between the mainshock motion and the aftershock motion. This plot is a conservative measure, since correlations would be more visible if passbands with higher linearity or more clustering of aftershock polarization were given more weight in the search for patterns. Note, for example, that the four passbands where the mainshock is most poorly polarized (2.5, 4.5, 5.5, and 9.5 Hz) show the least agreement between mainshock and aftershock directions for station 006/GA2.

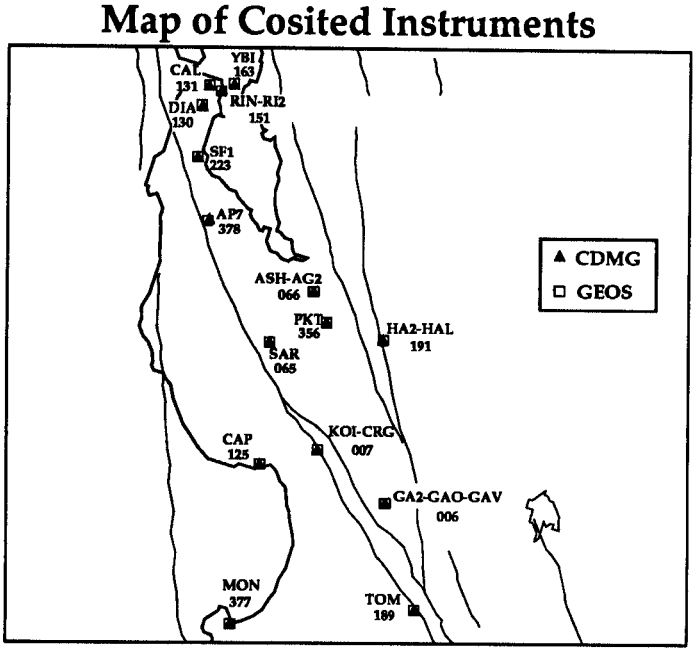

Figure 1. Map of stations recording both the mainshock and some of the aftershocks of the Loma Prieta sequence.

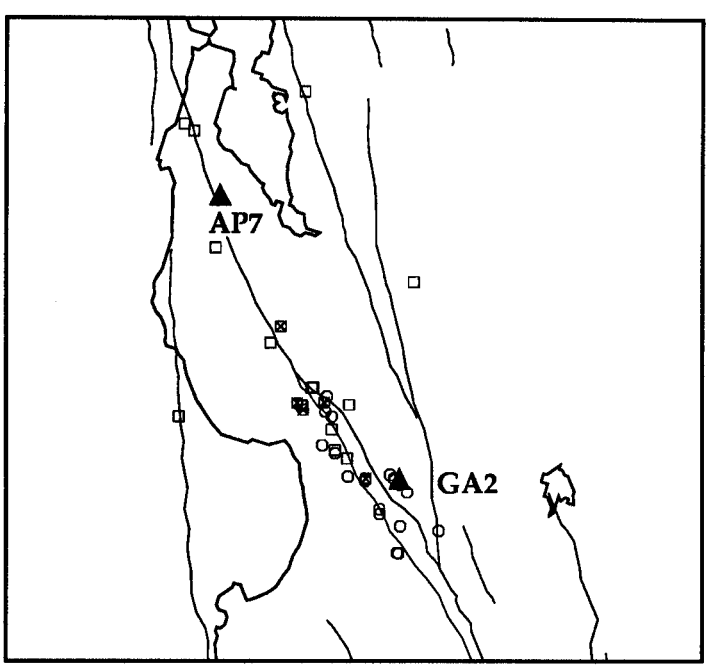

Figure 2. Map of the two stations (solid triangles) for which directional resonance analysis is presented. The locations of aftershocks analyzed at AP7 are shown by squares. The locations of aftershocks analyzed at GA2 are shown by circles. Aftershocks indicated by a cross were analyzed for both stations.

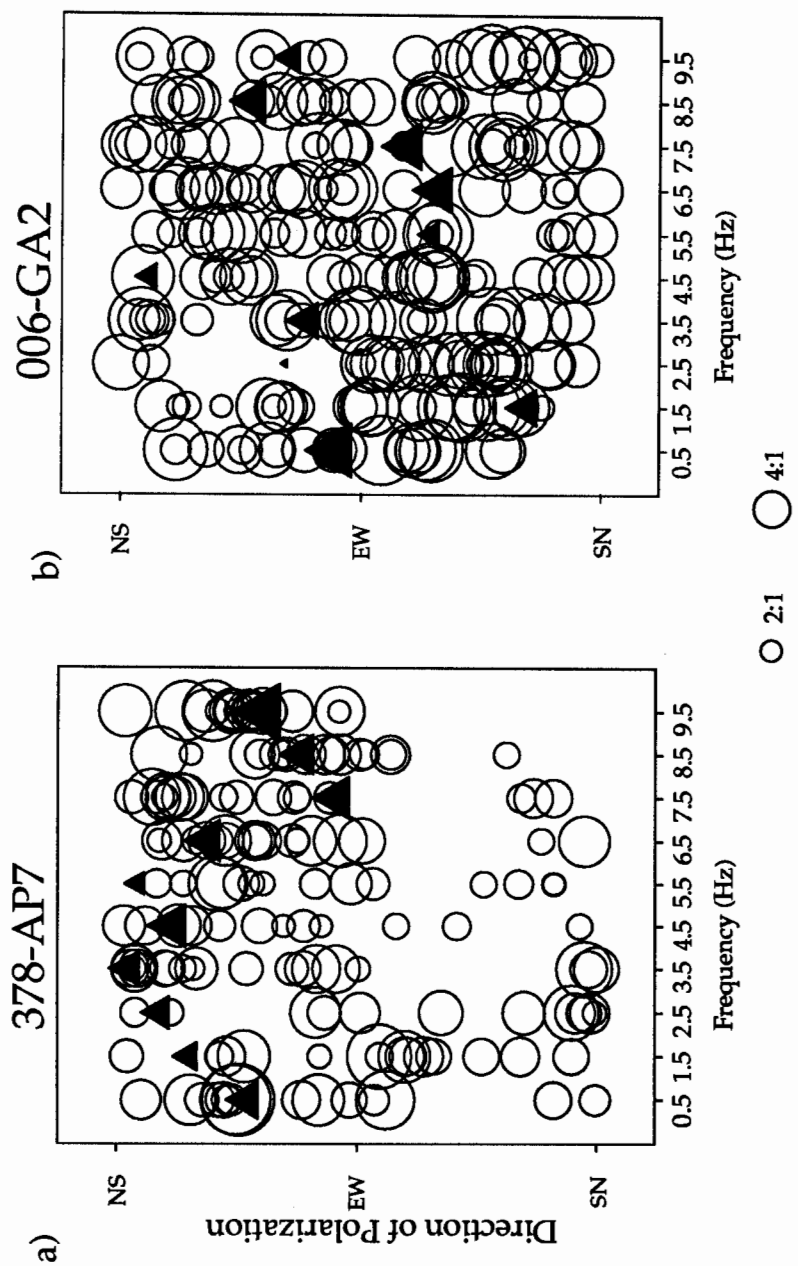

Figure 3. The preferred direction of motion plotted for each of the 10 frequency bands for each of the aftershocks. Larger symbols indicate more linear polarization. Solid triangles show the direction of polarization in the mainshock. Each frequency band is one Hz wide. a) Data from station 378/AP7. b) Data from station 006/GA2.

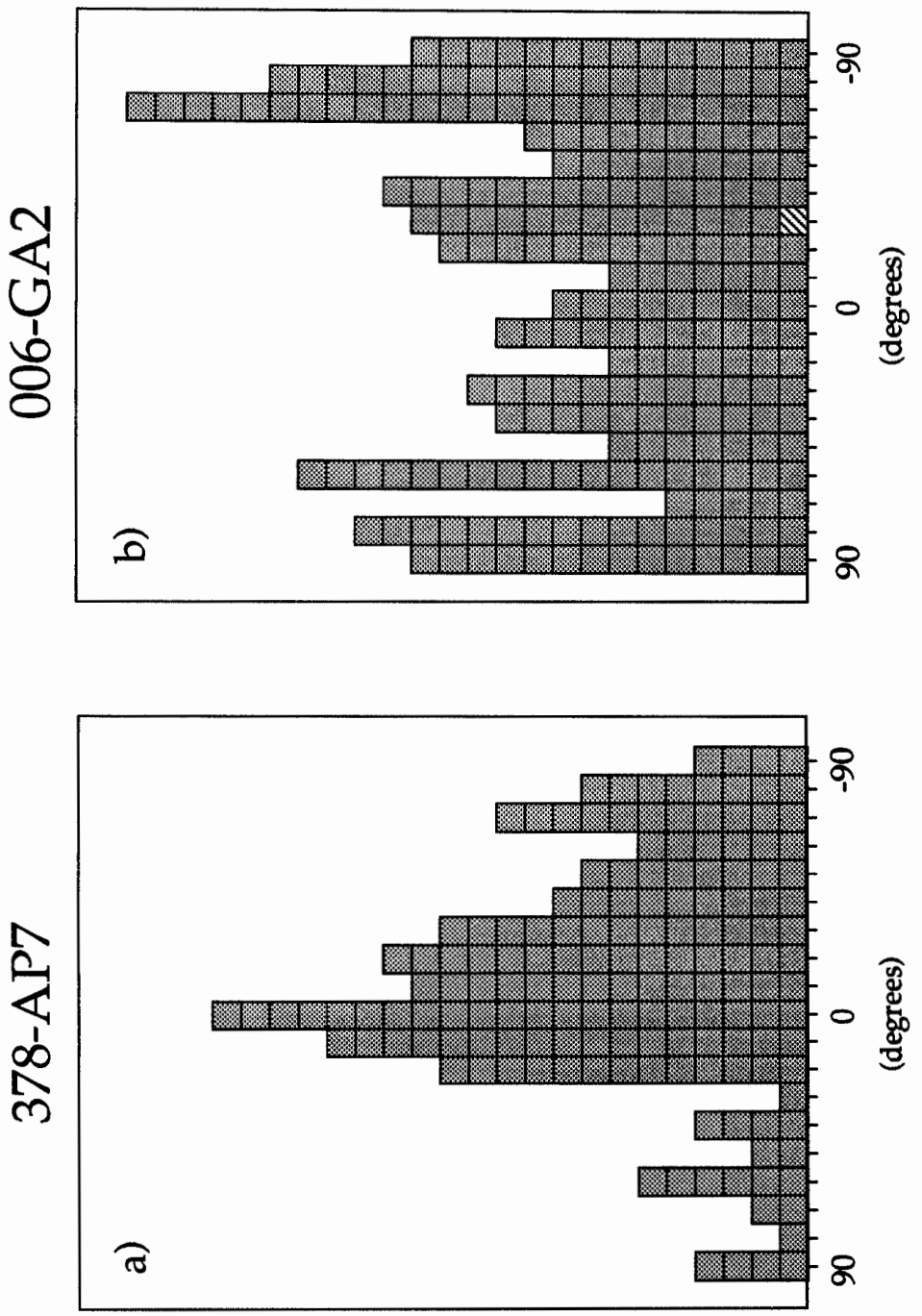

Figure 4. Histogram of azimuthal differences between the direction of strongest shaking in the mainshock and the direction of the strongest shaking in an aftershock for each aftershock and each frequency. a) Data from station 378/AP7. Note that the differences cluster around 0 to 20°. b) Data from station 006/GA2. The differences are not clustered.

Figure 5. The open triangles show the mean direction of strongest shaking for 22 aftershocks in each frequency band. The error bars indicate one standard deviation. The solid circles show the direction of strongest shaking observed in the mainshock. a) Data from station 378/AP7. b) Data from station 006/GA2.

The coherence estimated in Figure 4 is examined in more detail in Figure 5. Here, the *mean* direction of motion for each frequency from the aftershocks is shown by an open triangle. The standard deviation is indicated by the error bar. The direction of motion in the mainshock is shown by the solid circles. The agreement at station 378/AP7 is striking (Figure 5a). For 8 out of 10 passbands, the mainshock direction of motion is within 30° of the aftershock mean motion. Note the very good agreement between the direction of shaking in the mainshock and the mean direction of shaking for the aftershocks, less than 5°, at the frequencies wheere the aftershock directions are most tightly clustered (0.5, 6.5, and 9.5 Hz). Station 006/AP7, on the other hand, shows little correlation between the (mostly poorly clustered) aftershock mean directions of strongest shaking and the mainshock directions of strongest shaking. This plot is also conservative. For example, excluding the 4 passbands where the mainshock polarization is least linear, fair to good agreement is seen in 5 of 6 passbands.

It appears that about 20 aftershock recordings were sufficient to provide fairly accurate "predictions" of the mainshock motion at one of the two stations presented. Rather surprisingly, it is the hard site (sandstone) rather than the alluvium that showed the stronger tendency for directional site resonance, emphasizing our poor understanding of the influence of the near-surface weathered layer.

NON-LINEAR SITE EFFECTS?

Non-linear effects are known to diminish the amplitude of very strong ground motion through conversion of seismic energy into heat in anelastic deformation. An understanding of non-linear damping is important, since most earthquake hazard research relies on the study of small earthquakes to predict the effects of big events. Non-linear effects have recently been proposed to occur in shaking as weak as 10% g by Chin and Aki (1991) and Darragh and Shakal (1991). The work of Chin and Aki (1991) requires assumptions about the seismic source, the attenuation of amplitude with distance, and the relation between horizontal vertical site response, while the work of Darragh and Shakal (1991) compares hard site-soft site pairs of stations, with the assumption that the hard rock site is free of strong site effects.

Another approach is to compare the amplitude of motions at a set of stations for an aftershock with that from the mainshock. In the ideal case of identical source location, identical mechanism, and no non-linear effects, the ratio of mainshock and aftershock motions should be constant across all stations for each frequency. So a plot of mainshock versus aftershock motion would produce a straight line whose slope is proportional to the ratio of the two earthquakes' source strengths.

We choose the 11 aftershocks ranging from magnitude 2.5 to 4.5 that are shown in Figure 6. The north-south and east-west components of each record are filtered into the passbands 1-2, 2-4, 4-8 and 8-12 Hz for each aftershock and the mainshock. We measure the larger of the peak amplitudes of the two components, and compare the mainshock with the aftershock motions for each passband in Figure 7.

These results are preliminary. The apparent saturation of mainshock motions suggests, however, that some non-linearity is present. In other words, in several cases the amplification observed for the mainshock is less than that seen in aftershocks, which could be due to non-linear damping of the mainshock motions. We must still correct for the differing moments and corner frequencies of the aftershocks. Several of the most discrepant points arise from the station in Capitola, making it the leading candidate for non-linear motions.

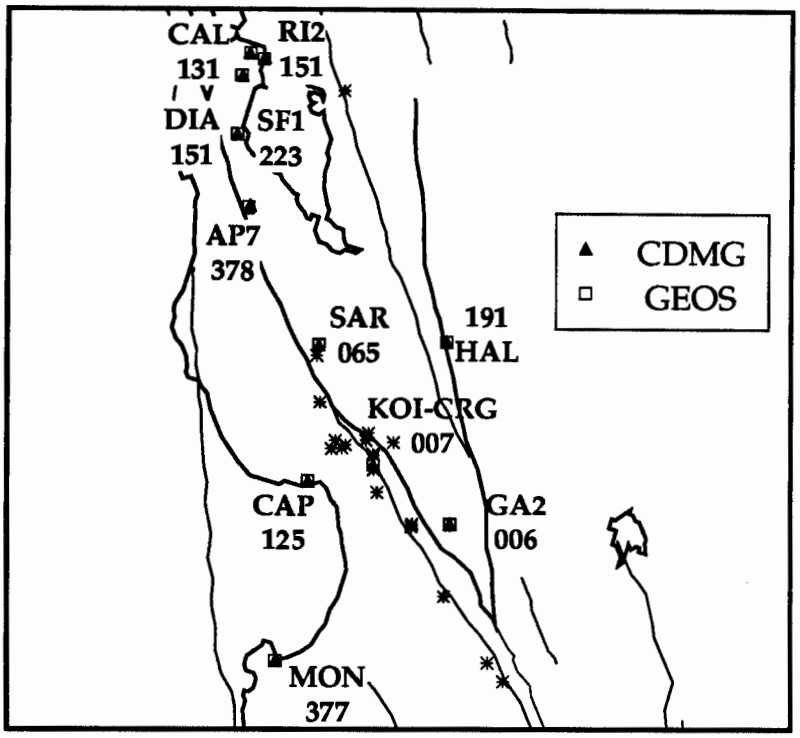

Figure 6. Map of the stations (triangles) that recorded the mainshock and the 11 aftershocks shown by circles.

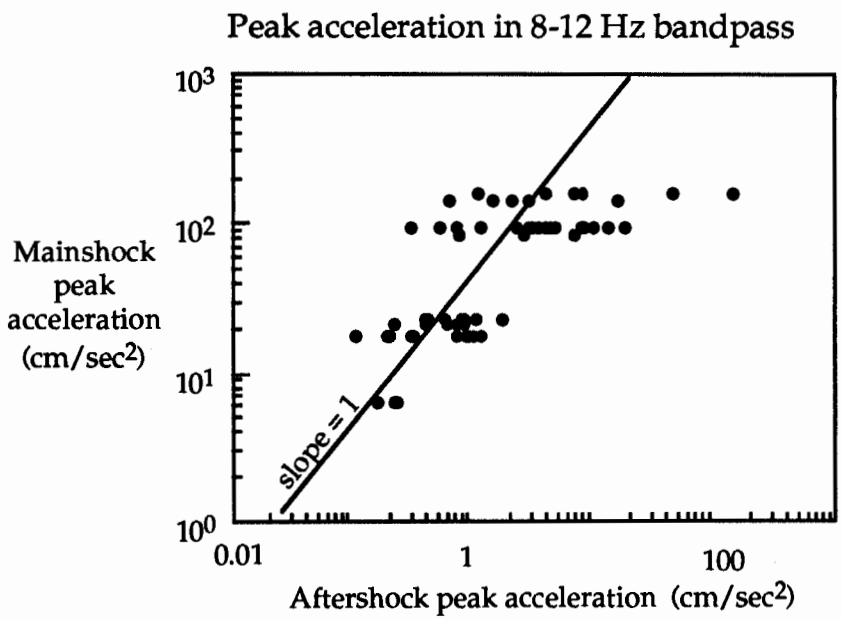

Figure 7. The amplitude of the peak motion in the mainshock plotted against the peak motion in each of the 11 aftershocks for the passband 8 to 12 Hz.

CONCLUSIONS AND UNANSWERED QUESTIONS

We have demonstrated that recordings of small earthquakes can provide useful estimates of directional resonance effects that occur in the mainshock. The evidence for non-linearity requires more thorough examination.

The remaining questions have advanced only incrementally since the meeting a year ago: Where are the geologic structures that strongly filter the high-frequency polarization characteristics? The low spatial coherence suggests shallow structure, borehole studies suggest shallow structure, and to the extent that common sense applies, the observation that the near surface is the least consolidated and most highly variable volume along the seismic ray path suggests that the structures lie near the surface. Candidates for these near surface structures include surface topography (Bard and Gariel, 1986, Kawase and Aki, 1989) and topography on the soil rock interface (Bard and Tucker, 1985). Candidates for wave interactions include focusing through seismic velocity gradients acting as lens (Rial, 1989, Langston and Lee, 1983), body-wave to surface-wave conversions at sharp, laterally heterogeneous velocity contrasts (Bard and Gariel, 1986, Vidale and Helmberger, 1988, Kawase and Aki, 1989), and energy that becomes trapped and reverberates between high contrast interfaces (Novaro et al., 1990).

The task remaining is the construction of simulations with methods like three-dimensional finite differences (Frankel *et al.*, 1990) that reproduce the complexity we observe in the seismic wavefield using realistic velocity models. This task relies on the equally difficult task of accurately estimating realistic three dimensional velocity models of the near surface.

REFERENCES

Abrahamson, N.A., J.F. Schneider, and J.C. Stepp, 1989. Spatial Coherency of strong ground motion for application to soil structure interaction, *Seism. Res. Lett.*, **60**, 3.

Aster, R., and P. Shearer, 1991. High-frequency seismic polarizations and site effects observed in boreholes in the San Jacinto fault zone, southern California. Part 1. Polarizations, *Bull. Seism. Soc. Am.* **81**,1057-1080.

Bard, P.-Y., and J.C. Gariel, 1986. The seismic response of two-dimensional sedimentary deposits with large vertical velocity gradients, *Bull. Seism. Soc. Am.*, **76**, 343-360.

Bard, P.-Y., and B.E. Tucker, 1985. Underground and ridge site effects: A comparison of observation and theory, *Bull. Seism. Soc. Am.*, **75**, 905-923.

Bonamassa, O., J.E. Vidale, H. Houston, and S.Y. Schwartz. Directional site resonances and the strong influence of near-surface geology on ground motion, *Geophys. Res. Lett.*, **18**, 901-904.

Bonamassa, O., J.E. Vidale, 1991. Directional site resonances observed from aftershocks of the 18 October 1989 Loma Prieta earthquake, *Bull. Seism. Soc. Am.*, **81**, 1945-57.

Borcherdt, R.D., 1970. Effects of local geology on ground motion near San Francisco Bay, *Bull. Seism. Soc. Am.*, **60**, 29-61.

Chin, B, and K. Aki, 1991. Simultaneous study of the source, path and site effects on strong ground motion during the 1989 Loma Prieta earthquake: A preliminary result on pervasive nonlinear site effects, *Bull, Seism. Soc. Am.*, **81**, 1859-1884.

Darragh, R.B., and A.F. Shakal, 1991. The site response of two rock and soil pairs to strong and weak ground motion, *Bull. Seism. Soc. Am.*, **81**, 1885-1899.

Dietel, C., B. Chouet, K. Aki, V. Ferrazzi, P. Roberts, and R.Y. Koyanagi, 1989. Data summary for dense GEOS array observations of seismic activity associated with magma transport at Kilauea Volcano, Hawaii, Open File Report, US Geological Society, 171 p.

Frankel, A., S. Hough, P. Friberg, R. Busby, 1991. Observations of Loma Prieta aftershocks from a dense array in Sunnyvale, California, *Bull. Seism. Soc. Am.*, **81**, 1900-1922.

Haukkson, E., T.-L. Teng, T.L. Henyey, 1987. Results from a 1500 m deep, three-level downhole seismometer array, *Bull. Seism. Soc. Am.*, **77**, 1883-1904.

Joyner, W.B., R.E. Warrick, T.E. Fumal, 1981. The effect of Quaternary alluvium on strong ground motion in the Coyote Lake, California, earthquake of 1979, *Bull. Seism. Soc. Am.*, **71**, 1333-1351.

Joyner, W.B., R.E. Warrick, and A.A. Oliver, III, 1976. Analysis of seismograms from a downhole array in sediments near San Francisco Bay, *Bull. Seism. Soc. Am.*, **66**, 937-958.

Kagami, H., S. Okada, K. Shiono, M. Oner, M. Dravinski, and A.K. Mal, 1986. Observation of 1-5 second microtremors and their application to earthquake engineering. Part III. A two-dimensional study of site effects in the San Fernando Valley, *Bull. Seism. Soc. Am.*, **76**, 1801-1812.

Kawase, H. and K. Aki, 1989. A study on the response of a soft basin for incident S, P, and Rayleigh waves with special reference to the long duration observed in Mexico City, *Bull. Seism. Soc. Am.*, **79**, 1361-1382.

Langston, C.A., and J. Lee, 1983. Effect of structure geometry on strong ground motions; the Duwamish river valley, Seattle, Washington, *Bull. Seism. Soc. Am.*, **73**, 1851-1863.

Malin, P.E., J.A. Waller, R.D. Borcherdt, E. Cranswick, E.G. Jensen, and N. Van Schaak, 1988. Vertical seismic profiling of Oroville microearthquakes: velocity spectra and particle motion as a function of depth, *Bull. Seism. Soc. Am.*, **78**, 401-420.

Menke, W., and A.Lerner-Lam, 1991. Observations of the transition from linear polarization to complex polarization in short-period compressive waves, *Bull. Seism. Soc. Am.*, **81**, 611-623.

Mueller, C., and G. Glassmoyer, 1990. Digital recordings of the aftershocks of the 17 October 1989 Loma Prieta, California, earthquake, US Geological Survey Open-file report 90-503, 147 p.

Novaro, O., T.H. Seligman, J.M. Alvarez-Tostado, J.L. Mateos, and J. Flores, 1990. Two-dimensional model for site effect studies of microtremors in the San Fernando Valley, *Bull. Seism. Soc. Am.*, **80**, 239-252.

Rial, J.A., 1989. Seismic wave resonance in 3-D sedimentary basins, *Geophys. J. Roy astr. Soc.*, **99**, 81-90.

Rogers, A.M., R.D. Borcherdt, P.A. Covington and D.M. Perkins, 1984. A comparative ground response study near Los Angeles using recordings of Nevada nuclear tests and the 1971 San Fernando earthquake, *Bull. Seism. Soc. Am.*, **74**, 1925-1949.

Vidale, J.E., 1986. Complex polarization analysis of particle motion, *Bull. Seism. Soc. Am.*, **76**, 1393-1406.

Vidale, J.E., and O. Bonamassa, 1992. Strong variations in strong motion recordings across San Francisco; the influence of near-surface geology, in press, *Loma Prieta Professional Paper*

Vidale, J.E., O. Bonamassa, and H. Houston, 1991. Directional Site Resonances Observed from the 1 October 1987 Whittier Narrows Earthquake and the 4 October Aftershock, *Earthquake Spectra.*, **7**, 107-126.

Vidale, J.E., and D.V. Helmberger, 1988. Elastic finite-difference modeling of the 1971 San Fernando, Ca. earthquake, *Bull. Seism. Soc. Am.*, **78**, 122-142.

EVALUATION OF CODE-ACCIDENTAL TORSION PROVISIONS USING EARTHQUAKE RECORDS FROM THREE NOMINALLY SYMMETRIC-PLAN BUILDINGS

Juan Carlos De la Llera and Anil K. Chopra

Department of Civil Engineering
University of California at Berkeley

ABSTRACT

A procedure is presented for evaluating building code provisions for accidental torsion from analysis of recorded motions of nominally symmetric-plan buildings during earthquakes. This procedure is utilized to analyze the motions of three buildings recorded during recent California earthquakes. The results demonstrate that the accidental torsion specified by the Uniform Building Code is adequate in representing the torsion in the recorded motions of these three buildings. It is also concluded, although somewhat speculatively, that accidental torsion need not be considered in the design of many buildings.

INTRODUCTION

Building codes require that the effects of torsion be considered by applying the equivalent lateral forces at a distance e_d from the center of rigidity (CR), resulting in story torques in addition to shears and overturning moments. The design eccentricity, e_d, specified in U.S. codes and design recommendations is of the form $e_d = e_s \pm 0.05b$, where e_s is the static stiffness eccentricity--i.e., the distance between the center of mass (CM) and CR--and b is the plan dimension of the building perpendicular to the direction of ground motion. The first term, e_s, is intended to account for the coupled lateral torsional response of the building arising from lack of symmetry in plan. The additional $\pm 0.05b$, known as *accidental eccentricity*, is introduced to account for building torsion arising from discrepancies between the mass, stiffness, and strength distributions used in analysis and true distributions at the time of an earthquake; torsional vibrations induced by a rotational component of ground motion; and other sources of torsion not considered explicitly in analysis. Accidental torsion is to be considered in the design of buildings with asymmetric plans as well as symmetric plans; in the latter case, this is the total torsion to be considered.

Most of the research investigations of coupled lateral-torsional response of buildings, including the work aimed toward evaluating the adequacy of torsional provisions in building codes, have been concerned with structures with asymmetric plan. Perhaps there are two major reasons. Firstly, buildings with asymmetric floor plan tend to suffer greater damage. Secondly, the dynamics of asymmetric-plan buildings are amenable to analytical study; elastic as well as inelastic systems have been investigated.

On the other hand, the subject of accidental torsion is not amenable to investigation by traditional analytical approaches. Standard dynamic analyses cannot predict torsion in symmetric-plan buildings. However, it has been possible to investigate analytically the torsional response of such buildings due to rotational ground motion [5]. These studies are based on ground motion assumptions which so far have not been verified for lack of suitable ground motion records. Therefore, analysis of recorded motions of nominally symmetric-plan buildings during earthquakes provides the most direct means of developing an understanding of the torsional responses of such buildings and for evaluation of building code provisions for accidental torsion. This is the approach adopted in this investigation.

BUILDINGS CONSIDERED AND RECORDED MOTIONS

Ideal for the purposes of this investigation would be buildings satisfying certain requirements--nominally-symmetric floor plans, rigid floor diaphragms, and negligible soil-structure interaction effects--that have experienced significant ground shaking, and three independent components of acceleration have been recorded at the ground level and at each floor. Three buildings which essentially satisfy the above requirements have been identified for the present study. A brief description of these three structures and their motions recorded during earthquakes is presented next.

BUILDING A

Identified as CSMIP Station No. 58506, this building is located in Richmond, California. A typical framing plan of this steel structure is shown in Fig. 1. The building has a nominally-symmetric floor plan. It consists of moment-resisting frames 1 and 7 in the Y-direction. Between frame lines 3 and 6, frames A and C are also designed for lateral load resistance. All other frames with semi-rigid connections are designed to carry only gravity loads. The floor decking system is formed by a steel corrugated metal sheet filled with lightweight concrete. The roof deck is lighter but has additional insulating concrete. The foundation system consists of rectangular column footings interconnected by grade beams. In the Y-direction only footings for columns of frames 1 and 7 are interconnected. Additional information about this building is presented in the complete report.

Accelerographs recorded the motion of the building during the Loma Prieta earthquake (October, 1989), including three channels of horizontal motion at the second floor, third floor, and roof levels, and two channels of motion at the first (or ground) floor level. The peak accelerations at the ground level are $0.083g$ in the X-direction and $0.11g$ in the Y-direction. These motions were amplified to $0.31g$ and $0.27g$, respectively, at the roof level. The building experienced no structural damage during the earthquake.

BUILDING B

Identified as CSMIP Station No. 23511, this building is located in Pomona, California. This reinforced concrete frame building has two stories and a partial basement, and a light penthouse structure. The building has a nominally-symmetric floor plan, as indicated by its framing plan. The lateral force-resisting system in the building consists of peripheral columns interconnected by longitudinal and transverse beams. The "L"-shaped exterior corner columns as well as the interior columns in the building are not designed especially for earthquake resistance. The floor decking system is formed by a 6" concrete slab. The building also includes walls in the stairwell system--concrete walls in the basement and masonry walls in upper stories. Foundations of columns and interior walls are supported on piles. Additional information about this building is presented in the complete report.

Accelerographs recorded the motion of the building during the Whittier (October, 1987) and Upland (February, 1990) earthquakes, including three channels of horizontal motion at the second floor and roof levels and at the basement of the building. During the Whittier earthquake, the peak accelerations at the basement level were $0.046g$ in the X-direction and $0.05g$ in the Y-direction. These motions were amplified to $0.15g$ in both directions at the roof level. During the Upland earthquake, the peak accelerations at the ground level were $0.12g$ and $0.13g$ in the X- and Y-directions, respectively. These motions were amplified to $0.24g$ in the X-direction and $0.39g$ in the Y-direction at the roof level. The building experienced no structural damage during either earthquake.

BUILDING C

Identified as CSMIP Station No. 57562, this building is located in San Jose, California. The building considered is one of four similar wings around a central building. Each wing is isolated from the central building by a separation joint. A typical framing plan of this three-story steel structure is shown in Fig. 3. The triangular portion of the building (shown in dashed lines) is not part of any lateral moment-resisting frame of the structure. Thus, the building has a nominally-symmetric floor plan consisting of moment-resisting frames A, B, C, and D in the X-direction and frames 1 through 9 in the Y-direction. All other frames are designed to carry only gravity loads. The floor decking system is formed by a steel corrugated metal sheet filled with lightweight concrete. The foundation system consists of rectangular column footings interconnected by grade beams. Additional information about this building is available in the complete report.

Accelerographs recorded the motion of the building during the Loma Prieta earthquake, including three channels of horizontal motion at each of the roof, third, and first (ground) floor levels. The peak accelerations at the ground level are $0.2g$ in both lateral directions, X and Y. These motions were amplified to $0.58g$ in the X-direction and $0.68g$ in the Y-direction at the roof level. The building experienced no structural damage during the earthquake. The two horizontal components of acceleration and rotational acceleration at the second floor without any accelerographs were estimated using the procedure described in the complete report.

DYNAMIC ACCIDENTAL ECCENTRICITY

We first determine the accidental eccentricity for a nominally symmetric-plan building with rigid floor diaphragms directly from the recorded motions. At the i^{th} floor these recorded accelerations are denoted by $a_{1i}(t)$, $a_{2i}(t)$, and $a_{3i}(t)$, and such data are assumed to be available for all floors $i = 1, 2, \ldots, N$ (Fig. 4(a)). From the recorded motions of the i^{th} floor the X and Y acceleration components at the CM of the floor, $a_{Xi}(t)$ and $a_{Yi}(t)$, and the torsional acceleration, $a_{\theta i}(t)$, of the i^{th} floor diaphragm can be determined by a simple geometric transformation. The associated inertia forces are $m_i\, a_{Xi}(t)$ and $m_i\, a_{Yi}(t)$ in the X- and Y-directions, respectively, and the associated torque is $I_{pi}\, a_{\theta i}(t)$ where m_i is the i^{th} floor mass and I_{pi} is the polar moment of inertia of the i^{th} floor mass about the CM of the floor (Fig. 4(b)). The shears and torques in the j^{th} story are determined by simple statics from the floor inertia forces which are known from the floor masses and recorded accelerations: $V_{Xj}(t) = \sum_{i=j}^{N} m_i\, a_{Xi}(t)$, $V_{Yj}(t) = \sum_{i=j}^{N} m_i\, a_{Yi}(t)$, and $T_j(t) = \sum_{i=j}^{N} I_{pi}\, a_{\theta i}(t)$. These story shears and torque are statically equivalent to each of the following force sets: (1) V_{Xj} at the CM and V_{Yj} at eccentricity e_{Xj} (Fig. 4(c)) given by $e_{Xj}(t) = T_j(t)/V_{Yj}(t)$; and (2) V_{Yj} at the CM and V_{Xj} at eccentricity e_{Yj} given by $e_{Yj}(t) = T_j(t)/V_{Xj}(t)$. The time-dependent quantities $e_{Xj}(t)$ and $e_{Yj}(t)$ may be interpreted as the instantaneous accidental eccentricities for the j^{th} story.

From the recorded motions these accidental eccentricities were computed for the three selected buildings. The results for the first story of Building B during the Upland earthquake are presented in Fig. 5 wherein the base shear and base torque are presented together with accidental eccentricities $e_{X1}(t)$ and $e_{Y1}(t)$. These computed eccentricity values grossly exceed the code value of $0.05b$ intermittently during the earthquake. However, this result does not imply that the code provisions are deficient.

This approach to compute the accidental eccentricity is appealing because it is based exclusively on recorded motions and does not require idealization or analysis--static or dynamic--of the structure. However, the numerical results are not especially useful because the largest peaks in the eccentricity-time plot are usually associated with small values of the base shear, and can occur even during the trailing, weak portions of the building motions. Therefore, a large value for the accidental eccentricity by itself is not meaningful and should be considered in conjunction with the instantaneous base shear value. In order to consider the combined effects of shear and torque in evaluating the code provisions, however, static analysis of the structure becomes necessary.

STRUCTURAL IDEALIZATION

The natural vibration frequencies and modes of the buildings are computed and static analyses are performed at many time instants, but no dynamic analyses were necessary. For these analyses the three buildings were idealized consistent with the ETABS computer program where in the building mass is assumed to be lumped at the floor levels and the floor diaphragms are assumed to be rigid. The compatibility of axial deformations required in columns belonging to more than one moment-resisting frame is considered by analyzing each structure as a single three-dimensional frame with six degrees of freedom per joint (in contrast to the more common type of analysis that considers the structure as an assemblage of independent planar frames). A brief summary of the structural idealization for each building is presented next; additional details are available in the complete report.

BUILDING A

This building was treated as fixed at the level defined by the slab on grade. Each frame was modeled with appropriate beam-column joints: moment-resistant (or rigid) connections and semi-rigid connections. The latter were divided into two groups: connections of column flanges with beams were modeled as rigid, and connections of column webs with beam webs as pinned. Computed by the ETABS program, the natural vibration frequencies and shapes of the first mode in the X-direction, the first mode in the Y-direction, and the first torsional mode are presented in Table 1. These computed results are similar to the "actual" vibration properties in Table 1 determined from the recorded earthquake motions by the procedure described in the complete report.

BUILDING B

This building was treated as fixed at the level defined by the base of the columns because the pile foundations are very stiff. The structural idealization considers all structural elements, including those not intended to provide lateral resistance, such as the masonry walls in the stairwell system, because they may cause torsion of the building and contribute to its accidental eccentricity. The effective moment of inertia in the beams was calculated assuming cracked sections and including the contribution of the concrete slab. The actual variation of moment of inertia along the span was considered in modeling the tapered beams along axes 2, 3, 4, and 5 (Fig. 2). The effective moment of inertia in columns was calculated assuming gross section properties.

Computed by the ETABS program, the natural vibration frequencies and shapes of the first mode in the X-direction, first mode in the Y-direction, and first torsional mode are presented in Table 1. These computed results agree reasonable well with the "actual" vibration properties determined from the recorded earthquake motions. As expected, the computed vibration properties are closer to the "actual" values from the less intense Whittier earthquake motions than from the more intense Upland earthquake motions. The higher intensity of shaking during the Upland earthquake, combined with the stiffness degradation during the earlier Whittier earthquake, leads to lower vibration frequencies during the Upland earthquake.

BUILDING C

This building was treated as fixed at the level of the slab on grade. The structural idealization includes all structural elements, including those that provide little lateral resistance, such as the triangular portion of the building (Fig. 3), because they may cause torsion of the building and contribute to its accidental eccentricity. Each frame was modeled with appropriate beam-column connections: moment-resistant (or rigid) connections and pinned connections as defined in the original structural drawings of the building. Computed by the ETABS program, the natural vibration frequencies and shapes of the first mode in the X-direction, the first mode in the Y-direction, and the first torsional mode are presented in Table 1. These computed results are similar to the "actual" vibration properties in Table 1 determined from the recorded earthquake motions by the procedure described in the complete report.

BASE SHEAR AND BASE TORQUE

As mentioned in a preceding section, the combined effects of shear and torque must be considered in evaluating the accidental torsion provisions in building codes. For each of the three buildings the base shears $V_{X1}(t)$ and $V_{Y1}(t)$ and base torque $T_1(t)$ have already been computed from the recorded accelerations. Consistent with the code approach of two independent lateral-force analyses in two orthogonal directions, X and Y, we consider the combined effects of V_{Y1} and T_1 separately from the combined effects of V_{X1} and T_1; only the first pair is considered in the following presentation and the modification for the other pair is obvious. Figure 6 shows the base shear $V_{Y1}(t)$ and base torque $T_1(t)$ for Building A during the recorded earthquake wherein each point (+) denotes the combination of V_{Y1} and T_1 values at a particular time instant; there are as many points as the time instants considered. The point C in Fig. 6 identifies the code value of base shear $V_{code} = (ZIC/R_w)W$ and base torque which, for a nominally-symmetric building, is $T_{code} = (0.05b)V_{code}$. In computing the coefficient C, the fundamental vibration period T was taken equal to the "actual" value in Table 1, and R_w as 12. The fact that the base shear during the earthquake exceeds the code value of base shear at many time instants is consistent with the well known fact that the actual capacity of most buildings is much larger than the design base shear. In order to evaluate the code-accidental torsion provisions, we also show the point C_a which denotes the maximum value of actual base shear $(V_{Y1})_o = \max_t |V_{Y1}(t)|$ and $T_1 = (0.05b)(V_{Y1})_o$. However, it is by no means obvious whether the pair of actual forces $V_{Y1}(t)$ and $T_1(t)$ at a particular time instant is more or less "critical" to the structure than the amplified "code" forces denoted by C_a. Note that so far no structural analysis was necessary.

In order to resolve this issue, we determine all combinations of base shear and base torque which, when considered as static forces, produce the same member force as the amplified code forces denoted by C_a. These code-equivalent combinations shown, for example, in Fig. 6 for Building A are determined by static analysis of the building as follows:

1. The maximum value of base shear $V = (V_{Y1})_o$ determined from floor accelerations may be defined as the amplified "code" base shear.

2. Analyze the structure using a static code-type analysis considering: (a) base shear as given in Step 1; (b) heightwise distribution of lateral floor forces according to the code; and (c) accidental eccentricity, equal to $0.05b$ in the Uniform Building Code, in the most unfavorable direction for each element. The resulting base shear V and base torque T are shown as point C in Fig. 8(e). A member force computed by this analysis is defined as a member "design" force. The analysis required in Step 2 is shown conceptually in Fig. 8(a), where F_i $(i = 1,2,3)$ are the lateral floor forces in the Y-direction, defined by Steps 2a and 2b. The resulting "design" shear V_{c1}^D in column 1 is obtained by applying the story lateral forces at a distance equal to $0.05b$ to the right of the CM. Analogously, the "design" shear V_{c2}^D in column 2 is obtained by applying the same floor forces at a distance of $0.05b$ to the left of the CM.

3. Determine the value of base shear and the associated lateral floor forces distributed over the building height according to the code which, applied at the CM (without any floor torques or eccentricity), produce the same member "design" force as determined in Step 2. This base shear is identified by points A_c and A'_c in Fig. 8(e). The analysis required in Step 3 is shown conceptually in Fig. 8(b). The building subjected to the lateral floor forces F_1, F_2, and F_3 of Steps 2a and 2b applied at the CM of the floors is analyzed to determine V_{c1}^S and V_{c2}^S, the shear forces in columns 1 and 2, respectively. The lateral forces F_i and base shear V multiplied by the ratio $V_{ci}^D / V_{ci}^S (i = 1,2)$ acting alone (without any floor torques or eccentricity) would produce in column "i" the shear force V_{ci}^D, which is equal to the member "design" force determined in Step 2. In the case of column 1 this base shear, $V_{c1}^o = (V_{c1}^D / V_{c1}^S) V$, defines the points A_{c1} and A'_{c1} in Fig. 8(e). Similarly, $V_{c2}^o = (V_{c2}^D / V_{c2}^S) V$ defines the points A_{c2} and A'_{c2} in Fig. 8(e).

4. Determine the value of base torque and the associated floor torques distributed over the building height in the same proportion as the lateral floor forces which alone (without any lateral forces) produce the same "design" force in a selected member as determined in Step 2. This torque is identified by points B_c and B'_c in Fig. 8(e). The analysis required in Step 4 is shown conceptually in Fig. 8(c). The building subjected to story torques T_i, where $T_i = 0.05b F_i$ and F_i are known from Steps 2a and 2b, is analyzed to determine V_{c1}^T and V_{c2}^T, the shear forces in columns 1 and 2, respectively. The floor torques T_i and base torque T multiplied by the ratio $V_{ci}^D / V_{ci}^T (i = 1,2)$ acting alone (without any lateral forces) would produce the "design" shear force V_{ci}^D in column "i." In the case of column 1 this base torque $T_{c1}^o = (V_{c1}^D / V_{c1}^T) T$ defines the points B_{c1} and B'_{c1} in Fig. 8(e). Similarly, $T_{c2}^o = (V_{c2}^D / V_{c2}^T) T$ defines the points B_{c2} and B'_{c2} in Fig. 8(e).

5. Each point on lines $A_{c1}B_{c1}$ and $A'_{c1}B'_{c1}$ denotes a combination of base shear and base torque, each being distributed over the building height according to the code (Steps 3 and 4) which produces the same member "design" force as determined in Step 2; hence, lines $A_{c1}B_{c1}$ and $A'_{c1}B'_{c1}$ are called "code-equivalent combinations" associated with column 1. Similarly, $A_{c2}B_{c2}$ and $A'_{c2}B'_{c2}$ are the "code-equivalent combinations" associated with column 2.

If at each time instant the "actual" base shear and base torque combination falls within the region enclosed by the code-equivalent limits, this implies that, during the earthquake, the force in the selected member did not exceed the "design" value determined in Step 2. Alternatively, such a situation indicates that the accidental eccentricity of $0.05b$ is conservative during the particular earthquake. Any point in the base shear-torque plot which falls outside the region enclosed by code-equivalent combination represents, at a particular time instant, a combination of base shear and base torque that produces in the selected member a force that is larger than its "design" value. Alternatively, this situation indicates that the accidental eccentricity of $0.05b$ is unconservative at that instant of time.

The above-described procedure was utilized to determine the code-equivalent combinations of base shear and base torque for Building A, and the results are presented in Fig. 6. Analysis for Y-lateral forces with the shear forces in columns 8 and 18 selected as the member "design" forces led to the code-equivalent combinations of Fig. 6(b). Similarly, analysis for X-lateral forces with the shear forces in columns 4 and 22 selected as the member "design" forces led to the code-equivalent combinations of Fig. 6(a). These results demonstrate that all points denoting "actual" values of base shear and base torque during the earthquake fall inside the region enclosed by the code-equivalent combinations with one exception: point A in Fig. 6(a), which indicates that only at that instant of time during the earthquake, the shear force in column 22 exceeds the "design" force. This observation is consistently confirmed by examining the code-equivalent limits for the "design" shear forces and bending moments in several other beams and columns. For

the recorded response of Building A during the Loma Prieta earthquake, the torsional effects are so small that it may not be necessary to consider accidental eccentricity at all. Figure 6 indicates that very few points fall outside the region enclosed by the code-equivalent combinations with zero accidental eccentricity.

Figure 9 shows the dynamic base shear-torque values, and code-equivalent combinations determined from the motions of Building B recorded during the Whittier earthquake. Similar results for the Upland earthquake are presented in Fig. 10. Analysis for X-lateral forces with the shear forces in columns 2 and 29 selected as the member "design" forces led to the code-equivalent combinations of Figs. 9(a) and 10(a). Similar analysis for Y-lateral forces with the shear forces in columns 8 and 25 selected as the member "design" forces led to the code-equivalent combinations of Figs. 9(b) and 10(b). Only at two time instants during the Whittier earthquake does the "actual" shear force in column 29 exceed the "design" force. During the Upland earthquake, the "actual" forces in all columns remain below their respective design values. In fact, the design value with zero accidental eccentricity is exceeded only once, suggesting that it is not even necessary to consider any accidental eccentricity for the recorded response of Building B during the Upland earthquake.

The actual values of the Y component of the base shear and base torque for Building C during the Loma Prieta earthquake are presented in Fig. 7(b). This plot shows a trend towards the second and fourth quadrants which implies that the dynamic forces in structural elements located on the left side of the CM of the structure (Fig. 3), e.g. column 1, and more likely to exceed their "design" values. This speculation is confirmed in Fig. 7 which shows that at a few time instants the actual shear force in the first story exceeds the design value.

MEMBER FORCES

An alternative procedure to the one presented in the preceding section for evaluating the code-accidental torsion provisions is to compare the member "design" forces defined in Step 2 of the preceding section with the time history of the "actual" member forces during the earthquake. At each time instant the "actual" member forces during the earthquake are determined by static analysis of the building subjected to the floor inertia forces $m_j a_{xj}(t)$, $m_j a_{yj}(t)$, and $I_{pj} a_{\theta j}(t)$ at all floors, i.e. $j = 1, 2, \ldots, N$ (Fig. 8(d)). If at all time instants the "actual" member force is less than its "design" value, the accidental eccentricity of $0.05b$ can be interpreted to be conservative during the particular earthquake. Conversely, the accidental eccentricity of $0.05b$ is unconservative at those time instants when the "actual" member force exceeds the "design" value. The two procedures are equivalent for a symmetric one-story system but differ slightly for multistory buildings because the actual heightwise distribution of lateral forces computed from recorded accelerations and floor masses is not identical to the heightwise distribution of lateral forces specified by the code.

The time variation of the "actual" shear force in the first-story columns 22 and 18 of Building A during the Loma Prieta earthquake is presented in Fig. 11, together with the "design" values of these forces obtained by static analysis of the building for amplified code forces in the X-direction (for column 22) and in the Y-direction (for column 18). The "actual" values of these member forces do not exceed their "design" values based on the specified accidental eccentricity and barely exceed the design values ignoring this eccentricity. The results for shear force and bending moment in all columns support this conclusion.

The time variation of the "actual" shear force in the first-story columns 8 and 26 of Building B during the Whittier earthquake is presented in Fig. 13, together with the "design" values of these forces obtained by static analysis for amplified "code" forces in the X-direction (for column 26) and in the Y-direction (for column 8). Similar results obtained from the Upland earthquake records are presented in Fig. 14. For both earthquakes the "actual" values for these member forces do not exceed their "design" values based on the code-specified accidental eccentricity and barely exceed the design values ignoring this eccentricity. The results for shear force and bending moment in all columns in the building support this conclusion.

The time variation of the "actual" shear force in the first-story columns 1 and 8 of Building C during the Loma Prieta earthquake is presented in Fig. 12, together with the "design" values of these forces obtained by static analysis of the building for amplified code forces in the X-direction (for column 8) and in the Y-direction (for column 1). The "actual" value of the X-component of the shear force in the first-story column 8 does not exceed its "design" value based on the code-specified accidental eccentricity and barely exceeds the design value ignoring this eccentricity. The results for shear forces and bending moments in all columns associated with motion of the building in the X-direction support this conclusion. The "actual" value of the Y-component of the shear force in the first-story column 1 exceeds its "design" value for a small fraction of a second three times during the earthquake. The maximum value of the "actual" shear during the earthquake is 10% greater than its "design" value. These observations are representative of other columns at the left edge of the plan. The "actual" forces in columns located to the right of the CM remain below their "design" values throughout the earthquake.

Accidental torsion is seen to be more significant in the response of Building C than the other two buildings. This may be the result of several-factors: the natural vibration periods of the first three--two lateral and one torsional--vibration modes are very close to each other--a situation known from forced vibration tests to create strong coupling of lateral and torsional motions even in nominally-symmetric buildings; the torsional component of the ground motion is significant; and the restraint provided by the adjacent building may have contributed to accidental torsion.

For the three buildings and their motions during past earthquakes considered in this investigation, the actual member forces exceed their design values based on the UBC-specified accidental torsion by at most 10% for a small fraction of a second three times during an earthquake. These discrepancies between the design force and the actual force are small when considered in the context of the many larger approximations inherent in building code provisions, uncertainties in building idealization and material properties, etc. Thus, the accidental torsion provisions in building codes are satisfactory in representing the torsional motions of these three buildings during the particular earthquakes.

The design values of member forces determined by ignoring the accidental torsion are, of course, exceeded more often and by a larger amount. During the earthquakes considered, a member design force is exceeded once for a small fraction of a second by less than 3% in Building A, once for a small fraction of a second by less than 10% in Building B, and five times, each for a small fraction of a second, by less than 38% in Building C. Such increased force demand should not be a problem for most well designed buildings with nominally-symmetric floor plan for two reasons. Firstly, the overstrength relative to design values that is typical of most buildings would, for moderate ground motion, be sufficient for the building to withstand the increased force demand essentially within the elastic range. Secondly, even if the force demands exceeded structural capacity because of accidental torsion, the damaging effects of the very few and small inelastic excursions of very short duration would be very small.

During strong ground motions, most buildings would be expected to deform beyond the elastic range and accidental torsion may increase the ductility demand for some structural frames or elements of a building designed without considering accidental eccentricity. However, the results from analyzing the recorded motions of these three buildings considered suggest that the additional ductility demand should be small. Thus, if these three buildings were designed ignoring accidental eccentricity, but detailed for sufficient ductility for the design earthquake, their performance should not be adversely affected by accidental torsion.

Thus, it seems that accidental torsion need not be considered in the design of these three buildings for the recorded ground motions or amplified versions of these ground motions. Although extrapolating these observations to other situations is somewhat speculative, it is difficult to visualize that the design of nominally-symmetric buildings would be influenced significantly by accidental torsion, or that torsional response could be a significant contributor to the damage such a building may experience during an earthquake. Exceptions may occur if the natural vibration periods of the fundamental lateral and torsional modes of the building are very close to each other, or the torsional vibration period is much longer than the lateral period, or if the ground motion contained an unusually strong torsional component of ground motion.

ACKNOWLEDGEMENT

The authors are grateful for the financial support provided by the Strong Motion Instrumentation Program, California Department of Conservation, that made this investigation possible.

Table 1: Natural Vibration Periods and Modes Shapes for Buildings A, B and C

Vibration Properties	X-lateral mode		Y-lateral mode		Torsional mode	
	Recorded	Computed	Recorded	Computed	Recorded	Computed
	Building A: Loma Prieta Earthquake					
Period (sec)	0.63	0.60	0.74	0.76	0.46	0.45
Mode Shape						
Roof	1.00	1.00	1.00	1.00	1.00	1.00
3^{rd} Floor	0.71	0.77	0.72	0.73	0.72	0.76
2^{nd} Floor	0.39	0.57	0.39	0.38	0.40	0.43
	Building B: Whittier Earthquake					
Period (sec)	0.29	0.28	0.27	0.27	0.20	0.20
Mode Shape						
Roof	1.00	1.00	1.00	1.00	1.00	1.00
2^{nd} Floor	0.62	0.61	0.39 ?	0.60	0.57	0.64
	Building B: Upland Earthquake					
Period (sec)	0.30	0.28	0.28	0.27	0.21	0.20
Mode Shape						
Roof	1.00	1.00	1.00	1.00	1.00	1.00
2^{nd} Floor	0.64	0.61	0.55	0.60	0.52	0.64
	Building C: Loma Prieta Earthquake					
Period (sec)	0.67	0.70	0.69	0.69	0.69 - 0.65	0.67
Mode Shape						
Roof	1.00	1.00	1.00	1.00	1.00	1.00
3^{rd} Floor	0.80	0.70	0.70	0.67	0.67	0.66
2^{nd} Floor	0.44	0.33	0.33	0.30	0.31	0.30

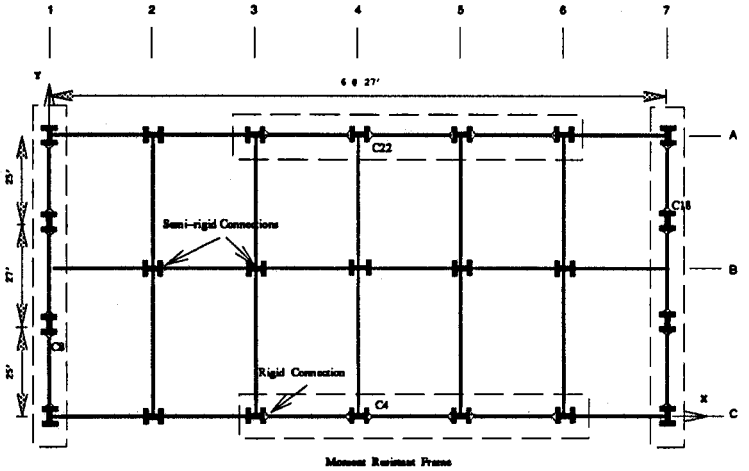

Figure 1 : Framing Plan of Building A

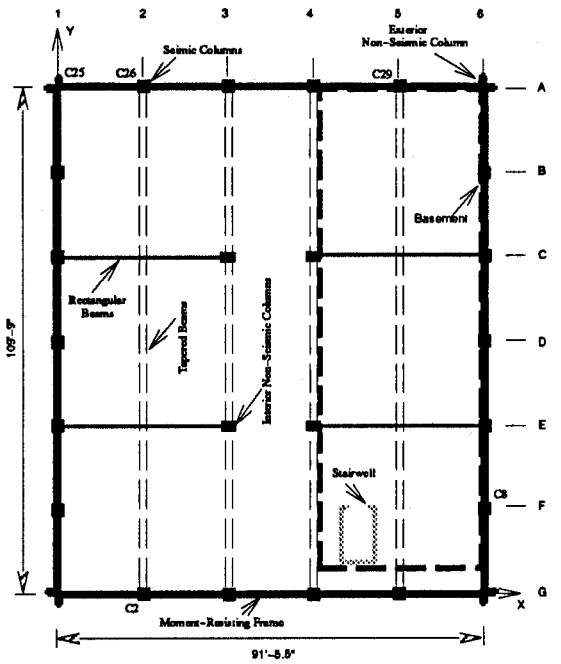

Figure 2 : Framing Plan of Building B

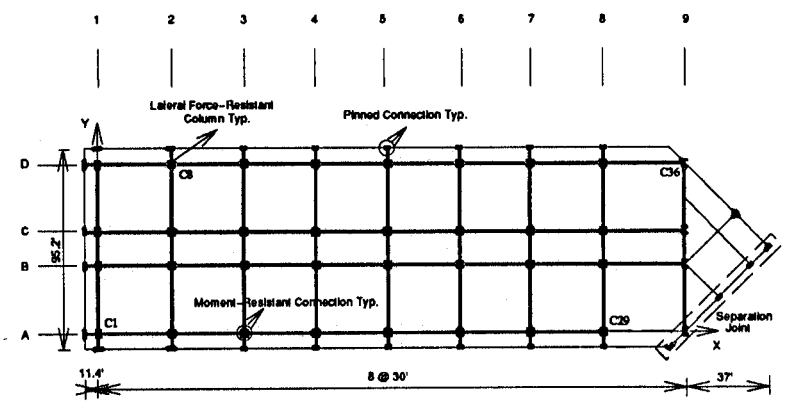

Figure 3 : Framing Plan of Building C

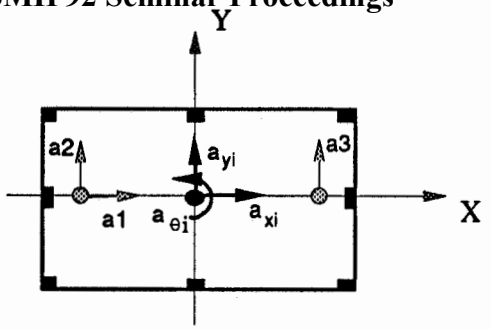

(a) Recorded Accelerations at ith Floor and Accelerations at the CM

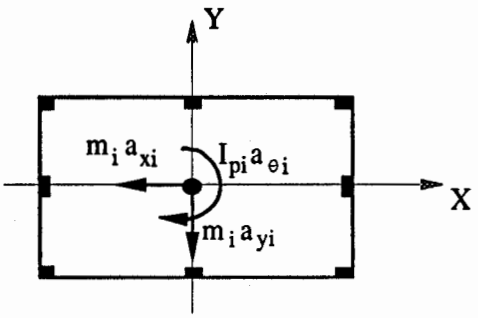

(b) Inertia Forces at ith Floor

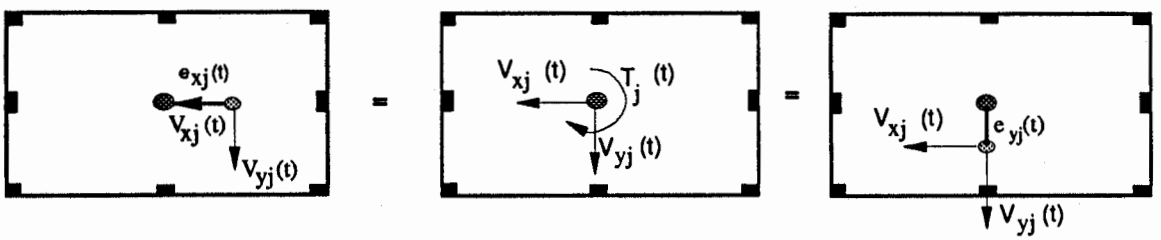

(c) Accidental Eccentricities for the jth Story

Figure 4 : Dynamic Accidental Eccentricity

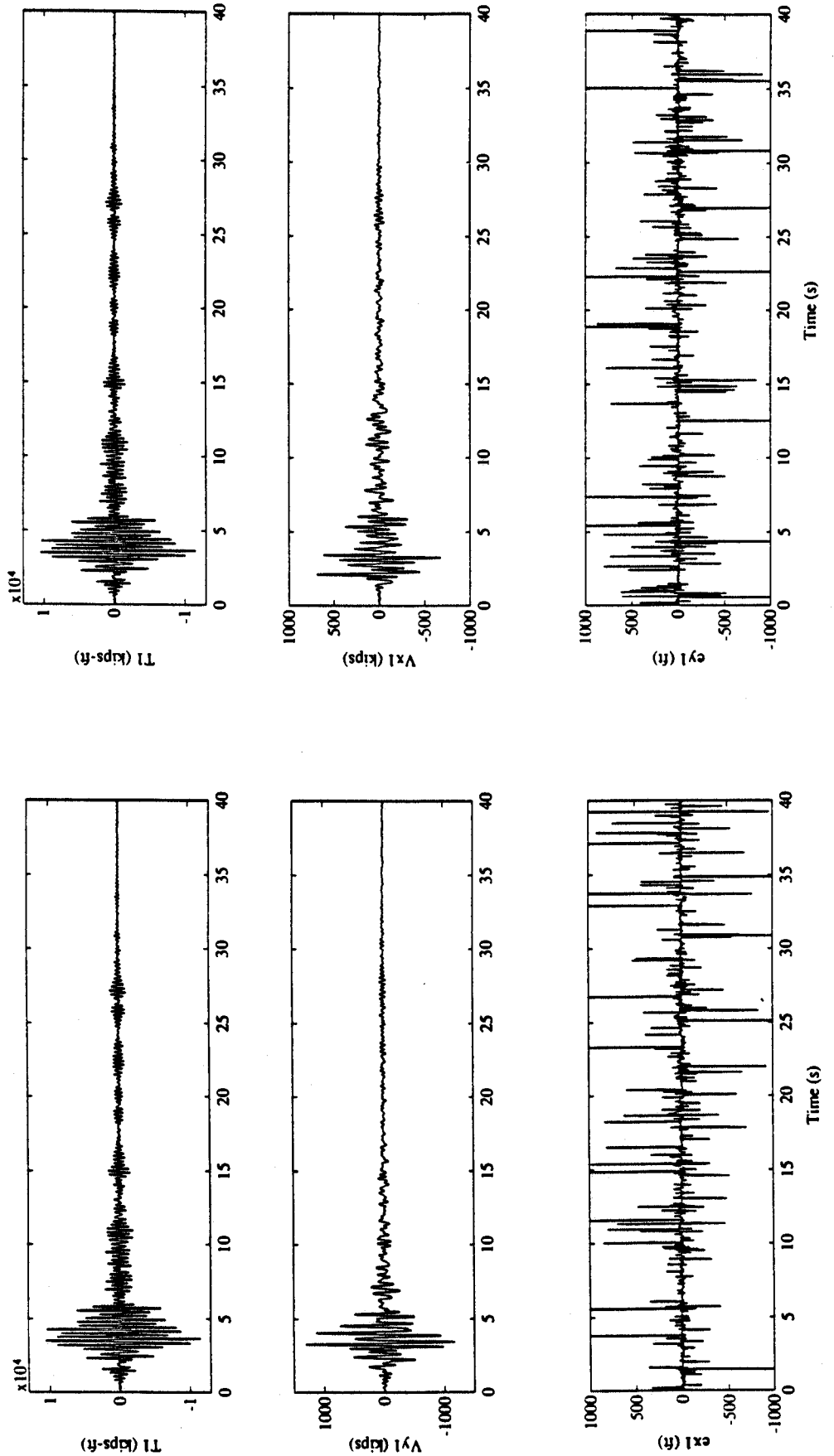

Figure 5: Base Shear, Base Torque and First Floor Accidental Eccentricities Computed from Recorded Accelerations in Building B During the Upland Earthquake

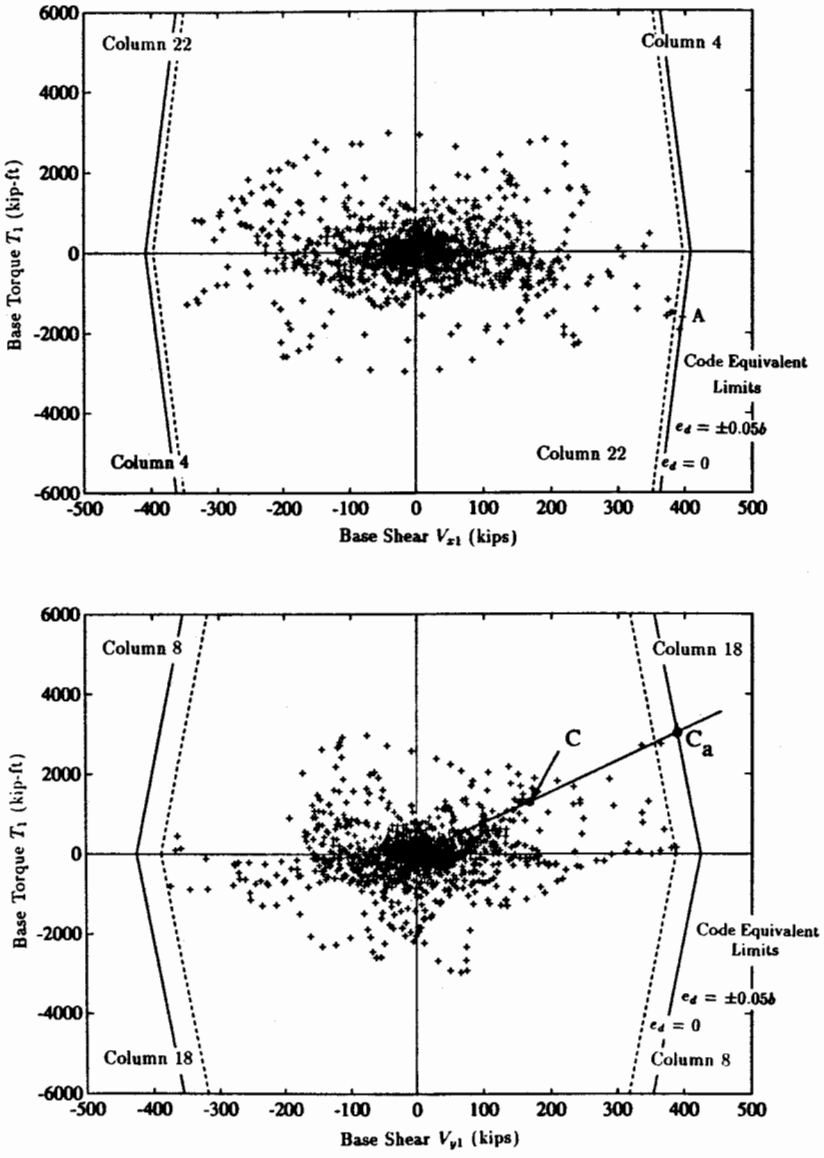

Figure 6: Comparison of Dynamic Base Shear, Base Torque and "Code Equivalent Combinations" in Building A During the Loma Prieta Earthquake

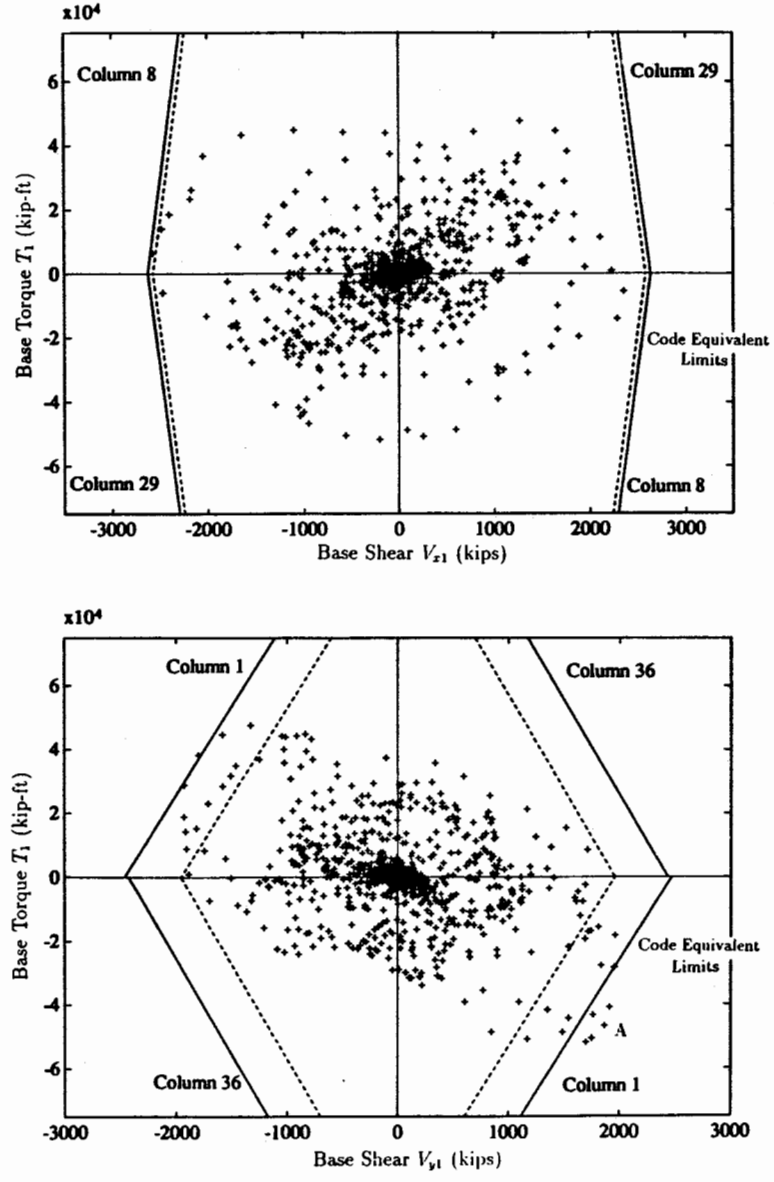

Figure 7: Comparison of Dynamic Base Shear, Base Torque and "Code Equivalent Combinations" in Building C During the Loma Prieta Earthquake

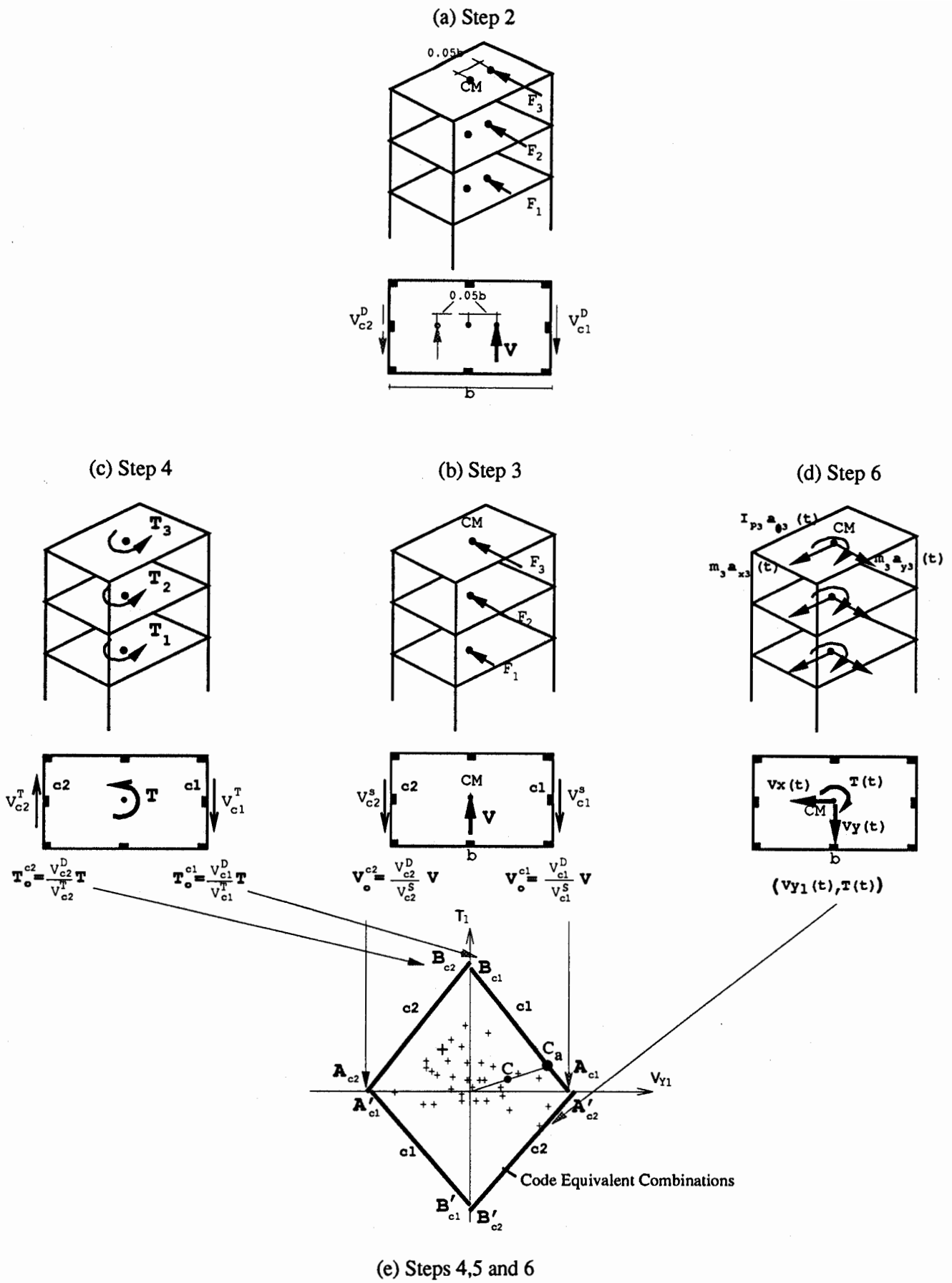

Figure 8: Computation of Design Member Forces, Base Shear, Base Torque, and Code Equivalent Limits

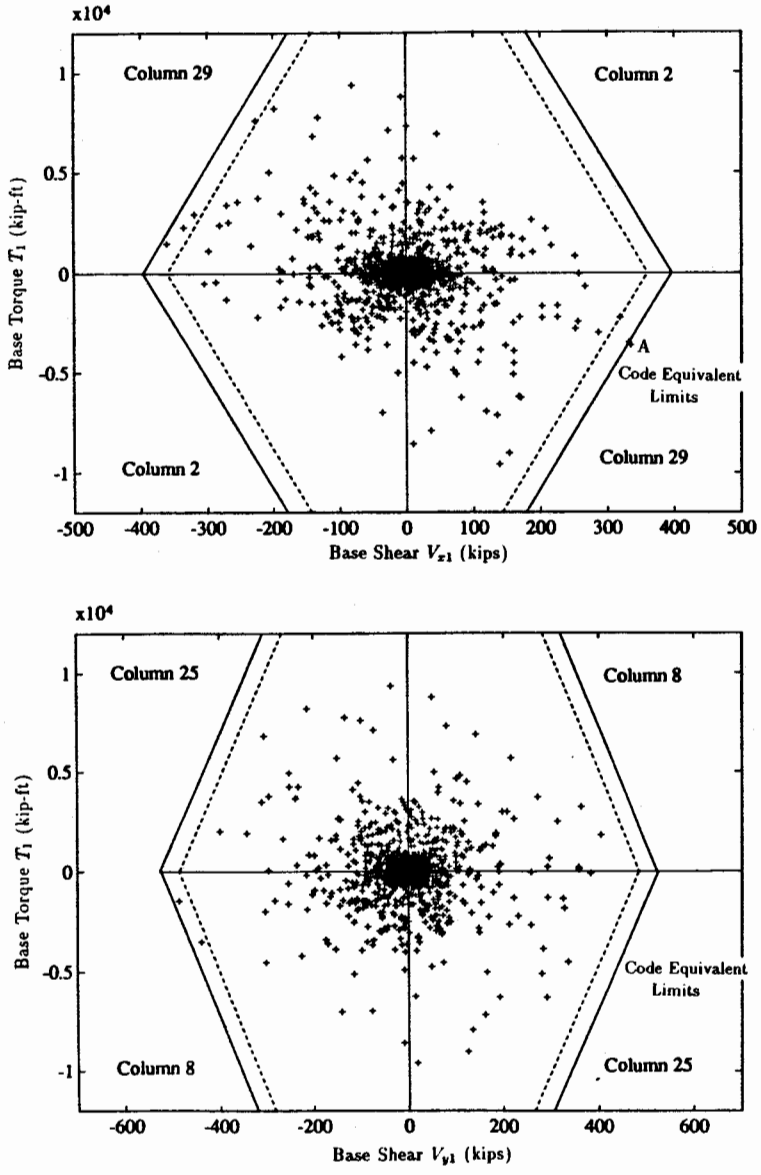

Figure 9: Comparison of Dynamic Base Shear, Base Torque and "Code Equivalent Combinations" in Building B During the Whittier Earthquake

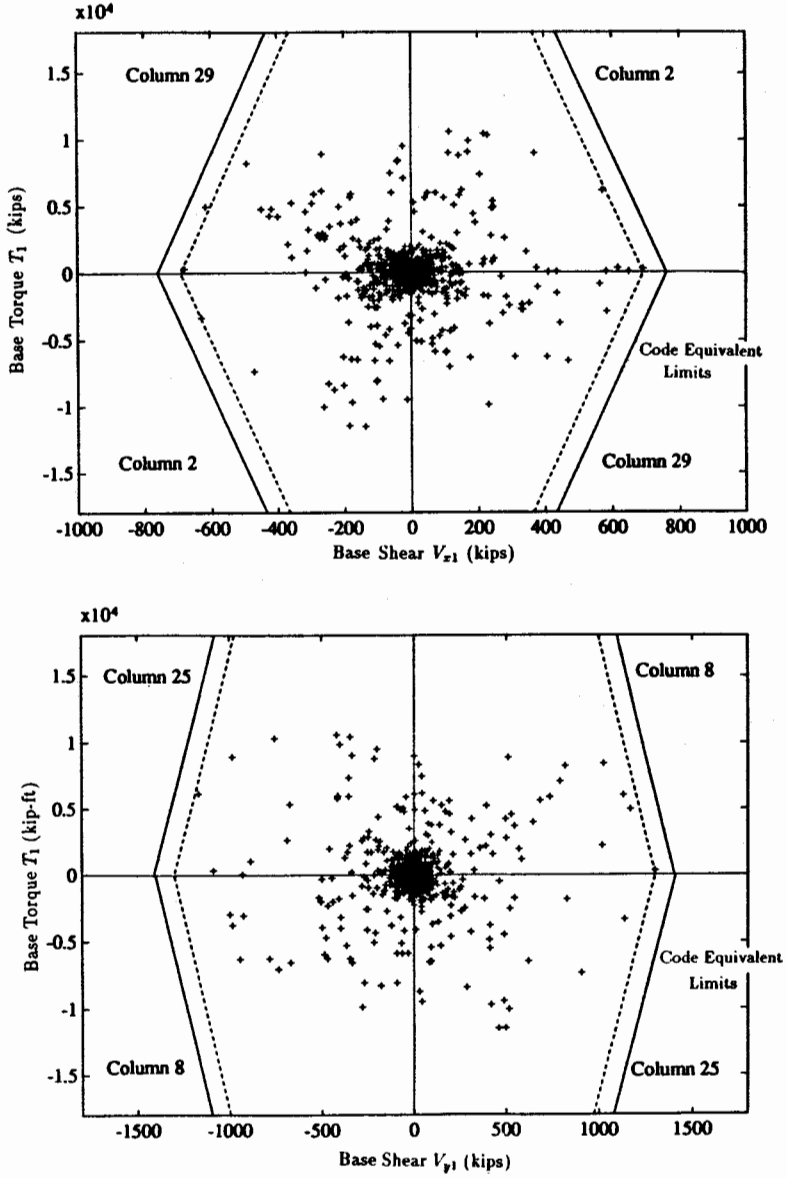

Figure 10: Comparison of Dynamic Base Shear, Base Torque and "Code Equivalent Combinations" in Building B During the Upland Earthquake

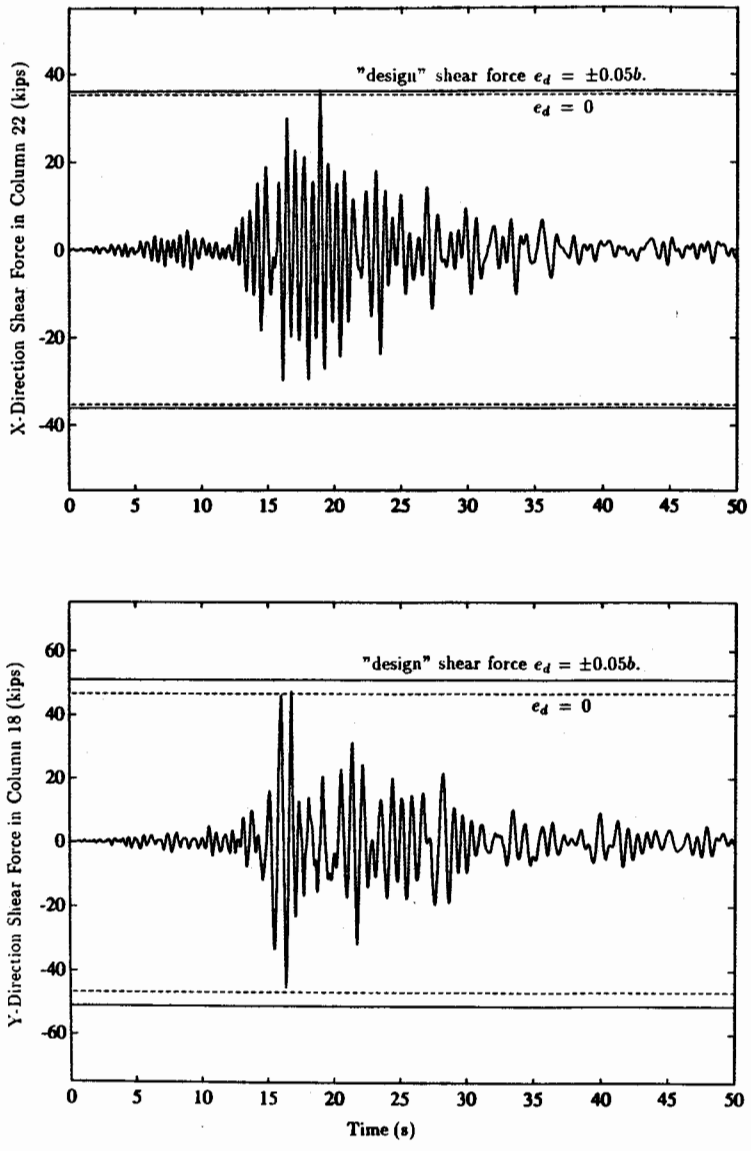

Figure 11: Comparison of Earthquake Induced Shears in Columns 22 and 18 with "Design" Shear Values, Building A (Loma Prieta Earthquake)

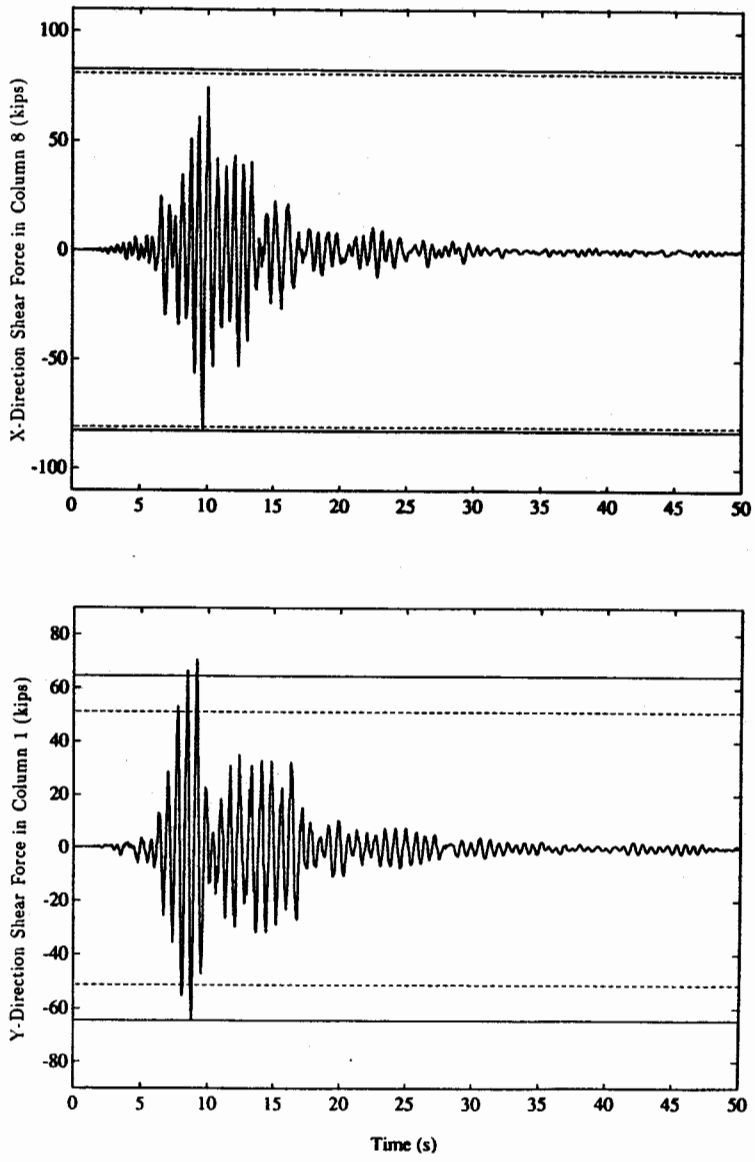

Figure 12: Comparison of Earthquake Induced Shears in Columns 8 and 1 with "Design" Shear Values, Building C (Loma Prieta Earthquake)

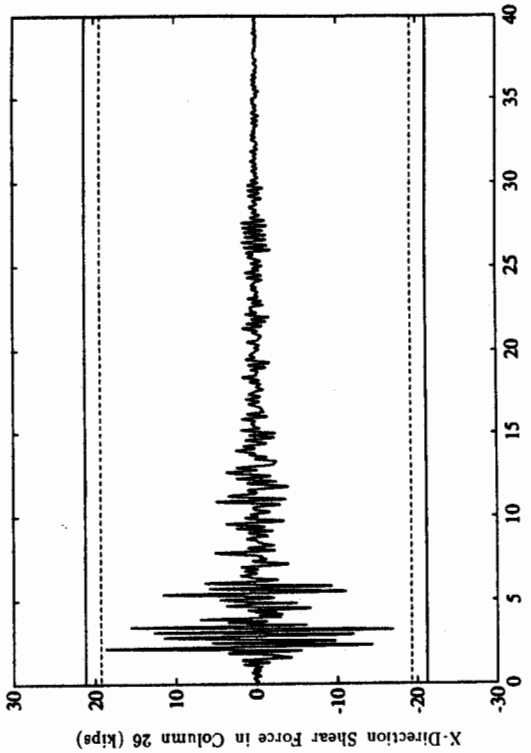

Figure 14: Comparison of Earthquake Induced Shears in Columns 26 and 8 with "Design" Shear Values, Building B (Upland Earthquake)

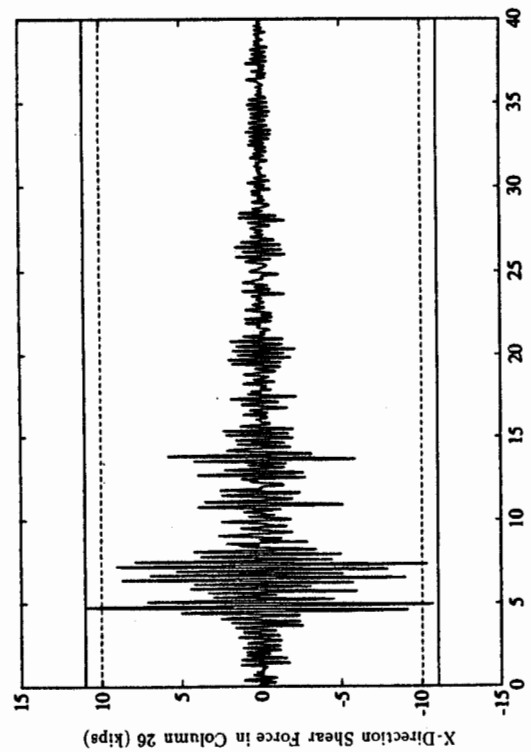

Figure 13: Comparison of Earthquake Induced Shears in Columns 26 and 8 with "Design" Shear Values, Building B (Whittier Earthquake)

Evaluation of Displacement Amplification Factor for Seismic Design Codes

Chia-Ming Uang
Assistant Professor, Northeastern University
Ahmed Maarouf
Graduate student, Northeastern University

ABSTRACT

To estimate the roof and story drifts occurring during severe earthquakes, the Uniform Building Code (UBC) uses $3R_w/8$ as a displacement amplification factor (*DAF*) to amplify elastic design drifts. A comparison of several seismic design codes shows that UBC's *DAF* is very low. A study conducted on four instrumented buildings indicates that the maximum story drifts developed in severe earthquakes are much higher than that predicted by the UBC. This study also shows that the *DAF* of multi-degree-of-freedom systems is similar to that of single-degree-of-freedom systems.

INTRODUCTION

Modern seismic design provisions assume that buildings will undergo inelastic deformations during severe earthquakes. Therefore, these provisions allow the designer to reduce the elastic seismic force demand by a force reduction factor (*FRF*). Since reduced seismic forces are used in design, the computed displacements from an elastic analysis have to be amplified in order to estimate the actual deformations that develop in severe earthquakes. Building codes usually use a displacement amplification factor (*DAF*) for this purpose.

Consider the typical lateral force versus deformation relationship of a structural system in Fig. 1. The elastic force demand, expressed in terms of a base shear ratio, for a severe earthquake is expressed as C_e. Idealizing the actual structural response curve by the linearly elastic-perfectly plastic curve in Fig. 1, the structural ductility factor can be defined as

$$\mu_s = \frac{\Delta_{max}}{\Delta_y} \tag{1}$$

where the deformation is expressed in terms of story drift Δ. The ratio between the elastic force demand (C_e) and the structure's yield strength level (C_y) is defined as the ductility reduction factor, R_μ:

$$R_\mu = \frac{C_e}{C_y} \tag{2}$$

Based on these definitions, the force reduction factor (*FRF*) for working stress design can be derived from Fig. 1 as follows (8):

$$FRF = \frac{C_e}{C_w} = R_\mu \frac{C_y}{C_w} \tag{3}$$

The displacement amplification factor (*DAF*) can also be derived from Fig. 1 as follows:

$$DAF = \frac{\Delta_{max}}{\Delta_w} = \frac{\Delta_{max}}{\Delta_y} \frac{\Delta_y}{\Delta_w} = \mu_s \frac{\Delta_y}{\Delta_w} \tag{4}$$

Since Δ_y/Δ_w is equal to C_y/C_w (see Fig. 1), it follows that

$$DAF = \mu_s \frac{C_y}{C_w} \tag{5}$$

From Eqs. 3 and 5, the ratio between *DAF* and *FRF* is

$$\frac{DAF}{FRF} = \frac{\mu_s}{R_\mu} \tag{6}$$

For a single-degree-of-freedom system, the ratio between μ_s and R_μ can be expressed as follows (4):

(a) in the velocity and displacement amplification regions:

$$\frac{\mu_s}{R_\mu} = \frac{\mu_s}{\mu_s} = 1 \tag{7a}$$

(b) in the acceleration amplification region:

$$\frac{\mu_s}{R_\mu} = \frac{\mu_s}{\sqrt{2\mu_s - 1}} \geq 1 \tag{7b}$$

If a multistory building tends to deform as a single-degree-of-freedom system, which appears to be a valid assumption if the structure deforms into a global mechanism in severe earthquakes, it follows from Eqs. 6 and 7 that the *DAF* should not be less than *FRF*.

A review of the 1991 Uniform Building Code (10) of the U.S.A., the 1990 National Building Code (3) of Canada, the 1987 Mexico Code (5), and the 1988 Eurocode (7) indicates that the ratios between the *DAF* and *FRF* vary considerably from one code to another. Table 1 lists the ratio between the *DAF* and *FRF* used in these codes. On one extreme, both the Mexico Code and Eurocode use a *DAF* which is no smaller than the *FRF*. At the other extreme, UBC uses a *DAF* which is only 3/8 that of the *FRF*.

OBJECTIVE AND SCOPE

The main objective of this research is to evaluate the appropriate *DAF* for seismic design of multi-story building frames. Dynamic analyses of four instrumented buildings in California (two steel and two reinforced concrete buildings) with fundamental periods ranging from 0.31 to 2.2 seconds were performed in order to investigate the relationship between the *DAF* and *FRF*.

METHOD OF ANALYSIS

The four buildings selected for this study have been instrumented by CDMG (6); they are designated as CSMIP 57357, 58496, 57355, and 58490. See Table 2 for a brief description of these buildings. For each building, the dynamic response was computed by the computer program DRAIN-2D (1). As input motions, eight historical earthquake records (see Table 3) were used. The average normalized response spectra of this set of earthquakes resembled the UBC elastic design spectra (see Fig. 2). By scaling the intensity of each earthquake record to different intensities, the roof drift and story drifts from the inelastic dynamic analyses were compared to those that would develop if the structure were to respond elastically. Referring to Fig. 1, the ratio between the inelastic drift (Δ_{max}) and elastic drift (Δ_e) is the same as the ratio between *DAF* and *FRF* because:

$$\frac{\Delta_{max}}{\Delta_e} = \frac{DAF\ (\Delta_w)}{FRF\ (\Delta_w)} = \frac{DAF}{FRF} \tag{8}$$

Both the ratios obtained from roof drift and story drifts were evaluated. The results obtained from the ratio of story drifts can be used to determine a suitable *DAF* for estimating the critical story drift, while the ratio of roof drifts can be used to determine an appropriate *DAF* for estimating the required building separations in order to avoid pounding. For each scaled earthquake record, the scale factor is defined as the ratio between the average pseudo-acceleration (*PSA*), expressed in terms of the gravitational acceleration, at the fundamental period of the structure and the UBC prescribed design base shear ratio, C_w. For the buildings and earthquake records selected in this study, the results of elastic dynamic analyses indicate that the base shear ratio, C_e, approximately equals the average *PSA*. Therefore, the earthquake scale factor can also be expressed as the ratio between C_e and C_w.

SUMMARY OF RESULTS

CSMIP Building No. 57357 — The lateral-force-resisting system of this building is a steel moment-resisting space frame (R_w = 12); the fundamental period is 2.18 seconds. A review based on the 1991 UBC indicates that story drift limit controlled the design (9). A 2-D interior frame in the E-W direction was modeled for dynamic analysis (see Fig. 3a). Elastic analysis of a 3-D mathematical model of the building using the ETABS program (2) indicated that the reactive mass associated with the selected frame is about 11% of the total building mass.

To calibrate the properties of the 2-D model, nonlinear dynamic analyses were performed using the 1989 Loma Prieta earthquake acceleration record as the input ground motion at the building base. In the analysis, the damping ratios were assumed to be 5% of critical damping for the first two modes. Fig. 4a shows that the displacements computed from the model correlate very well with the measured responses from the Loma Prieta earthquake. A nonlinear static analysis was also conducted to determine the lateral strength of the building; the UBC lateral load profile was used. The analysis indicated that the lateral load

capacity of the building significantly exceeds the UBC design seismic forces (see Fig. 5a). The figure also shows that the failure mechanism is initiated at the base and continues to the seventh floor.

By scaling the earthquake record to different intensity levels, nonlinear dynamic analyses were performed for eight earthquake records to calculate the ratios between Δ_{max} and Δ_e (i.e., *DAF/FRF*). Fig. 6a shows that the displacement ratio at the roof level is slightly less than one; the ratio is about 0.8 at the UBC severe design earthquake level (i.e., $C_e/C_w = 12$.) Fig. 7a shows that the ratio of story drifts tends to be larger than one if the earthquake intensity is increased; the ratio is about 1.1 at the UBC design earthquake level. Therefore for this type of long period structures the UBC approach of using 3/8 of the *FRF* as *DAF* may significantly underestimate the roof and story drifts.

CSMIP Building No. 58496 — The lateral-force-resisting system of this hospital building (see Table 2) in the E-W direction consists of two eccentrically braced and one moment-resisting steel frames (see Fig. 3b); the fundamental period is 0.31 seconds. A low frequency noise was observed in the relative displacement records of this building. This noise was filtered for the dynamic correlation study. Fig. 4b shows that the displacements computed from a 2D mathematical model correlate reasonably well with the measured responses from the Loma Prieta earthquake. Fig. 5b shows that the lateral load capacity of the building is 5.8 times greater than the UBC prescribed design base shear. Fig. 6b shows that the ratio of roof displacements remains smaller than 1.0 as the earthquake intensity is increased; the ratio equal 0.8 at the level of the UBC severe design earthquake (i.e., $C_e/C_w = R_w = 12$.) For a structure of such a short period, Fig. 6b indicates that the ratio may be greater than 1.0 if the intensity is further increased; this is consistent with the observations for single-degree-of-freedom systems (4). Fig. 7b shows the variations of the ratio for story drifts; the trend is similar to that observed in the previous long-period structure. Since the ratio from Fig. 7b is about 1.0 at the UBC severe design earthquake level, it appears that for such a short period structure the *DAF* should also be equal to *FRF*.

CSMIP Building No. 57355 — The lateral-force-resisting system of this building (see Table 2) in the N-S direction consists of four reinforced concrete ductile moment-resisting frames; the fundamental period is 0.96 seconds. An interior frame was selected for the dynamic analysis (see Fig. 3c). Elastic analysis of a 3-D mathematical model of the building indicated that the reactive mass associated with this frame is about 19% of the total building mass. Fig. 4c shows that displacements computed from the 2D mathematical model correlate reasonably well with measured responses from the Loma Prieta earthquake; the dynamic analysis indicated that some minor yielding might have occurred in a number of beams. Fig. 5c shows that the ultimate base shear of the building is about four times the UBC prescribed design base shear. The figure also shows that the building has a partial failure mechanism (from the base to the seventh floor). Since this is a reinforced concrete frame, the Takeda model was used to simulate the stiffness degradation of the members. Fig. 6c shows that the effect of stiffness degradation on the ratio of roof drifts is small; the ratio is about 0.8. Fig. 7c shows that the ratio of story drifts increases with the ground

motion intensity. At the UBC severe design earthquake level, the ratio is about 1.2, much higher than the 3/8 recommended by the UBC.

CSMIP Building No. 58490 — The lateral-force-resisting system of this building (see Table 2) in the N-S direction consists of two perimeter moment-resisting frames; the fundamental period is about 0.84 seconds. The design of this building satisfies the UBC strength and stiffness requirements; the lateral strength controlled the design. Fig. 4d shows that displacements computed from the 2D mathematical model correlate well with the measured responses from the Loma Prieta earthquake; dynamic analysis indicated that some yielding might have occurred in a number of beams. Fig. 5d shows the overstrength of this building is relatively low, which is expected for perimeter frame systems. The ultimate base shear of the building is about 2.6 times the UBC prescribed design base shear. Since the column and beam strengths are constant along the height of building, the failure mechanism consists of a soft first story (see Fig. 5d). During severe earthquake excitation, it is expected that most of the damage will concentrate in the first story. Fig. 6d shows that the ratio of roof drifts is about 0.9 at an earthquake intensity similar to that of the UBC severe design earthquake. For the critical story drift, Fig. 7d shows that the ratios are 1.7 and 1.3 for models with and without stiffness degradation, respectively. These ratios are much greater than 3/8, as recommended by the UBC.

CONCLUSIONS AND RECOMMENDATIONS

Based on the observed dynamic responses of four regular planar frames subjected to eight historic earthquake records, the following conclusions and recommendations can be drawn.

(1) For steel frames, the ratio of *DAF/FRF* for estimating the critical story drift ranges from 1.0 to 1.3. For reinforced concrete frames with stiffness degradation, the ratio can be as high as 1.7. To estimate roof drift, the ratio of *DAF/FRF* ranges from 0.8 to 0.9.

(2) The ratio of *DAF/FRF* is insensitive to the fundamental period of the building. One flexible steel frame (T = 2.2 sec.) and one stiff eccentrically braced frame (T = 0.3 sec.) gave practically the same *DAF/FRF* ratio.

(3) The ratio of *DAF/FRF* for estimating the story drift is affected by the type of failure mechanism under severe ground shaking. For the two reinforced concrete frames studied, the 6-story perimeter frame having a soft first story exhibits a higher *DAF/FRF* ratio.

(4) Stiffness degradation has insignificant effect on roof displacement response. For frames with a soft story, the stiffness degradation effect is more pronounced on story drifts.

(5) This study shows a similarity of the *DAF/FRF* ratio for single- and multi-degree-of-freedom systems. The UBC recommended ratio of 3/8 is too low. For simplicity, it is recommended that a *DAF* equal to *FRF*, which is the approach used by the Eurocode and Mexico Code, be used for estimating both the story drift and roof drift.

ACKNOWLEDGMENTS

This research is supported by a grant from the Strong Motion Instrumentation Program of the California Department of Conservation (Contract No. 1090-526). Much appreciation is given to the staff of the SMIP, especially Drs. M. J. Huang and A. F. Shakal, for providing processed data and design drawings.

REFERENCES

1. Kannan, A. E. and Powell, G. H., "DRAIN-2D: A General Purpose Computer Program for Dynamic Analysis of Inelastic Plane Structures," *Report No. UCB/EERC-73/6*, Earthquake Engrg. Res. Ctr., Univ. of California, Berkeley, 1973.
2. Maison, B. F. and Neuss, C. F., "SUPER-ETABS: An Enhanced Version of the ETABS Program," Technical Report to the National Science Foundation, J. G. Bouwkamp, Inc., Berkeley, Calif., 1983.
3. *National Building Code of Canada (NBCC)*, Nat. Res. Council Canada, Ottawa, Ontario, 1990.
4. Newmark, N. M. and Hall, W. J., *Earthquake Spectra and Design*, Earthquake Engrg. Res. Inst., 1982.
5. "Seismic Design Regulations of the 1976 Mexico Building Code," *Earthquake Spectra*, vol. 4, no. 3, pp. 427-439, Earthquake Engrg. Res. Inst., (translated by Garcia-Ranz and R. Gofnez), 1988.
6. Shakal, A., et al., "CSMIP Strong-Motion Records of the Santa Cruz (Loma Prieta) California Earthquake of 17 October, 1989," *Reprt OSMS 89-06*, Calif. Strong Motion Instrumentation Program, Calif. Div. Mines Geology, Sacramento, Calif., 1989.
7. "Structures in Seismic Regions," *Eurocode No. 8*, Commission of the European Communities, Luxembourg, 1988.
8. Uang, C.-M., "Establishing R (or R_w) and C_d Factors for Building Seismic Provisions," *J. Struct. Engrg.*, vol. 117, no. 1, pp. 19-28, ASCE, 1991.
9. Uang, C.-M. and Maarouf, A., "An Investigation of UBC Seismic Serviceability Requirements from Building Responses Recorded during the 1989 Loma Prieta Earthquake," *Report No. CE-91-6*, Final Report submitted to Calif. Dept. of Mines and Geology, Dept. of Civil Engr., Northeastern Univ., Boston, Mass., 1991.
10. *Uniform Building Code (UBC)*, Int. Conf. of Bldg. Officials, Whittier, Calif., 1991.

Building Code	FRF	DAF	$\frac{DAF}{FRF}$
UBC (1991)	R_w	$\frac{3R_w}{8}$	0.375
NBCC (1990)	$\frac{R}{0.6}$	R	0.6
Mexico (1987)	Q^*	Q	1.0
Eurocode (1988)	q	q	1.0

* less than Q in short period range

Table 1 *DAF/FRF* Ratios in Four Building Codes

CSMIP Bldg. No.	Construction Material	Reactive Weight (kips)	C_w	R_w	Direction of Frame	Period (sec)		
						UBC	Measured	Model
57357	13-story steel	25,200	0.043	12	E-W	1.77	2.18	2.20
58496	2-story steel	4,550	0.115	12	E-W	0.22	0.31	0.31
57355	10-story R.C.	24,500	0.058	12	N-S	1.11	0.96	1.19
58490	6-story R.C.	6,430	0.049	12	N-S	0.79	0.84	1.06

Table 2 Description of Buildings

Earthquake	Station	Comp.	PGA (g)	EPA (g)
Imperial Valley (1940)	EL Centro	S90E	0.35	0.28
Washington (1949)	Olympia	S86W	0.28	0.22
Kern County (1952)	Taft	S69E	0.18	0.15
Parkfield (1966)	Cholane	N85E	0.43	0.33
San Fernando (1971)	Pacoima Dam	S16E	1.17	0.80
Imperial Valley (1979)	I. V. C.	S40E	0.33	0.20
Loma Prieta (1989)	Corralitos	S00E	0.63	0.52
Loma Prieta (1989)	Santa Cruz	S90E	0.41	0.33

Table 3 Earthquake Records

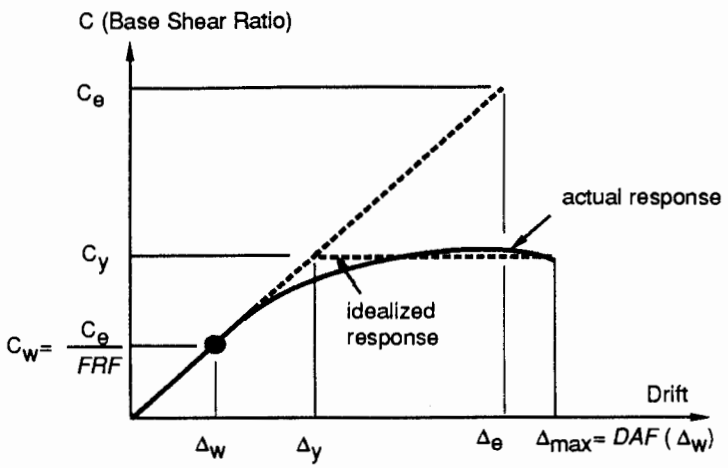

Fig. 1 General Structural Response

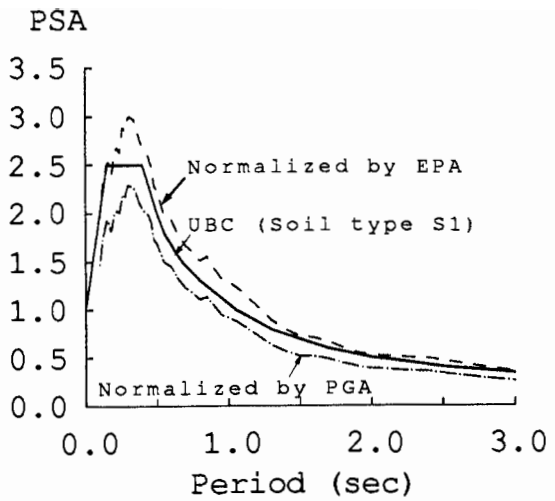

Fig. 2 Normalized Response Spectra (5% damping ratio)

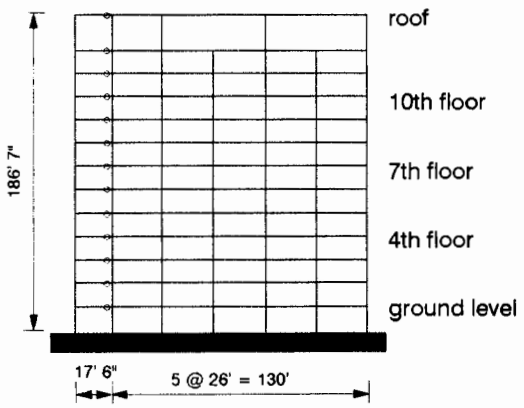

(a) SMRSF of Bldg. CSMIP57357 (E-W)

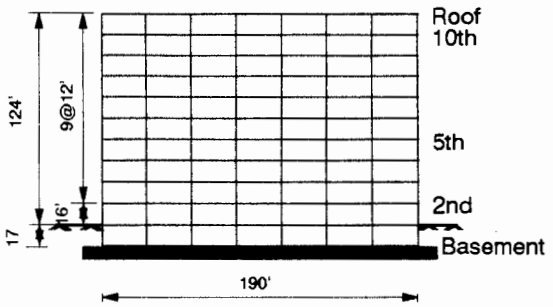

(c) SMRSF of Bldg. CSMIP57355 (N-S)

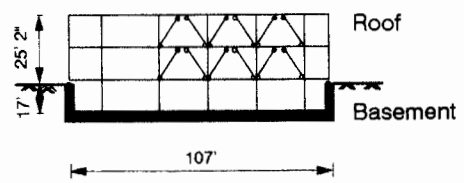

(b) EBF of Bldg. CSMIP58496 (E-W)

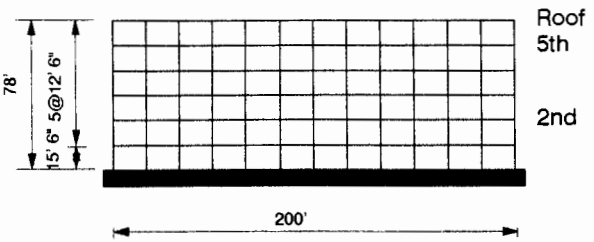

(d) SMRSF Bldg. CSMIP58490 (N-S)

Fig. 3 Elevations of Building Frames

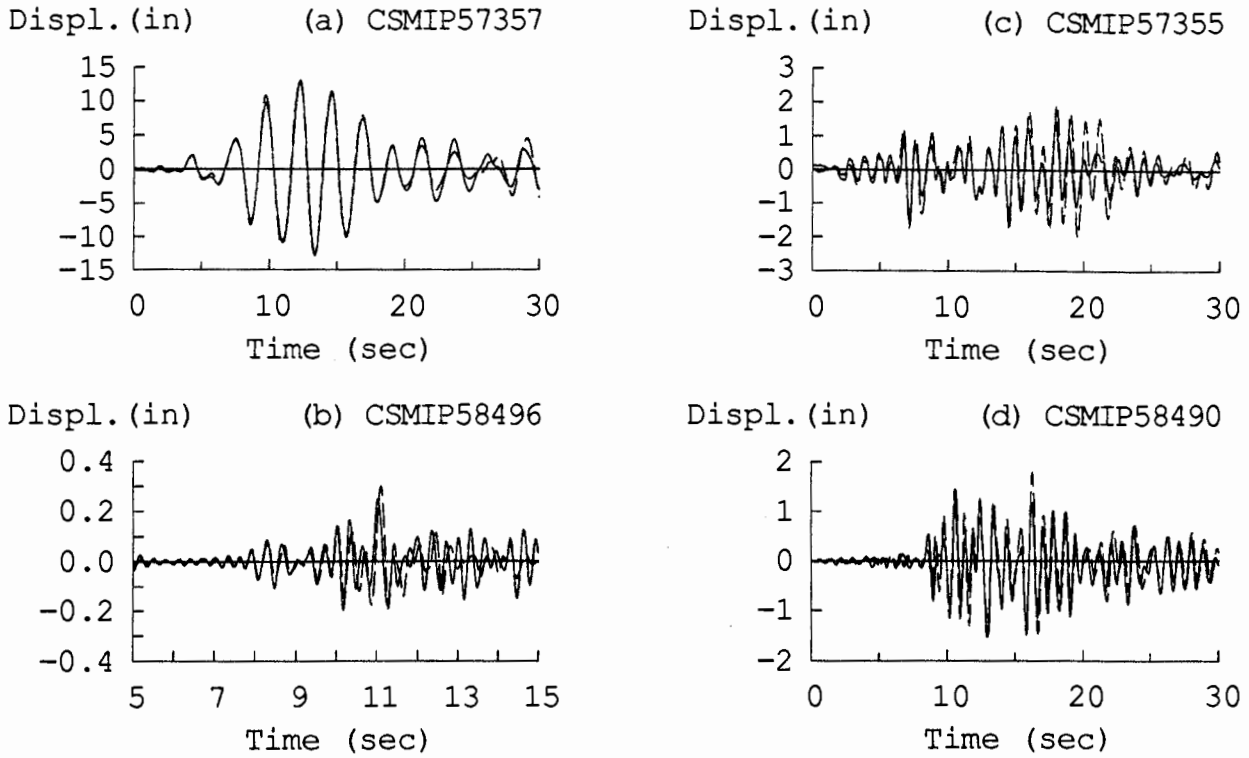

Fig. 4 Dynamic Correlation of Roof Response

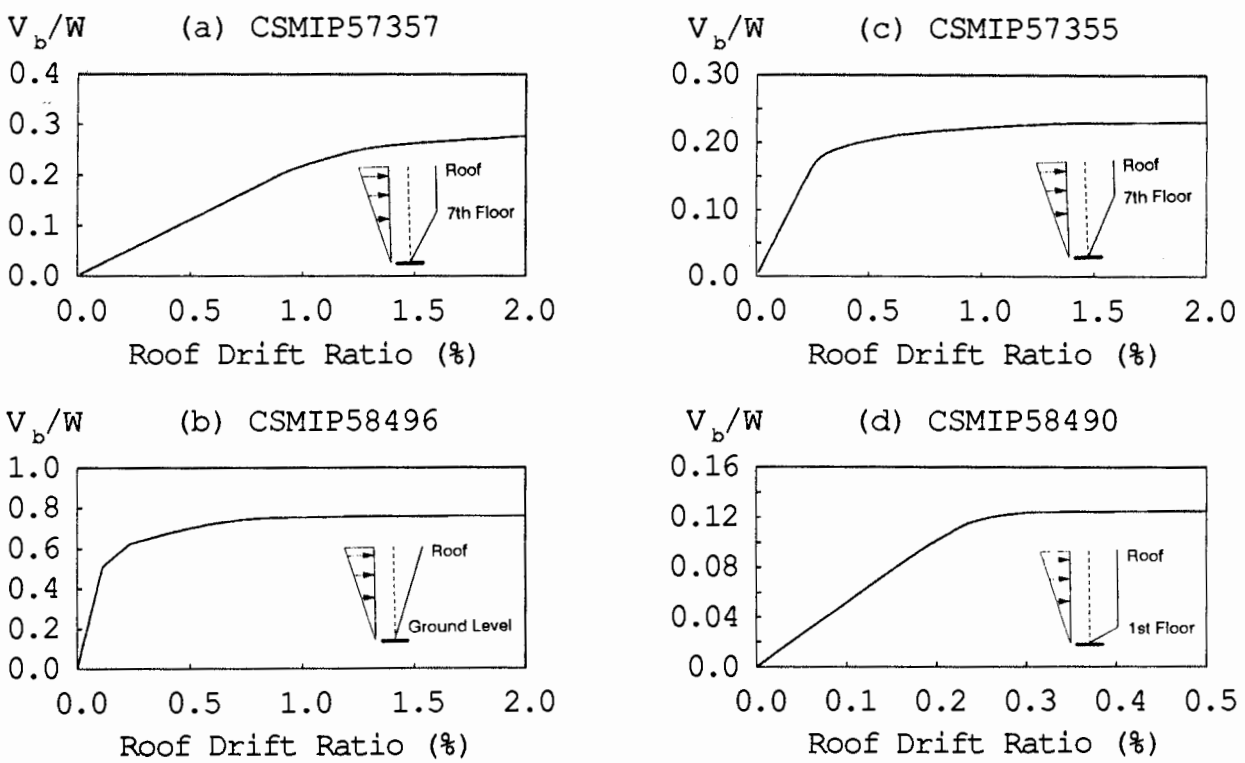

Fig. 5 Structural Lateral Strength and Collapse Mechanism

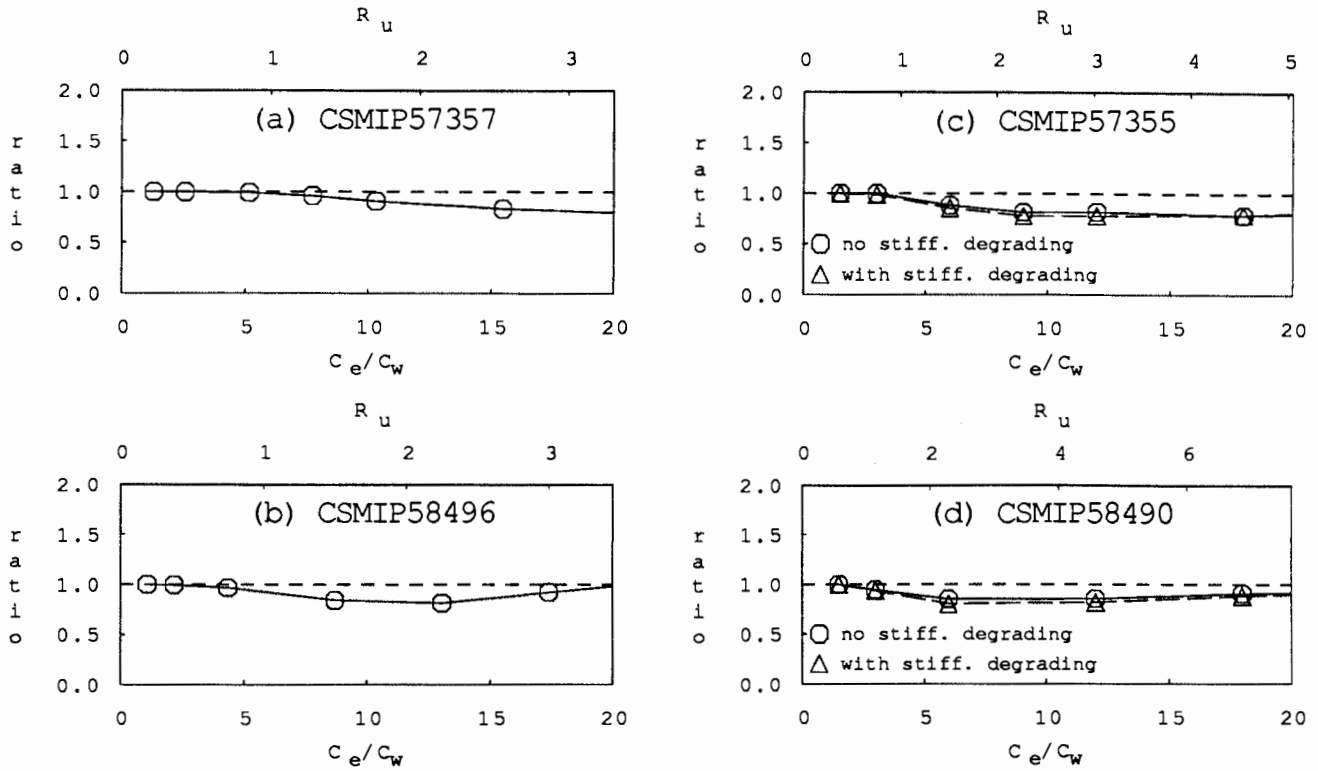

Fig. 6 Mean $\frac{\Delta_e}{\Delta_{max}}$ Ratios for Roof Drift

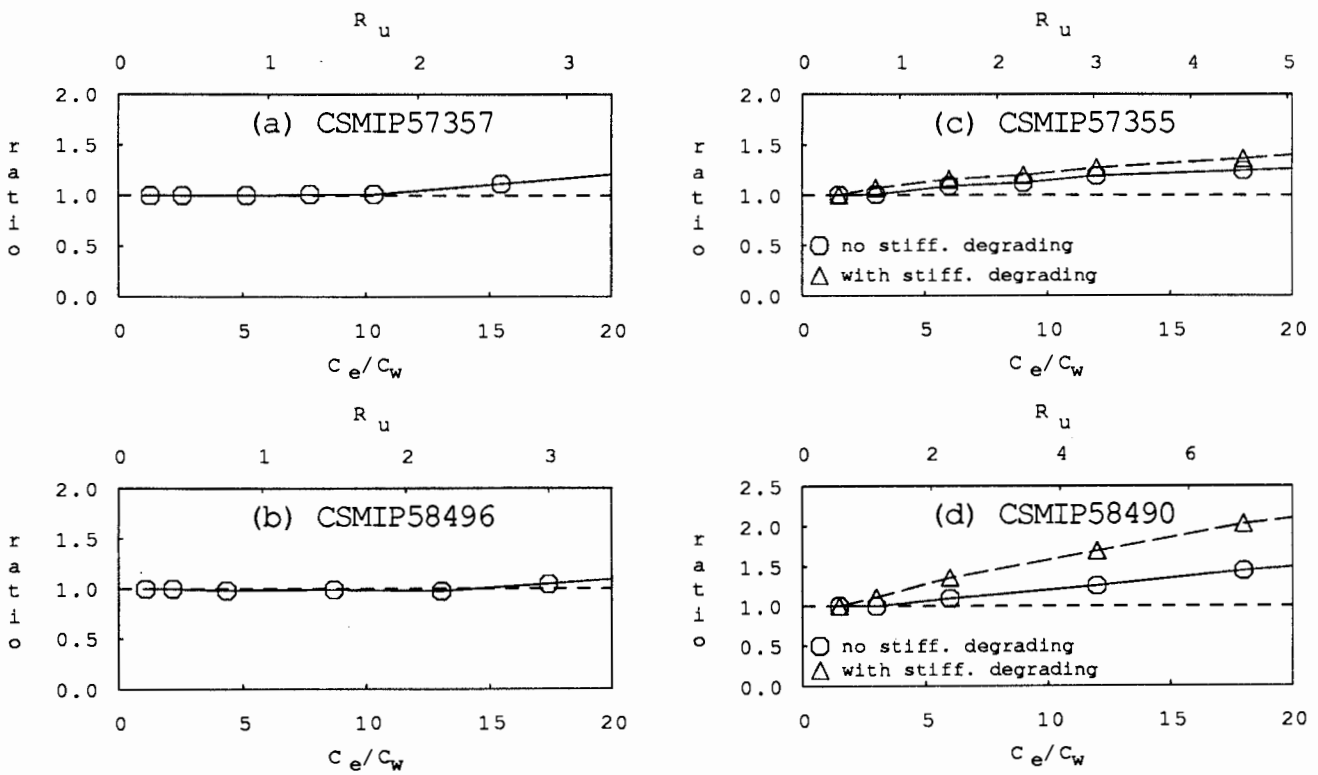

Fig. 7 Mean $\frac{\Delta_e}{\Delta_{max}}$ Ratios for Story Drift

ANALYSIS OF RECORDED BUILDING DATA TO VERIFY OR IMPROVE 1991 UNIFORM BUILDING CODE (UBC) PERIOD OF VIBRATION FORMULAS

Eugene E. Cole
Cole, Yee, Schubert & Associates

Christos V. Tokas
Cole, Yee, Schubert & Associates

John F. Meehan
Consulting Structural Engineer

ABSTRACT

A data base of 64 buildings was developed to investigate their fundamental period of vibration recorded during recent California earthquakes. These periods are compared with those calculated from the 1991 **Uniform Building Code** (1991 UBC) and the 1990 Structural Engineers Association of California **Recommended Lateral Force Requirements** (Blue Book). Steel moment frames, braced frames, concrete moment frames, and shear wall buildings are included in the data base. Also included in the study are buildings from the Gates & Foth report [12].

INTRODUCTION

The 1991 UBC establishes two methods of determining the fundamental period of vibration of buildings when the static force procedure is used. This report analyzes strong motion records from the California Strong Motion Instrumentation Program (CSMIP) and others to compare the fundamental period of vibration of buildings determined from these records and the calculated periods from the 1991 UBC. Graphs are presented showing the instrumented building periods and those obtained from the 1991 UBC period equations. These graphs indicate close correlation for steel moment frame and concrete moment frames. Shear wall periods are also shown. Insufficient data is available for braced frames and eccentrically braced frames. Further study is necessary to determine the accuracy of period formulas for shear wall buildings.

OBJECTIVE

The primary objective of this study is to review strong motion data to verify or recommend improvements in current seismic code formulas for the fundamental period of vibration of buildings.

METHODOLOGY

A data base of instrumented buildings that have experienced recorded ground motion of more than 0.05g was developed. This data base was obtained from information provided by CSMIP reports.

The buildings were tabulated and classified within one of the following lateral resisting system categories: Steel moment frames, concrete moment frames, concentric and eccentric braced frame, shear walls, and mixed lateral systems. Construction drawings of 64 buildings contained in the CSMIP archives were reviewed to verify the building classification.

Only regular buildings, instrumented by CSMIP or others, of a type contemplated by the 1991 UBC are included in this study. These buildings are shown in Tables 1, 2, and 3. The following unusual building types were omitted: Buildings containing a flexible first story, buildings constructed with base isolation devices, a building constructed in a pyramid shape, buildings with offset shear walls, buildings with mixed lateral systems, and buildings using a flat slab or a waffle slab as the horizontal moment frame member.

The fundamental period was obtained by scaling the processed data, adopting published values determined by other researchers, or by performing a non-parametric system identification procedure in the frequency domain.

The scaling process involves averaging the time interval between the peaks of the roof acceleration or displacement time-history curves processed by CSMIP in that portion of the record after the initial strong input motion. These values, however, include the influence of the site on the period. For flexible buildings, the values are competent. For stiff buildings, the scaling process is inaccurate since the displacement of the roof at the top of the wall is essentially the same as the ground. The following non-parametric system identification procedure in the frequency domain was used to identify the fundamental period of vibration for several of the buildings:

1) The Fourier amplitude spectrum graphs were computed from the corrected acceleration records by Fourier Transformations. The Fourier amplitude spectrum graph for the roof and base of a building were developed for each of the orthogonal building directions.

2) The transfer functions were computed by dividing the Fourier amplitude spectrum of acceleration recorded at the roof of the building by that recorded at the base. Thus, the building response was isolated from the soil-structure system, and therefore, the transfer function exhibited the dynamic characteristics of the building without the influence of the site.

3) The natural periods of the building can be obtained from the frequencies at which the peak values of the transfer function occur. The fundamental period is calculated from the frequency value at the first peak of the transfer function.

RESULTS

General: The building periods inferred from the strong motion records of the recent California Earthquakes are plotted against story height in Figures 1, 2, and 3 for moment resisting steel frame, moment resisting reinforced concrete frame, and shear wall buildings. Two values of period are shown for each building, and are joined with a connecting line. These values represent periods in each orthogonal direction. The graphs in Figures 1 and 2 were expanded by including buildings from the Gates & Foth Report [12].

A curve representing the period ,T_A, obtained from the code formula using Method A which is given in Section 2334(b) 2.A 1991 UBC, is shown on Figures 1, 2, and 3. It should be noted that this curve indicates shorter period values than the actual building periods obtained from the strong motion records for the moment resisting frame structures.

The UBC also allows the use of Method B for determining the period. When this method, based on the Rayleigh Formula, is used a limitation is placed on C of 80% of the value of C obtained by using T from Method A for regular buildings. This places an upper limit on the value of T obtained from Method B. This period is shown in Figures 1 and 2 as T_{MOD} ($T_{MODIFIED}$). T_{MOD} is calculated using the following procedure:

$$T_A = C_t (h_n)^{3/4} \quad (1)$$

$$C_A = 1.25\ S \div T_A^{2/3} \quad (2)$$

$$C_{MOD} = .80\ C_A = 1.25\ S \div T_{MOD}^{2/3} \quad (3)$$

Solving equation (3) for T_{MOD}

$$T_{MOD} = [(1.25\ S \div (0.8\ C_A)]^{3/2} \quad (4)$$

Combining equations (2), (3), and (4):

$$T_{MOD} = \{1.25\ S \div [(0.8)\ (1.25\ S \div T_A^{2/3})]\}^{3/2} \quad (5)$$

Simplifying further equation (5) becomes:

$$T_{MOD} = 1.4\ T_A \quad (6)$$

Steel Moment Frames: In Figure 1, for building heights above 75 feet, the curve of the Method A period, T_A, is below the data points giving shorter periods than the records. The difference between the period value given by this curve and the actual data is large for taller buildings. The T_{MOD} curve provides a conservative, yet reasonable, approximation of the measured period for all buildings above 75 feet in height with the exception of two buildings from the Gates & Foth study [12]. The lateral load systems of both of these buildings were investigated and it was found that a steel tubular framing system was used for one, and composite concrete and steel column with steel truss girders was used for the other. These buildings are not included in Figure 1.

Concrete Moment Frames: In Figure 2, the curve for Method A period, T_A indicates shorter periods than those determined from the records. Six buildings from the Gates & Foth study are not included. The lateral load resisting system of these six buildings did not have a 100% moment resisting frame in one of the directions. For the remaining buildings, the T_{MOD} curve provides a reasonable approximation of the measured period.

Shear Walls: Figure 3 summarizes the data obtained from the shear wall buildings. The curve , T_A, obtained from the code formula using Method A is shown in Figure 3. The periods from the records are academically interesting; however, they have little significance for short period buildings since the maximum value of the spectral amplification factor C equal to 2.75 (regardless of soil type) establishes the lower limit for periods of shear wall buildings.

$$C = 1.25\ S \div T^{2/3}$$

For soil type S_1, $2.75 = 1.25\ (1.0) \div T^{2/3}$

Therefore, $T^{2/3} = 1.25\ (1.0) \div 2.75 = 0.455$

and , $T = 0.31$

Therefore, only shear wall building periods longer than the lower limit set by the code at 0.31, 0.40, 0.56, and 0.81 seconds for soil types S_1, S_2, S_3, and S_4, respectively, affect the base shear coefficient. These values are plotted on Figure 3.

A recent CSMIP study of a low-rise stiff shear wall building with a flexible diaphragm shows that the response of this structure was dominated by the dynamic properties of the flexible roof diaphragm [26]. Conventional code design procedures for buildings with this type of lateral load resisting system assume dynamic amplification in the shear walls and a uniform acceleration of the diaphragm, which does not correlate with the observations of the above study.

Braced Frames: Insufficient data is available to develop a comparison between code period formulas for braced frames and those determined from instrumented buildings.

SUMMARY AND CONCLUSIONS

This study compares the results given from the code empirical formulas for estimating the fundamental period of building structures to the fundamental periods obtained from the strong motion records. The primary results of this study may be summarized as follows:

1) Steel and Concrete Moment Frames

   A) The fundamental periods of vibration of the buildings obtained from the strong motion records are longer than the period values computed by the Method A equations given in Section 2334 (b) 2.A 1991 UBC.

   B) The 80% limitation on C from Method A, when Method B (Section 2334 (b) 2.B 1991 UBC) is used, results in a maximum period from Method B of 1.4 times the period determined from Method A. This modified period correlates well with results obtained from the data.

2) Shear Walls

   A) Although measured periods of shear wall buildings indicate much lower values than the code formulas estimate, these lower measured periods have no effect on the base shear calculations since the upper limit of 2.75 is placed on the value of C. It is appropriate to re-evaluate this limit since it has the effect of negating soil amplification in short period buildings.

FUTURE RESEARCH

1) More data is necessary to evaluate periods for concentrically and eccentrically braced frames.

2) Further study is necessary to determine the accuracy of period formulas for shear wall buildings.

3) Investigate the influence of softer soils and flexible diaphragms on short period buildings to determine if these conditions cause larger forces than currently anticipated by the code.

4) The 1991 UBC requires only a single value for building period for both principal axes when both axes are framed in the same framing system. The stiffnesses along each orthogonal axes of a building may be different. This will result in different values for the fundamental period of vibration along each axis. Recent studies have shown that in buildings where a stiffer lateral load resisting system is employed in one direction than the other, the predominant motion occurs in the softer direction [17, 18]. Therefore, the building response along one principal axis is not only dependent on the period along that axis, but also relates to the building period in the other principal axis. This condition should be further studied and the code revised accordingly.

ACKNOWLEDGEMENTS

The assistance, cooperation, and many helpful suggestions of Dr. Anthony F. Shakal and Dr. Moh-Jiann Huang of the Office of Strong Motion Studies of the California Division of Mines and Geology is greatfully appreciated.

The contents of this report were developed under Contract No. 1090-524 from the California Department of Conservation, Division of Mines and Geology, Strong Motion Instrumentation Program. However, these contents do not necessarily represent the policy of that agency nor endorsement by the State Government.

REFERENCES

[1] Structural Engineers Association of California (SEAOC) Seismology Committee
"Recommended Lateral Force Requirements", 1990

[2] International Conference of Building Officials
"Uniform Building Code", 1991 Edition

[3] A.F Shakal, M.J. Huang, et. al.
"CSMIP Strong Motion Records from the Santa Cruz Mountains (Loma Prieta) California Earthquake of October 17, 1989"
Report No. OSM 89-06, California Department of Conservation, Division of Mines and Geology, Office of Strong Motion Studies, November 1989

[4] California Department of Conservation, Division of Mines & Geology, Office of Strong Motion Studies
"Processed Strong Motion Data from the Loma Prieta Earthquake of 17 October 1989"
Report No. OSMS 91-07

[5] A.F. Shakal, M.J. Huang, et. al.
"CSMIP Strong Motion Records from the Whittier, California Earthquake of October 1, 1987"
Report No. OSM 87-05, California Department of Conservation, Division of Mines and Geology, Office of Strong Motion Studies, October 1987

[6] California Department of Conservation, Division of Mines & Geology, Office of Strong Motion Studies
"Processed Strong Motion Data from the Whittier Earthquake of 1 October 1987"

[7] A.F. Shakal, M.J. Huang, et. al.
"CSMIP Strong Motion Records from the 1984 Morgan Hill Earthquake"
Report No. OSMS 85-05, California Department of Conservation, Division of Mines and Geology, Office of Strong Motion Studies, October 1987

[8] M.J. Huang, A.F. Shakal, et. al.
"CSMIP Strong Motion Records from the Sierra Madre California Earthquake of 28 June 1991"
Report No. OSMS 91-03, California Department of Conservation, Division of Mines and Geology, Office of Strong Motion Studies

[9] M.J. Huang, et. al.
"CSMIP Strong Motion Records from the Palm Springs California Earthquake of 8 July 1986"
Report No. OSMS 86-05, California Department of Conservation, Division of Mines and Geology, Office of Strong Motion Studies

[10] California Department of Conservation, Division of Mines & Geology, Office of Strong Motion Studies
"Processed Strong Motion Data from the Palm Springs Earthquake of 8 July 1986"

[11] L.D. Porter, et. al.
"Processed Data from the Strong Motion Records of the Santa Barbara Earthquake of 13 August 1978"
Special Report 144, Volume 3, California Department of Conservation, Division of Mines and Geology, Office of Strong Motion Studies

[12] Gates, W.E. and Foth, V.A.
"Building Period Correlation" Report to the Applied Technology Council

[13] McVerry, G.H.
"Frequency Domain Identification of Structural Models from Earthquake Records"
Report No. EERI 79-02, California Institute of Technology, Pasadena, California, 1979

[14] J.C. De la LLera, A.K. Chopra
"Evaluation of Code Accidental Torsion Provisions Using Strong Motion Records from Regular Buildings"
Preprints, SMIP91 Seminar, CDMG, Sacramento, California 1991

[15] A. Astaneh, D. Bonowitz, C.Chen
"Evaluating Design Provisions and Actual Performance of a Modern High-Rise Steel Structure"
Preprints, SMIP91 Seminar, CDMG, Sacramento, California 1991

[16] H. Sedarat, S. Gupta, S.D. Werner
"Torsional Response Characteristics of Regular Buildings Under Different Seismic Excitation Levels"
Preprints, SMIP91 Seminar, CDMG, Sacramento, California 1991

[17] V. Bertero, Bendimerad M.F., and Shah H.C.
"Fundamental Period of Reinforced Concrete Moment-Resisting Frame Structures"
Technical Report No. 87, The John A. Blume Earthquake Engineering Center, Stanford University, Stanford, California, 1988

[18] F. Bendimerad, H.C. Shan, T. Hoskins
"Extension of Study on Fundamental Period of Reinforced Concrete Moment-Resisting Frame Structures"
Technical Report No. 96, The John A. Blume Earthquake Engineering Center, Stanford University, Stanford, California, June 1991

[19] M. Celebi, L.T. Phan, R.D. Marshall
"Dynamic Characteristics of Five Buildings Determined from Their Responses to the 10/17/1989 Loma Prieta (California) Earthquake and Low-level Amplitude Tests"
(Obtained from Authors)

[20] C. Uang, A. Maaroof
"An Investigation of Serviceability Requirements of the 1988 UBC Seismic Provisions"
Preprints, SMIP91 Seminar, CDMG, Sacramento, California 1991

[21] R.L. Boroschenek, S.A. Mahin, C.A. Zeris
"Seismic Response and Analytical Modeling of Three Instrumented Buildings"
Proceedings of Fourth U.S. National Conference on Earthquake Engineering, May 20-24, 1990, Palm Springs, California, Volume 2

[22] NOAA/EERI, Murphy, L.M., Editor
"San Fernando, California Earthquake of February 9, 1971"
NOAA U.S. Department of Commerce, Volumes I, II, and III, 1973

[23] F.C. Fillippou
"Correlation Studies of Seismic Response of Reinforced Concrete Moment Resisting Frames"
Preprints, SMIP 89 Seminar, CDMG, Sacramento, California, 1989

[24] J.P. Moehle
"Implications of Strong Motion Data for Design of Reinforced Concrete Bearing Wall Buildings"
Preprints, SMIP 89 Seminar, CDMG, Sacramento, California, 1989

[25] E. Miranda, J.C. Anderson, V.V. Bertero
"Seismic Response of a Thirty-Story Building During the Loma Prieta Earthquake"
Proceedings of the Second Conference on Tall Buildings in Seismic Regions, 55th Regional Conference, May 16 and 17, 1991, Los Angeles, California

[26] J.B. Bauwkamp, R.O. Hamburger, J.D. Gillengerten
"Degradation of Plywood Roof Diaphragms Under Multiple Earthquake Loading"
Preprints, SMIP 91 Seminar, CDMG, Sacramento, California, 1991

TABLE 1

STEEL MOMENT RESISTING FRAME STRUCTURES AND RELATED PERIODS

BLDG No.	BUILDING NAME	CSMIP STATION No.	EARTHQUAKE	HEIGHT H (ft)	PERIOD T, (sec)			
					UBC MTHD-A	UBC T-MOD.	TRANS.	LONG.
1	Burbank 6-story	24370	Whittier	82.50	0.96	1.34	1.30	1.32
2	Long Beach 7-story	14323	Whittier	91.00	1.03	1.44	1.50	1.19
3	Palm Springs 4-story	12299	Palm Springs	51.50	0.67	0.94	0.63	0.71
4	Richmond 3-story office	58506	Loma Prieta	44.00	0.60	0.84	0.76	0.60
5	San Bernardino 3-story	23516	Whittier	42.00	0.58	0.81	0.46	0.50
6	San Francisco 18-story	58480	Loma Prieta	230.00	2.07	2.89	3.33	2.26
7	San Francisco 47-story	58532	Loma Prieta	564.00	4.05	5.66	5.00	6.50
8	San Jose 13-story	57357	Loma Prieta	186.60	1.77	2.47	2.23	2.23
9	San Jose 3-story	57562	Loma Prieta	49.50	0.65	0.91	0.69	0.69
10	South San Francisco - 4-story	58261	Loma Prieta	52.50	0.68	0.95	0.71	0.71

TABLE 2

CONCRETE MOMENT RESISTING FRAME STRUCTURES AND RELATED PERIODS

BLDG No.	BUILDING NAME	CSMIP STATION No.	EARTHQUAKE	HEIGHT H (ft)	PERIOD T, (sec)			
					UBC MTHD-A	UBC T-MOD.	TRANS.	LONG.
1	Los Angeles 5-story	24463	Whittier	119.00	1.08	1.51	1.30	1.40
2	N.Hollywood 20-story	24464	Whittier	169.00	1.41	1.97	2.21	2.15
3	Pomona 2-story	23511	Whittier	30.00	0.38	0.54	0.80	0.70
4	San Bruno 6-story	58490	Loma Prieta	78.00	0.79	1.10	1.10	0.85
5	Sherman Oaks 13-story	24322	Whittier	187.50	1.52	2.12	2.30	1.90
6	Van Nuys 7-story	24386	Whittier	65.71	0.69	0.97	1.20	1.40
7	Emeryvile 30-story	USGS	Loma Prieta	300.00	2.16	3.02	2.80	2.80

TABLE 3

SHEAR WALL BUILDINGS AND RELATED PERIODS

BLDG No.	BUILDING NAME	CSMIP STATION No.	EARTHQUAKE	HEIGHT H (ft)	PERIOD T, (sec)		
					UBC MTHD-A	TRANS.	LONG.
	R/C SHEAR WALL BUILDINGS						
1	Belmont 2-story	58262	Loma Prieta	28.00	0.24	0.20	0.13
2	Burbank 10-story	24385	Whittier	119.00	0.72	0.51	0.57
3	Goleta 3-story	25213	Santa Barbara	33.00	0.28	0.35	0.30
4	Hayward 4-story	58488	Loma Prieta	50.00	0.38	0.22	0.15
5	Long Beach 5-story	14311	Whittier	71.00	0.49	0.34	0.17
6	Los Angeles 17-story	24601	Sierra Madre	149.72	0.86	1.00	1.00
7	Oakland 24-story	58483	Loma Prieta	219.00	1.14	3.23	2.32
8	Palm Desert 4-story	12284	Palm Springs	50.20	0.38	0.60	0.50
9	Piedmont 3-story	58334	Loma Prieta	36.00	0.29	0.18	0.18
10	Pleasant Hill 3-story	58348	Loma Prieta	40.58	0.32	0.46	0.38
11	San Bruno 9-story	58394	Loma Prieta	104.00	0.65	1.30	1.20
12	San Jose 10-story resid.	57356	Loma Prieta	96.00	0.61	0.42	0.70
13	Saratoga 1-story	58235	Loma Prieta	33.00	0.28	0.18	0.31
14	Watsonville 4-story	47459	Loma Prieta	66.33	0.46	0.35	0.24
	R. MASONRY SHEAR WALL BUILDINGS						
15	Concord 8-story	58492	Loma Prieta	74.92	0.51	0.38	0.74
16	Lancaster 3-story	24517	Whittier	41.50	0.33	0.20	0.21
17	Palo Alto 2-story	58264	Loma Prieta	23.83	0.22	0.34	0.27

FIGURE 1. STEEL MOMENT RESISTING FRAMES

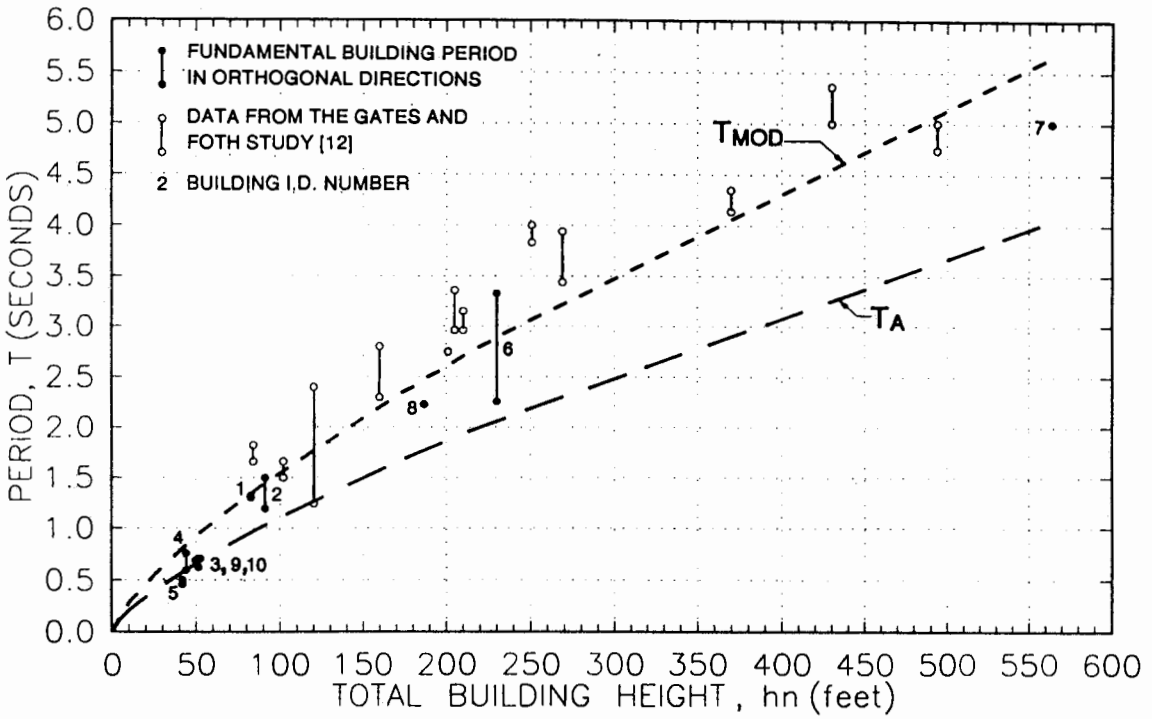

FIGURE 2. R/C FRAMES

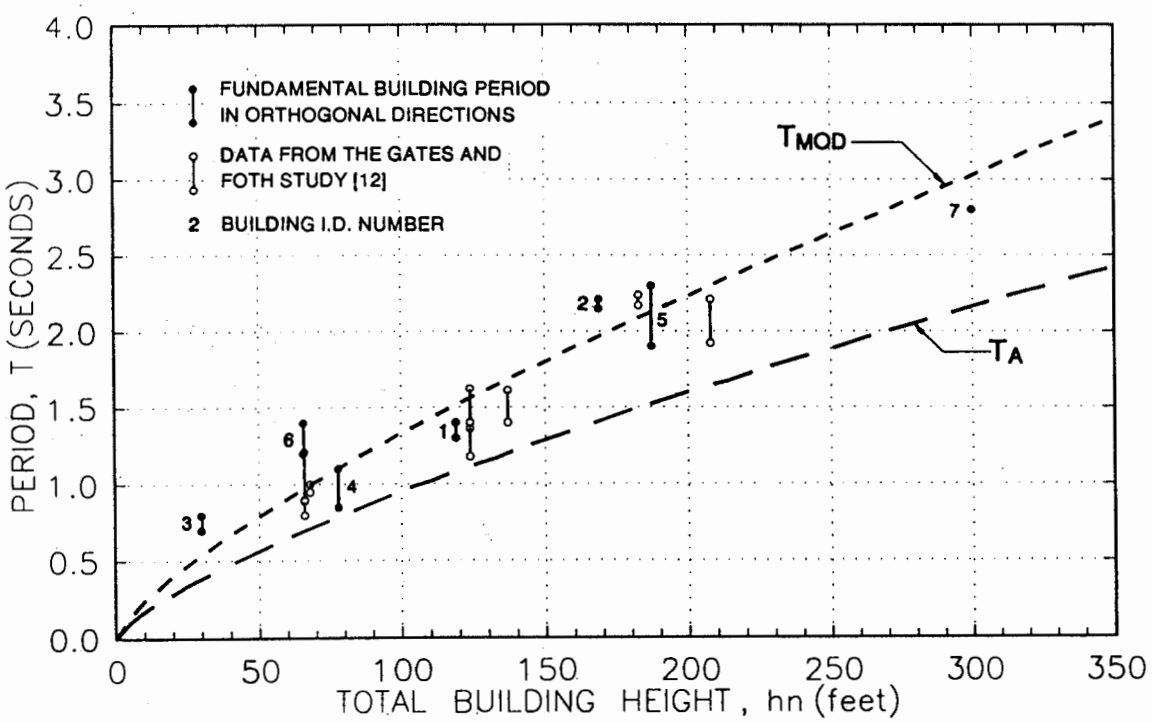

FIGURE 3. SHEAR WALL BUILDINGS
REINFORCED CONCRETE AND MASONRY

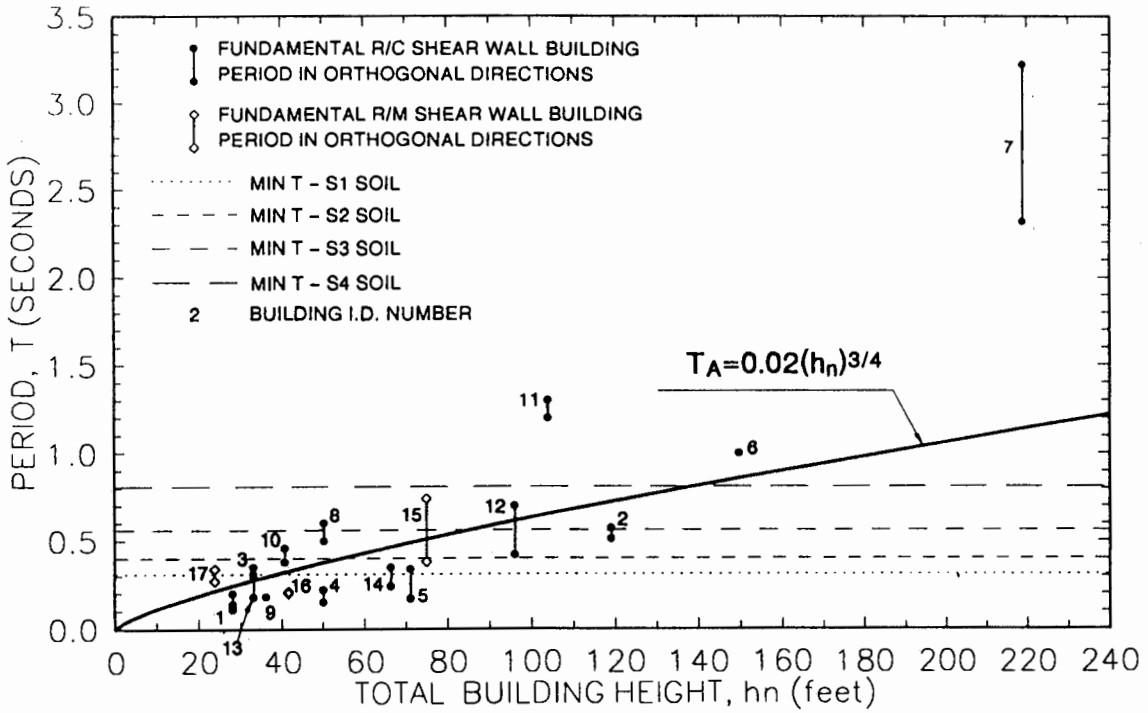

EFFECTS OF DURATION ON STRUCTURAL RESPONSE FACTORS AND ON GROUND-MOTION DAMAGEABILITY

Robert T. Sewell

Risk Engineering, Inc.
Golden, Colorado

ABSTRACT

Ground-motion records from the California Strong Motion Instrumentation Program (CSMIP) and from other sources are used to examine relationships between strong-motion duration, elastic strength demands, structural response factors, and inelastic strength demands, as derived from analytical study.

Structural response factors R are found to have generally slight systematic dependence on strong-motion duration, but they do have a more direct, if not fundamental, relationship to characteristics of elastic response spectra. In addition to the general lack of correlation between R and duration, both elastic and inelastic strength demands (and hence, ground-motion damageability also) show little apparent consistent systematic correlations with duration.

Results of this study imply that seismic load specifications, for safety analysis or design of buildings, can generally be adequately described by appropriate ground-motion spectra without the need to explicitly specify an associated duration.

INTRODUCTION

Intuition leads one to believe that duration plays a key role in the damage effectiveness of strong ground motion. Clearly, if a motion has insignificant duration with respect to the periods of dominant participating modes of vibration for a particular building, it should generally possess little potential to affect response, much less damage, in that building. In addition, short-duration motions do not have the potential to induce several hysteretic cycles of response which are associated with the type of non-linear "ratcheting" often thought to be necessary to damage ductile structures.

Structural response factors, R, describe allowable yield-force reduction factors associated with a given (tolerable) state of damage (as may be characterized, for example, by ductility, normalized hysteretic energy, cumulative damage measures, etc.). Expecting that duration is relevant to motion damageability, therefore, one might logically expect that values of R should depend on duration. In particular, if long-duration motions are more damaging, lower values of R (i.e., lower allowable yield-force reductions for a given damage state) would be expected (and accepted) for such long-duration motions, whereas higher values of R would be acceptable for short-duration records. Stated alternatively, if two motions (one of long-duration and one of

short-duration) produce the same elastic force in a given structure, and the structure is designed to yield at a force level equal to that elastic force divided by a given factor R, then a greater level of damage would generally be expected for the long-duration record, assuming that damage is relevant to duration.

A significant objective of this study has been to test this hypothesis, and to clarify the role of duration by investigating the dependence of R factors, elastic strength demands, and inelastic strength demands on duration. A key question to be addressed is: Given the common engineering intuition and observations that duration has an important influence on motion damageability, should R factors be specified explicitly on the basis of design-motion durations? If not, then how do we insure that the impacts of duration have been adequately considered in design?

The variety and significance of ground-motion records obtained by the CSMIP lead to a productive basis for conducting this investigation.

BACKGROUND

Results of previous research [1-4], not directly aimed at evaluating the effects of strong-motion duration, strongly imply that structural response factors do not have a clear systematic dependence on duration. Rather, these studies suggest that values of R may be only indirectly related to strong-motion duration through the intrinsic effects that duration has on the characteristics (namely, amplitude and breadth of frequency content) of the elastic response spectrum, and through systematic effects that the elastic response spectrum has on R factors.

To illustrate this point, we compare the seismic demands imposed by two motions, of differing durations, which were obtained by CSMIP following the 10/17/89 Loma Prieta, California earthquake. Figure 1 shows 5%-damped linear response spectra for the 0-deg component of the UCSC/Lick Lab., Santa Cruz recording and the 0-deg component of Aloha Ave., Saratoga recording, both scaled to a PGA of 0.5g. These two records are selected because the UCSC recording has a substantially (about 60%) longer duration than the Saratoga recording (see Figures 2 and 3). Using a duration measure T'_D proposed by Kennedy *et al.*[4], for instance, the strong motion duration of the UCSC and Saratoga records are, respectively, 5.96 and 3.78 seconds. Note also that at 2.0 Hertz, the spectral accelerations are equal for the two records. Hence, if ground-motion damageability is strongly dependent on duration, one would expect the 2.18-second-longer UCSC record to more damaging to a 2.0-Hz structure designed for a given spectral reduction (R) factor. Table 1 shows, however, that this is not the case; for identical design yield forces associated with an R factor of 4.0, all damage parameters computed for the Saratoga record exceed quite substantially those computed for the UCSC record. In addition, the computed R factors for a constant level of normalized hysteretic energy (NHE) equal to 10.0 are 4.3 and 2.9, respectively, for the UCSC and Saratoga records; hence, the 2.0-Hz structure, would have to be designed to have a yield force 50% greater in the case of the Saratoga record (vis-á-vis the UCSC record) to limit the NHE damage parameter to 10.0, despite the facts that the duration of the UCSC record is substantially greater and the spectral amplitudes at 2.0 Hz for the

two records are the same.

One important reason the Saratoga record is more damaging than the UCSC record, despite its shorter duration, is that its energy content (linear spectral amplitudes) at all frequencies less that 2.0 Hz is substantially greater than that for the UCSC record (as can be seen in Figure 1). Hence, when the structure yields, and its predominant frequency decreases (due to stiffness-reduction softening), it becomes more desensitized to the UCSC input than the Saratoga input, because the Saratoga input has substantially greater energy at frequencies lower than 2.0 Hz.

In this case (and most cases), this spectral effect is much more significant than any direct effect of duration; although duration can have a significant effect for certain cases. Clearly, there are simple academic cases where, given a fixed elastic spectral demand, duration can be found to have an important impact on damage. Real-earthquake motions, however, typically exhibit a characteristic pattern of nonstationarity (i.e., build-up phase, single strong-motion phase, and decay phase) that acts to de-sensitize damage models to duration (i.e., because the response is constrained such that most of the damage accumulates in a few characteristic peak cycles in the strong-motion phase). The use of real earthquake records is therefore essential in studying the impact of duration on R factors, both in analytical studies, as well as in laboratory tests. Certain real ground motions can be expected to reveal an explicit dependence of R on duration--for instance, a so-called "double-event" recording; however, it is anticipated that the number of such records in the ground-motion database may be comparatively few.

STUDY APPROACH

With this background, the approach in this study has been to undertake a direct investigation of the relationship of strong-motion duration, elastic and inelastic strength demands, and structural response factors, based on analytical results pertaining to a comprehensive set of ground-motion records.

Whereas R factors are conventionally thought to be inherent properties of structural systems, this study assesses and treats R factors as characteristics of ground motions (for given structures), just as peak ground accelerations, velocities, displacements, and elastic response spectra are routinely assessed and reported as characteristics of ground motions. For any given ground motion, R depends on the structural vibration frequency, the value of damping, the type of structural system, and the damage parameter of interest.

Here, we examine a set of 262 ground-motion records. For each ground motion, we considered 91 structural vibration frequencies, ranging from .067 to 25.0 Hz. Hysteretic models characterizing bilinear behavior and shear-wall type behavior were both used for nonlinear analyses in each case. A damping ratio of 5% (proportional to elastic stiffness) has been used for all analysis. For a given type of hysteretic behavior, four levels of damage for each of six damage measures were considered in evaluating R factors. These damage indices include, for instance, four values of ductility (e.g., 2,4,6,8), normalized hysteretic energy, cumulative damage measures, and state variables based on ductility and hysteretic-energy demand parameters. These

damage models are representative of modern methods for measuring or characterizing damage, and they include both what may be categorized as duration-sensitive (e.g., normalized hysteretic energy) and duration-insensitive (e.g., ductility) models. Conventionally, analytically derived R factors are computed based on ductility response. Because, however, ductility does not increase directly with numbers of nonlinear cycles (and hence, duration) it, by itself, does not provide a suitable basis for examining the effects of duration on R factors.

Two methods are used for assessing strong-motion duration in this study. The first measure of duration, T'_D, is defined as [4]:

$$T'_D = Max \begin{bmatrix} T_{75\%} \\ T_{pga} \end{bmatrix} - T_{5\%}$$

where $T_{x\%}$ is the time at which x% of the input energy is achieved. Input energy at time T is given by [5,6]:

$$E_T = \int_0^T a^2(t)\, dt$$

where a(t) is the ground acceleration at time t. T_{pga} is the time of occurrence of the peak ground acceleration. The second duration measure, T_D, is given as:

$$T_D = T_{95\%} - T_{5\%}$$

SAMPLE STUDY RESULTS

An extensive database of results on inelastic demands, structural response factors, and ground-motion durations have been obtained from this project, both for use in this study as well as for use by the research community. Figures 4 to 11 illustrate one use of this data--in investigating potential relationships between strong-motion duration and structural response factors R for the present study. Figures 4 to 7 show (respectively, for vibration frequencies of 0.1, 1.0, 10 and 25 Hz) plots of structural response factors versus strong-motion duration T_D, based on an inelastic-response/damage measure of NHE = 16.4 and bilinear hysteretic behavior. Similar results have been obtained for other damage measures and for the duration measure T'_D. Figures 8 to 11 show corresponding results for shear-wall hysteretic behavior (with NHE=11.1). In Figures 4 and 8 (for 10 Hz), the only dependence of R on duration is that low values of R occur systematically in instances where the duration is lower than the predominant period of vibration; otherwise no meaningful correlation between R and T_D can be observed. However, for higher frequencies, a generally increasing (inverse) correlation, although slight, is observed between R and T_D. These results reveal that nonlinear-response based factors have surprisingly little dependence on strong motion duration. Based on numerous other results obtained in this

study, this observation appears to be robust with respect to damage model, hysteretic behavior, duration measure, and all other parameters of importance in assessing ground-motion damageability based on analysis.

Whereas, values of R cannot be shown to have a clear relationship to duration, a fundamental dependence of R on elastic demand spectra can be clearly demonstrated. Figure 12, for instance, shows how R may be accurately predicted based on a simple function of elastic response spectral ordinates alone, without regard to duration. In this case, the equation used to predict R is given by Kennedy, *et. al* [4] as:

$$R_{\mu}=\mu\left(\frac{f_e}{f}\right)^2\left[\frac{S_a(f,\xi)}{S_a(f_e,\xi_e)}\right]$$

where f and f_e are, respectively, the initial frequency and effective frequency; ξ and ξ_e are values of initial and effective damping; and S_a denotes the elastic demand (i.e., spectral acceleration). For shear-wall type behavior, a ductility factor of 4.0, and initial damping of ξ=5%, values of (f_e/f)=0.6 and an effective damping of ξ_e=10% of critical, describe appropriate values of effective frequency and damping. Hence, values of R for ductility response in a shear-wall type structure may be simply estimated from the following equation:

$$R_{\mu=4}=1.44\left[\frac{S_a(f,.05)}{S_a(0.6f,0.1)}\right]$$

The results in Figure 12 show very good correlation using this formula. Similar formulas are expected to produce good correlations for other damage models. Hence, values of R are predominately effected by the spectral effect discussed earlier, and are related to a simple ratio of elastic demands factored by a constant, without explicit consideration of duration effects.

Figures 13 and 14 illustrate that elastic and inelastic spectral demands also have little consistent relationship to strong-motion duration. These figures show a marked lack or correlation with duration, whereas some cases that produce a slight correlation may be found. Because inelastic demand spectra characterize the damage potential of ground motion [1,8], it is difficult to conclude (based on analysis) that ground-motion damageability has a clear, or even meaningful, dependence on strong-motion duration.

Following the 10/17/89 Loma Prieta earthquake, a number of experts were quoted as saying that the damage from the earthquake would have been much greater if the duration had been significantly longer. While such a statement may be conditionally true (for instance, a greater earthquake magnitude may be needed for a greater duration) it encourages the public to

doubt that duration has been meaningfully factored into the seismic design process by structural engineering professionals.

As the results here confirm, however, the meaningful effects of duration are factored into the design process through the selection of appropriate design spectra. This confirmation, however, is conditional on the applicability of modern analytical models and procedures.

CONCLUSIONS

Structural response factors R have a fundamental relationship with elastic spectral demands. Elastic and inelastic spectral demands show inconsistent correlation with strong-motion duration. Additionally, values of R, themselves, show only slight correlation with duration.

In the SMIP91 proceedings, a paper by Miranda and Bertero [7] concluded that structural response factors are strongly affected by natural period of vibration, the level of inelastic deformation, and local site conditions. The results of this study and previous studies [1,4,8] echo these conclusions. Because of correlation between elastic demands and R factors, for design, it is best to specify site-dependent inelastic spectra directly for a particular state of damage (inelastic response) of interest. (Methods for obtaining probabilistic-based inelastic spectra for limit-state design based on probabilities of tolerable damage levels may be found in Reference [1]).

This study demonstrates that the effects of duration which are important for design are intrinsic to elastic (or inelastic) spectral demands. Therefore, seismic load specification can in most cases, be adequately described by appropriate inelastic ground-motion spectra, without the need to explicitly specify (or separately account for) an associated duration.

ACKNOWLEDGEMENTS

This study was supported by the Strong-Motion Instrumentation Program of the California Division of Mines and Geology, Contract No. 1090-525. Dynamic response analyses conducted for strong-motion records other than those provided by CSMIP, were conducted with support of the National Science Foundation, Grant No. BCS-9003588. The author appreciates the support of these funding agencies. In addition, the author thanks Dr. Moh Huang for his assistance in providing a large volume of strong-motion data and earthquake reports for this project.

REFERENCES

[1] Robert T. Sewell. *Damage Effectiveness of Earthquake Ground Motion: Characterizations based on the performance of structures and equipment.* Dept. of Civil Engineering, Stanford University, Stanford, CA, 1988.

[2] Robert T. Sewell, Gabriel R. Toro, and Robin K. McGuire. *Impact of Ground Motion Characterization on Conservatism and Variability in Seismic Risk Estimates*. U.S. Nuclear Regulatory Commission, 1991.

[3] C. Allin Cornell and Robert T. Sewell. "Non-linear-behavior intensity measures in seismic hazard analysis." In *Proceedings of the International Seminar on Seismic Zonation*. Guangzhou, China, December 1987.

[4] Robert P. Kennedy, S.A. Short, K.L. Mertz, F.J. Tokarz, I.M. Idriss, Maury S. Power and K. Sadigh. *Engineering Characterization of Ground Motion - Task I: Effects of characteristics of free-field motion on structural response*. NUREG/CR-3805, Vol. 1. U.S. Nuclear Regulatory Commission, February 1984.

[5] A. Arias. *A Measure of Earthquake Intensity*. Seismic Design for Nuclear Power Plants. MIT Press, Massachusetts Institute of Technology, Cambridge, MA, 1970.

[6] G.W. Housner. "Measures of Severity of Earthquake Ground Shaking." In *Proceedings of the U.S. National Conference on Earthquake Engineering*. Ann Arbor, Michigan, June 1975, pp. 25-33. Sponsored by the Earthquake Engineering Research Institute (EERI).

[7] Eduardo Miranda and Vitelmo V. Bertero. "Evaluation of Structural Response Factors Using Ground Motions Recorded During the Loma Prieta Earthquake." In SMIP91: *Proceedings of Seminar on Seismological and Engineering Implications of Recent Strong-Motion Data*. Sacramento, California, May 1991.

[8] Helmut Krawinkler, Aladdin Nassar, and Mohsen Rahnama. "Damage Potential of Loma Prieta Ground Motions." *Bulletin of the Seismological Society of America*. Vol. 8, No. 5, October 1991.

Table 1. Damage Measures and R Values for the UCSC and Saratoga, Loma Prieta Records

Record	Ductility	NHE
UCSC, Santa Cruz	3.27	8.54
Saratoga, Aloha Ave.	7.83	22.38

Record	R Factors for NHE=10
UCSC, Santa Cruz	4.32
Saratoga, Aloha Ave.	2.86

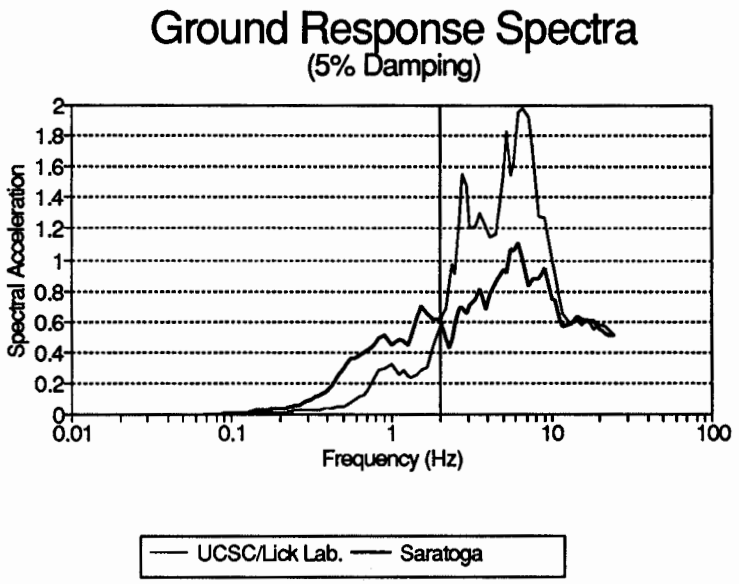

Figure 1. Ground response spectra for the UCSC/Lick Lab, Santa Cruz (0°) and Aloha Ave., Saratoga (0°) recordings from the Loma Prieta earthquake. (Each record has been scaled to have 0.5g PGA).

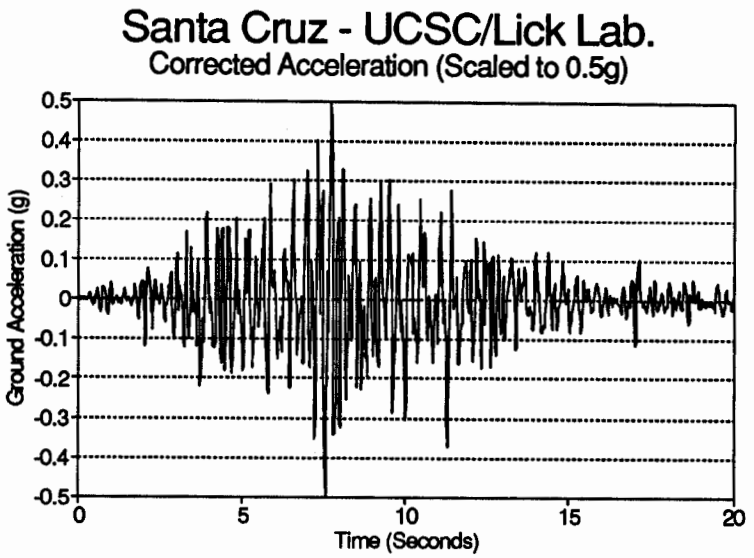

Figure 2. Acceleration time history of the UCSC/Lick Lab, Santa Cruz, (0°) ground motion recording from the Loma Prieta earthquake, scaled to 0.5g PGA.

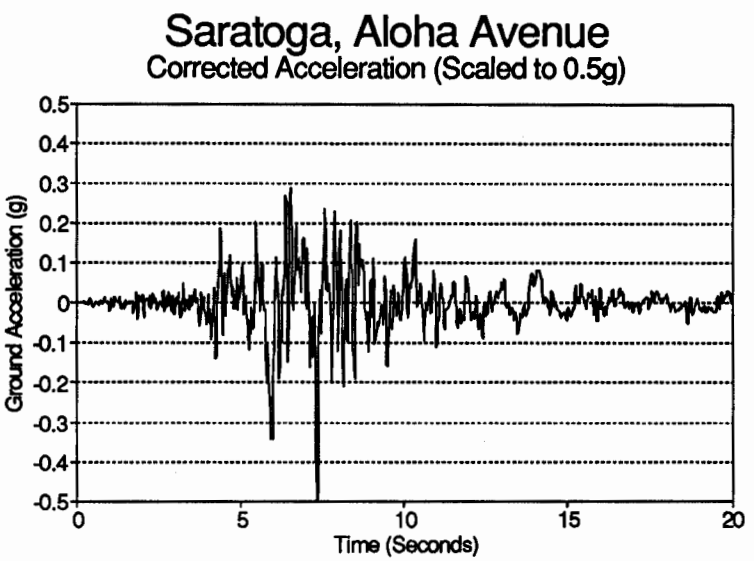

Figure 3. Acceleration time history of the Aloha Ave., Saratoga (0°) ground motion recording from the Loma Prieta earthquake, scaled to 0.5g PGA.

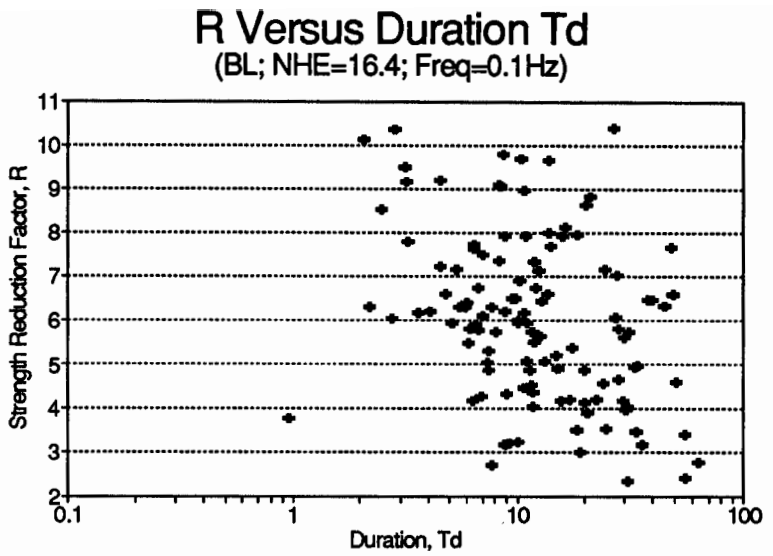

Figure 4. Inelastic strength reduction factor R versus duration T_D based on bilinear behavior and frequency of 0.1 Hz.

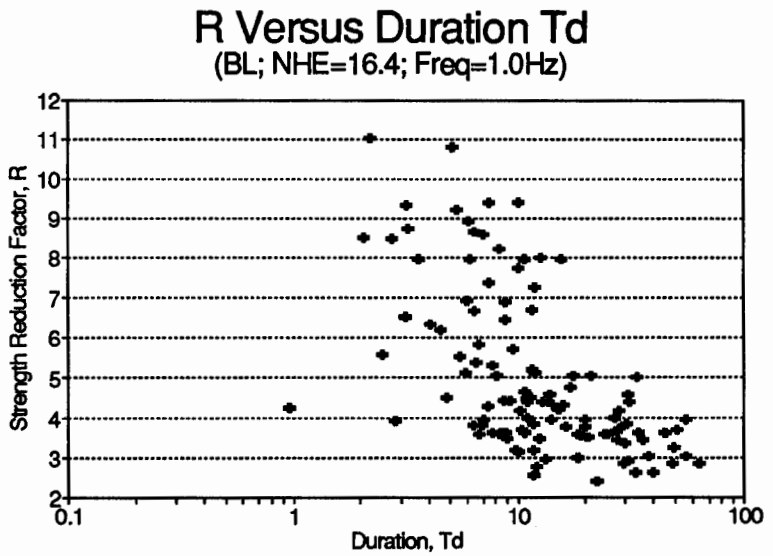

Figure 5. Inelastic strength reduction factor R versus duration T_D based on bilinear behavior and frequency of 1.0 Hz.

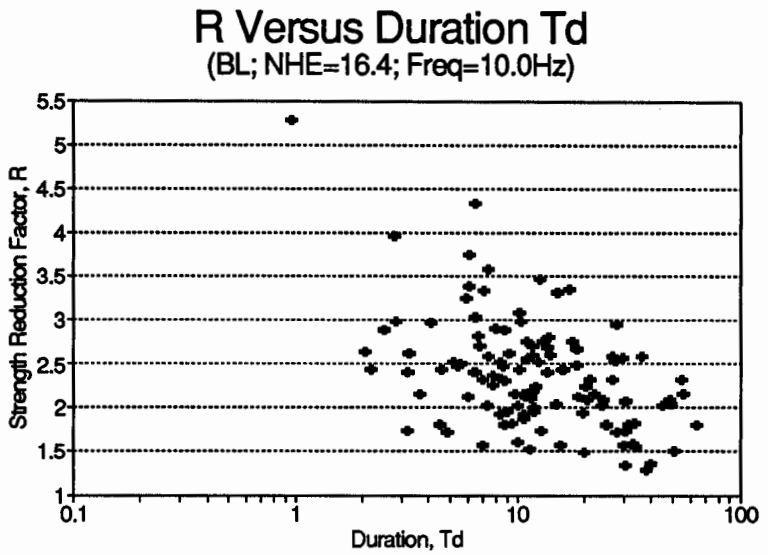

Figure 6. Inelastic strength reduction factor R versus duration T_D based on bilinear behavior and frequency of 10.0 Hz.

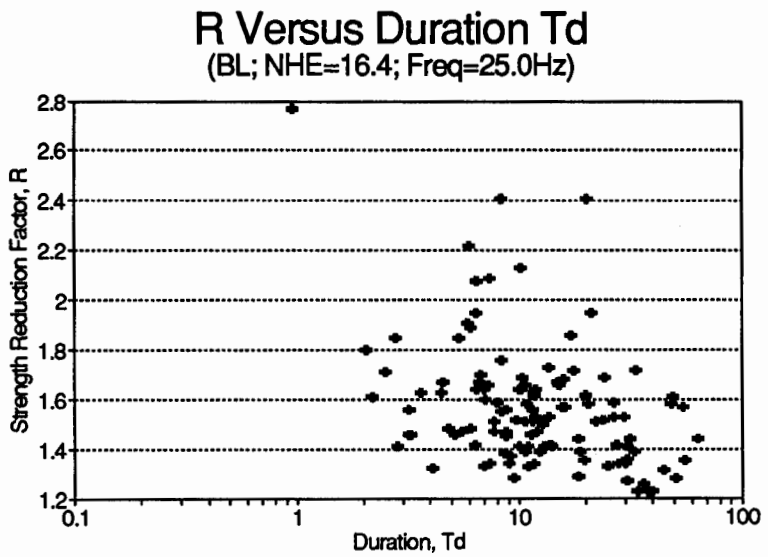

Figure 7. Inelastic strength reduction factor R versus duration T_D based on bilinear behavior and frequency of 25.0 Hz.

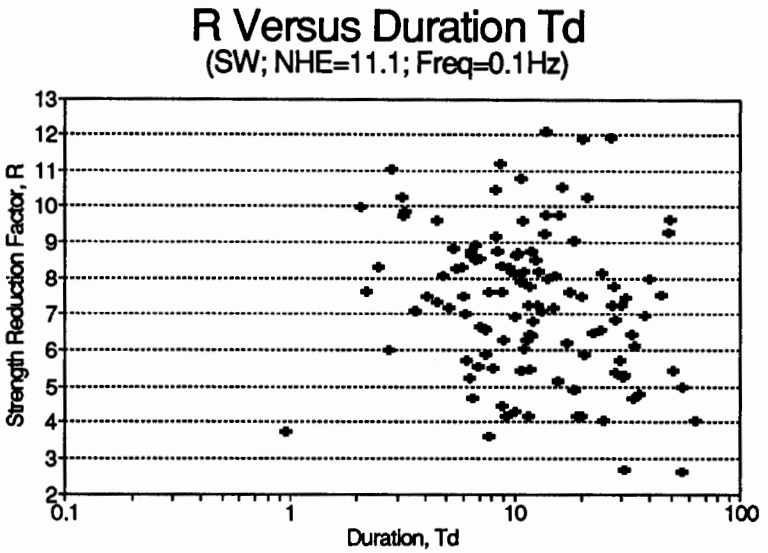

Figure 8. Inelastic strength reduction factor R versus duration T_D based on shear-wall behavior and frequency of 0.1 Hz.

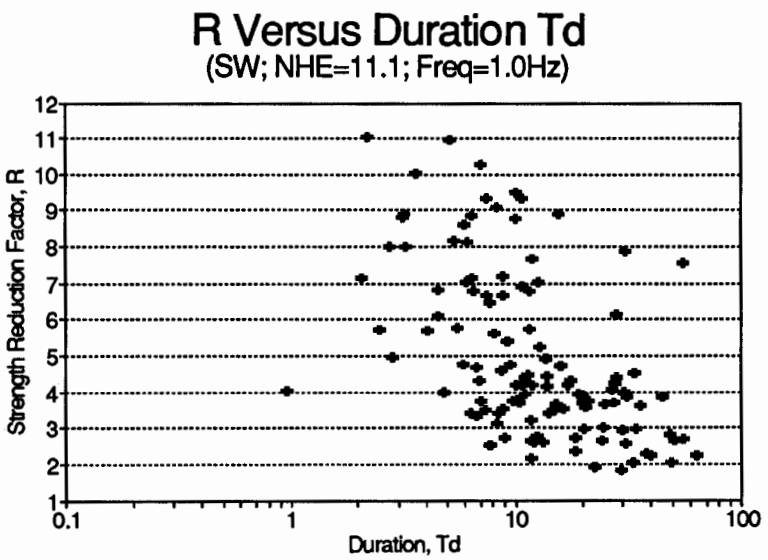

Figure 9. Inelastic strength reduction factor R versus duration T_D based on shear-wall behavior and frequency of 1.0 Hz.

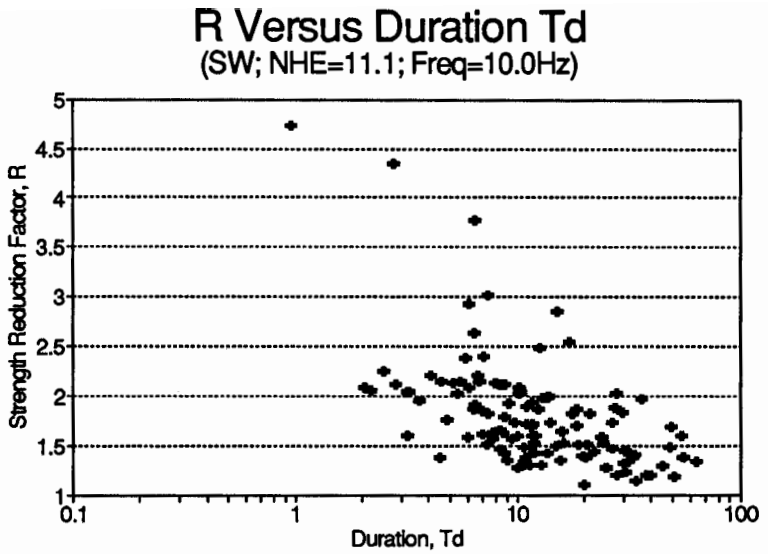

Figure 10. Inelastic strength reduction factor R versus duration T_D based on shear-wall behavior and frequency of 10.0 Hz.

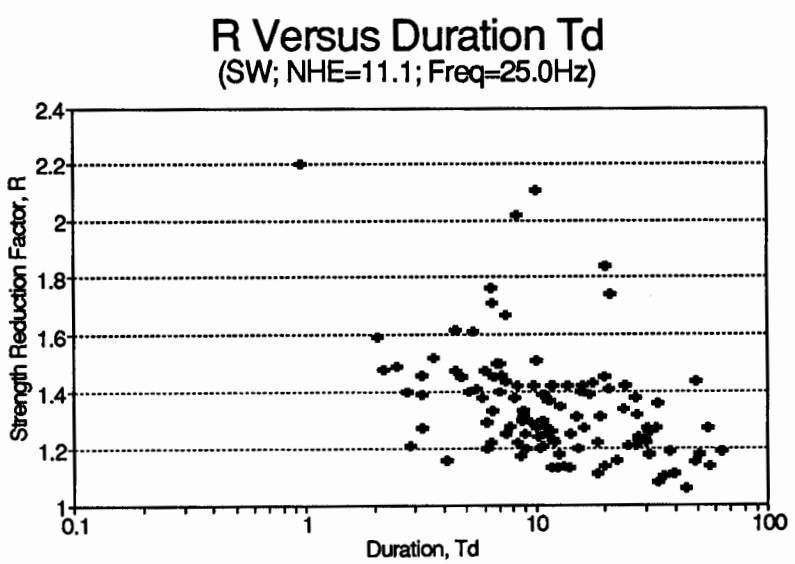

Figure 11. Inelastic strength reduction factor R versus duration T_D based on shear-wall behavior and frequency of 25.0 Hz.

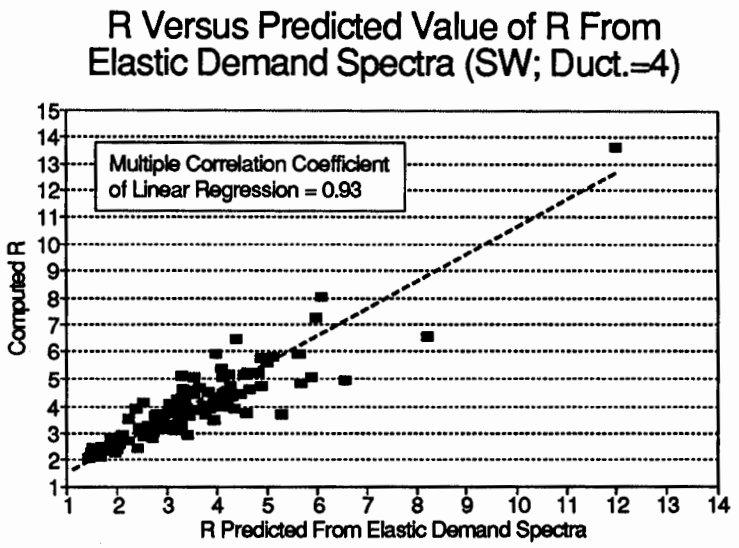

Figure 12. Prediction of R from elastic spectral demand ratios alone, without explicit consideration of motion duration (shear-wall behavior, ductility ratio of 4.0)

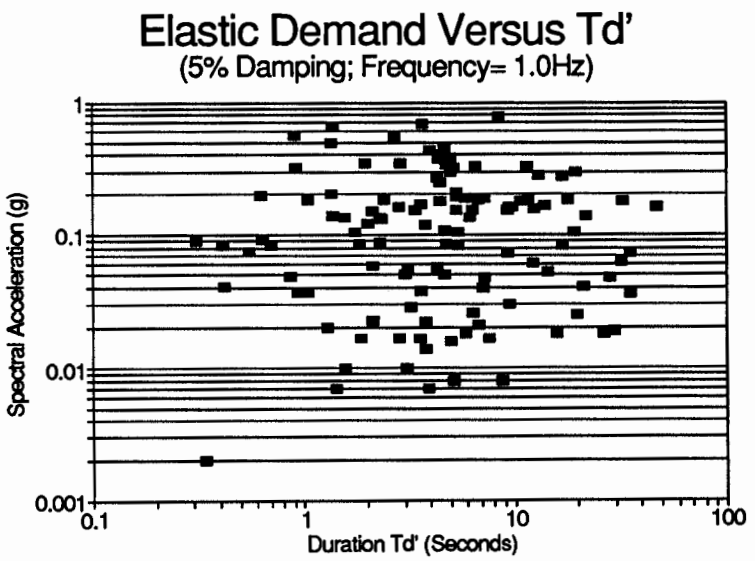

Figure 13. Elastic strength demand versus duration T'_D for freq uency of 1.0 Hz.

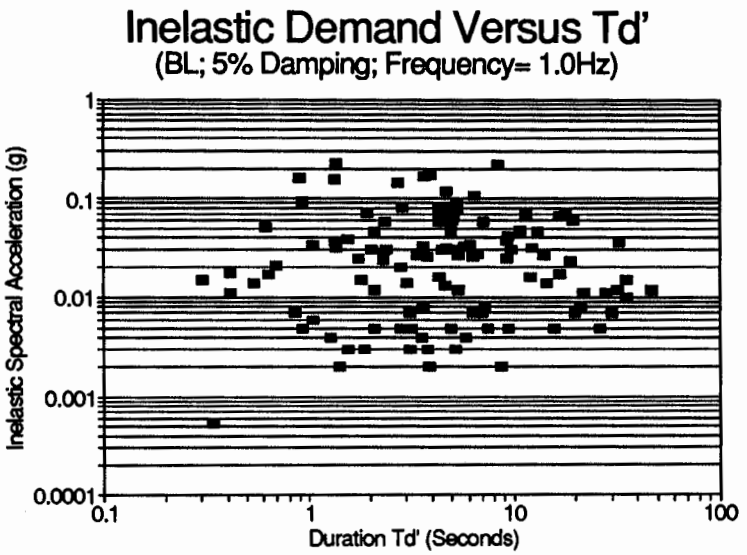

Figure 14. Inelastic strength demand versus duration $T'_{D,}$ based on bilinear behavior and frequency of 1.0 Hz.

VERIFICATION OF A METHOD FOR ESTIMATING OVERTURNING MOMENT OF TALL BUILDINGS

Ma-Chi Chen

Collaborative Engineering Service, Cupertino

ABSTRACT

The objective of this research is to verify a newly developed method ,time delay (TD) method, for earthquake analysis using data from strong motion instrumentation program (SMIP), and then applying the TD method to calculate overturning moment of structures. The TD method incorporates the attribute of finite wave speed propagating upward into the structure.

One detailed 3-dimensional model and nine simplified 2-dimensional models were used for study. The effects on the overturning moment due to the use of TD method varies depending upon the predominant period of the input earthquake motions and the structures. The concept of the TD method is verified with the measured data.

INTRODUCTION

The traditional equation of motion for single degree-of-freedom (SDOF) and multiple degree-of-freedom (MDOF) lumped-mass systems under earthquake excitation has the same general form (Refs.,1 to 4):

$$M\ddot{u} + C\dot{u} + K u = P_{eff}(t) \qquad (1)$$

For a ground motion acceleration time history $\ddot{u}_g(t)$, the effective earthquake force vector of a MDOF system for a multistory building as shown in Figure 1 is

$$P_{eff}(t) = - M \{ 1 \} \ddot{u}_g(t) \qquad (2)$$

In which {1} is a column vector of ones. Mathematically this implies that at a certain instant ti, all the masses in the structure are subjected to the same ground excitation without any spatial variations. Conceptually this means that the incident earthquake wave propagates throughout the entire structure instantaneously with an infinite speed, once it reaches the base of the structure. As is well known in classic mechanics, disturbances into a system of Eq.(1) will propagate with a finite speed into the solution domain, instead of an infinite speed as used in the traditional approach (Ref.5).

The TD method incorporates the attribute of finite wave speed in the forcing function, $P_{eff}(t)$ The following sections describe the conceptual and mathematical development, verification procedures using SMIP data, and application to calculate overturning moment of structures.

CONCEPTUAL AND MATHEMATICAL DEVELOPMENT

The two basic principles, equilibrium and compatibility, are the basis for the development of structural mechanics. When they are applied alone without wave propagation, the principles can be satisfied both locally and globally. With wave propagation, they are satisfied only locally or in the subdomain of solution and not necessarily the whole global domain of solution at certain instant.

An example, to illustrate the principle of compatibility coupling with wave propagation, is the motion of a hanging flexible string as shown in Figure 2(a). When one moves the string horizontally but slowly enough so not to generate any vibratory motion, as shown in Figure 2(b), an amount of translation at the top end produces the same amount of translation along the whole string at the same instant (i.e., there is rigid body motion compatible with the boundary condition of the string.). This apparently trivial case is actually of importance, since this is in fact the basis for developing the temporal variation only forcing function of earthquake motion, i.e. Eq.(2).

As one moves the string just fast enough to produce a swinging motion (or 1st mode of vibration), as shown Figure 2(c), the time variation of the input motion along the string is such that the spatial distribution of the effective force along the string is almost uniform. The characteristics of the motion are predominantly first mode. This therefore would be the case if one assumes a "temporal variation only" forcing function, and the motion of the hand is close to the fundamental mode of the string.

As one then vibrates the string faster , one can easily see the travelling of the motion along the string, and that the string vibrates in higher modes,as shown in Figure 2 (d). This last demonstration illustrates the main idea of this paper that a transient disturbance to the system will travel with finite speed, and the portion nearest the disturbance moves first followed very closely by the other portions. Namely, the top portion is subjected to force first, while the lower portions are subjected to the same force later. At a certain instant, there is nonuniform distribution of inertia force along the string. Therefore, the forcing function does not only have temporal variation but also spatial distribution.

Mathematically, the inertia force generated due to the wave motion thus has both spatial distribution and temporal variation. This spatio-temporal forcing function therefore has the following form in contrast to Eq.(2)

$$P(x,t)=M\ddot{U}g(x-ct) \qquad (3)$$

Pictorially, the existing method assumes the ground motion propagates through the structure instantaneously, and the masses at various levels are subjected to the same force simultaneously, as shown in Eq.(2) and in Figure 3(a). With the inclusion of finite

wave speed, the masses at various levels are not subjected to the same force simultaneously as shown by Eq. (3), and in Figure 3(b).

VERIFICATION PROCEDURES FOR THE TD METHOD

A total of 10 buildings with earthquake records from California Strong Motion Instrumentation Program (CSMIP) were selected for study. One of the buildings was selected for detailed modeling and nine others were used for simplified analysis. The 10 buildings selected for analysis are listed in Table 1.

The building selected for detailed analysis was modeled as a 3-dimensional model as shown in Figure 4. All major structural frames were included; floor diaphragm was assumed rigid. A time-history analysis was then performed. This building was also modeled as a simplified model similar to Figure 1. The other nine buildings were modeled using simplified models only, similar to Figure 1. Time history analyses were performed for each building.

APPLICATION TO OVERTURNING MOMENT CALCULATION

The calculation of overturning of a building at its foundation seems simple, but is actually one of the most perplexing problems in design practice. Since the inclusion of seismic loads into the UBC (Ref.6), the overturning problem has been treated from a very conservative manner to relatively liberal manner, then adjusted to be conservative again as shown in Figure 5.

Initially the overturning stability problem was treated statically same as the lateral wind load with the requirement of overturning moment to be one-half (1/2) of the resisting moment. In the 1961 UBC, a J factor was introduced to reduce the overturning in recognition of the participation of higher modes of vibration. However, the code still required a comparison of wind and seismic overturning effects to select the governing load. In recent years, the requirement for comparing the wind load with seismic load for overturning effects was dropped. This essentially eliminates the requirement for overturning moment to be less than two-third (2/3) of the resisting moment. As the code stands today, UBC-91 does not require the overturning moment to be less than the resisting moment at the foundation-soil interface.

The new proposed TD method was used to study the overturning moment at the base of structure by comparing the maximum overturning moment (OTM) calculated from time history analyses with and without time delay.

SUMMARY OF FINDINGS

Table 2 summarizes the results in terms of predominant period of the input earthquake motions, the fundamental period of the structure, the displacement at the top of structure and overturning moment at the base of structure with and without time delay.

The results of the studies indicate that the input motion considering time delay tends to excite the higher modes of the structure. However, the effects on structural response depend on several factors including the relationship between the predominant period of the input earthquake motions and the structure, stiffness and height of the structure. Following are some major observations:

1. Where the predominant period of the input earthquake motions is close to the higher modes of structure, the structural response will be predominantly in the higher modes. For the case of 47-story office building, the input earthquake has the predominant period of 1 second, and the major response at 44th floor is also 1 second, Figures 6 (a) and (b). According to the analysis, this is close to the 3rd mode of the structure. The frequency analysis and the time history at the 44th floor indicate a fundamental building period of about 5.2 sec, Figure 6(c). For this case, the TD method shows higher responses than method without time delay, as shown in Case 5 of Table 2 and Figure 6. Case 1, the S.F. 18-story, has similar result.

2. Where the period of the input earthquake motions is close to the fundamental period of the structure, the TD method shows lower responses than method without time delay as shown in Cases 2,3,4,6 and 10 of Table 2.

3. Where the buildings damping ratio is unusually high, both the responses with and without time delay are very close. The Long Beach City Hall indicates a high damping ratio of 17%. This can also be seen from the damped-out roof displacement in the trailing portion of the recorded time history shown in Figure 7.

CONCLUSIONS

1. The TD method considering input motion with time delay tends to excite the higher modes of the structures. Therefore, the overturning moment calculated using the fundamental mode may be too conservative for high rise structures.

2. Where the predominant period of the input earthquake motion is in the higher modes of the structure, the TD method shows higher responses than method without time delay.

3. Where the period of the input earthquake motion is close to the fundamental period of the structure,the TD method shows lower responses than method without time delay.

4. For highly damped structures, the effects of time delay are negligible.

5. The TD method considering input forcing function with time delay is conceptually and mathematically sound. It effects may be significant depending on the predominant period of the input earthquake motion and the characteristics of the structures.

REFERENCES

1. Housner, G.W.,and McCann,G.D., "The Analysis of Strong-motion Earthquake Records with Electric Analog Computer,"Bull., Seism. Soc. Am., Vol.39, No.1, Jan. 1949, P47-57

2. Clough, R.W., and Penzien, J., "Dynamics of Structures," McGraw Hill, Inc., 1975

3. Newmark, N.M., Rosenblueth, E.,"Fundamentals of Earthquake Engineering,"Prentice-Hall,Inc. 1971

4. Chopra, A.K., "Dynamics of Structures, A Primer," Earthquake Engineering Research Institute, 1980

5. Crandall,S.H.,"Engineering Analysis," McGraw Hill Book Company, New York, 1956

6. ICBO, "Uniform Building Code," 1937 to 1988 Ed.

TABLE 1

Buildings elected For Analyses

Name	EQ Record	PGA AT Base	Lateral Force Resisting System
1. S.F. 18-Story Commercial bldg.	Loma Prieta Oct.17, 1989	0.17g	Steel Moment-Resisting Frame
2. San Jose 13-Story Government Office Building	"	0.11g	Steel Moment-Resisting Frame
3. San Bruno 6-Story Office Building	"	0.14g	Concrete Moment -Resisting Frame
4. So. S.F. 4-Story Hospital	"	0.14g	Concrete shear wall at 1st. fl. Steel Moment-Resisting Frame above
5. S.F. 47-Story Office Building	"	0.13g	Steel Moment-Resisting Frame
6.San Jose 3-Story Office Building	"	0.10g	Concrete Moment-Resisting Frame and Shear Walls
7. Burbank 6-Story Calif. Federal Saving Building	Whitter, Oct. 1,1989	0.22g	Steel Moment Resisting Frame
8. Long Beach City Hall 15-Story	"	0.06g	Steel Moment-Resisting Frame
9. Long Beach Harbor Administration Building, 7- Story	"	0.07g	Steel Frame
10 Van Nuys Holiday Inn, 7-Story	"	0.17g	Concrete Moment-Resisting Frame

TABLE 2

SUMMARY OF RESULTS

Case	EQ Predominant Periods Second	Structural Periods Second	Displacement At Roof		O.T.M. Ratio Delay / No Delay
			W/o Delay	W/ Delay	
1. S.F. 18-Story	1.0 and less	$T_1 = 2.4$ $T_2 = 0.67$	3.3"	3.7"	1.47
2. San Jose 13-Story	2.8 and less	$T = 2.3$	16.6"	15.3"	0.89
3. San Bruno 6-Story	1.3 and less	$T = 0.85$	2.19"	2.05"	0.92
4. S.F. 4-Story	0.7 and less	$T = 0.7$	3.8"	4.4"	0.85
5. S.F. 47-Story	1.0 and less	$T_1 = 5.2$ $T_2 = 2.0$ $T_3 = 1.2$	3.1"	6.4"	1.19
6. San Jose 3-Story	1.0 and less	$T = 0.65$	3.1"	2.9"	0.86
7.Burbank 6-Story	1.0 and less	$T = 1.30$	1.57"	1.57"	1.06
8. Long Beach 15-Story	1.5 and less	$T = 3.2$	1.4"	1.53"	1.02
9. Long Beach 7-Story	1.0 and less	$T = 1.4$	1.2"	1.3"	0.97
10. Van Nuys 7-Story	0.5 and less	$T = 1.2$	1.19"	1.14"	0.97

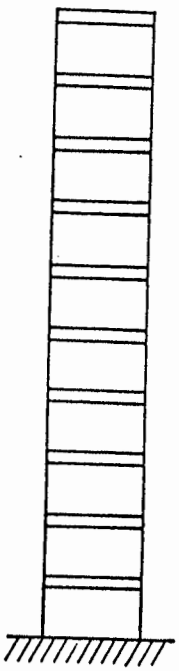

FIGURE 1 MDOF SYSTEM

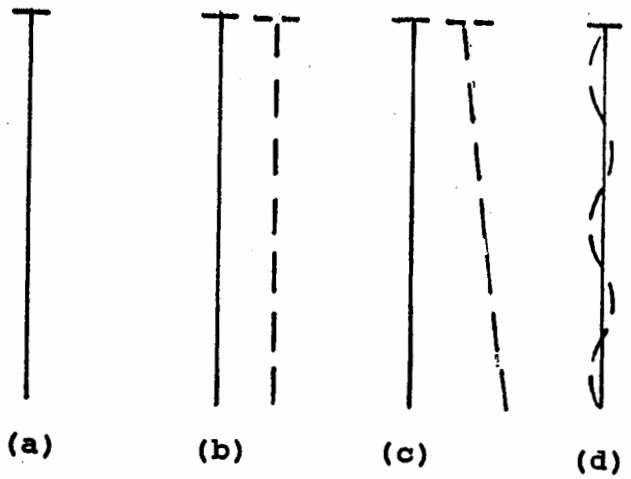

FIGURE 2 VIBRATION OF FLEXIBLE STRING

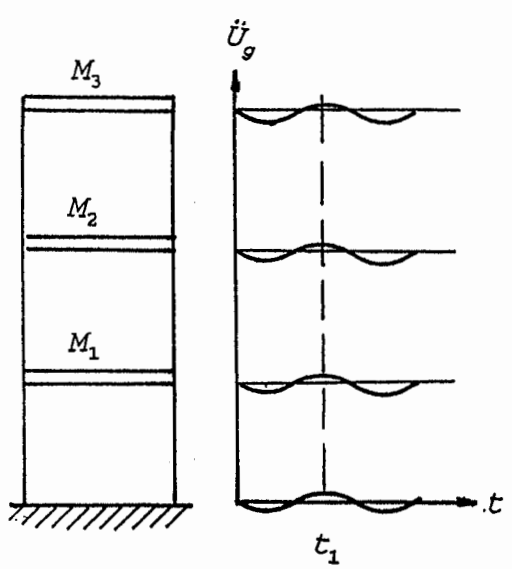

(a) INFINITE SPEED

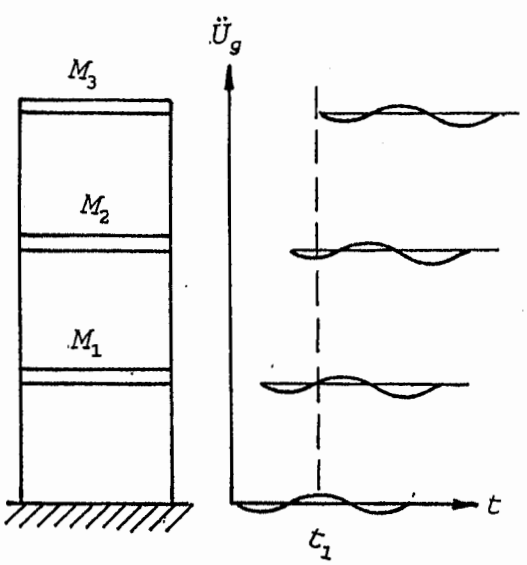

(b) FINITE SPEED

FIGURE 3 INPUT MOTION PROPAGATION WITH INFINITE AND FINITE SPEED

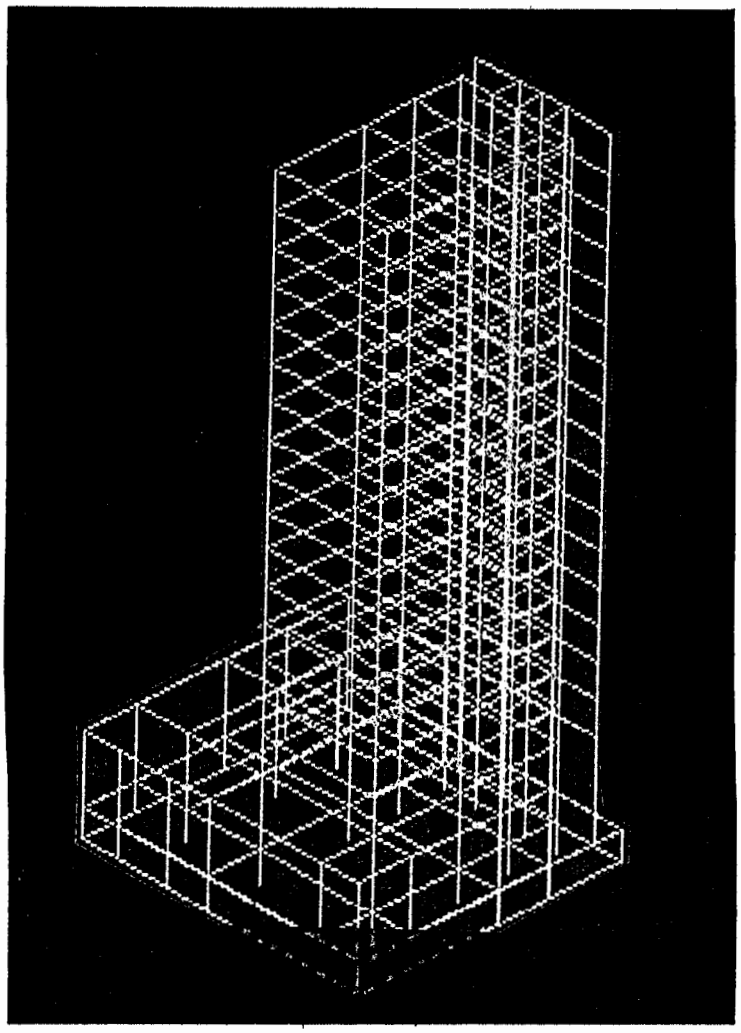

FIGURE 4 3-D MODEL OF S.F. 18-STORY BUILDING

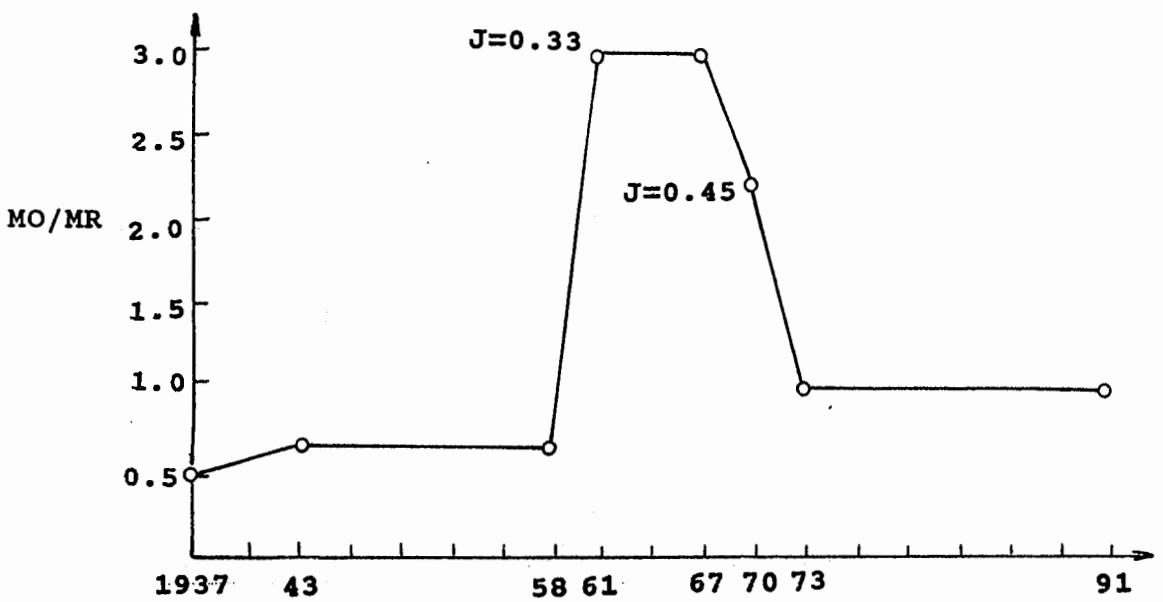

FIGURE 5 RATIO OF MO/MR, UBC

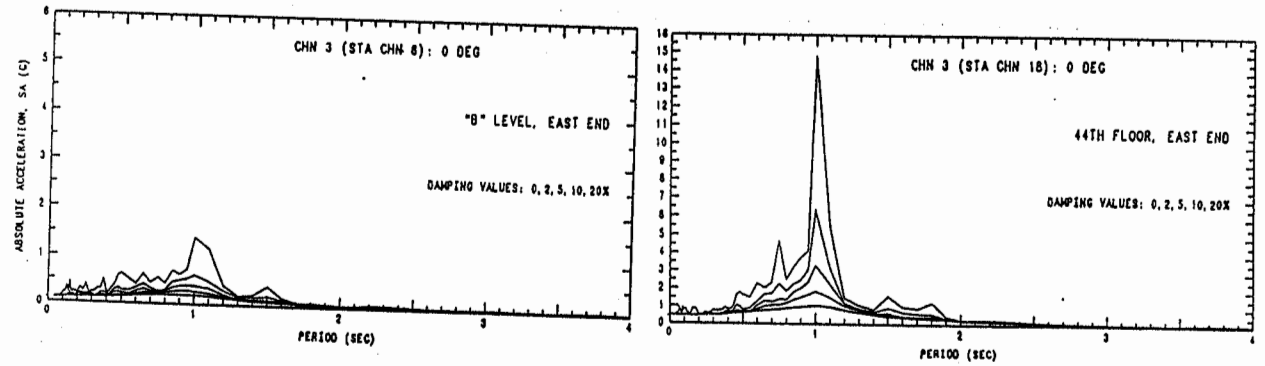

(a) RESPONSE SPECTRA AT "B" LEVEL (b) RESPONSE SPECTRA AT 44TH FL.

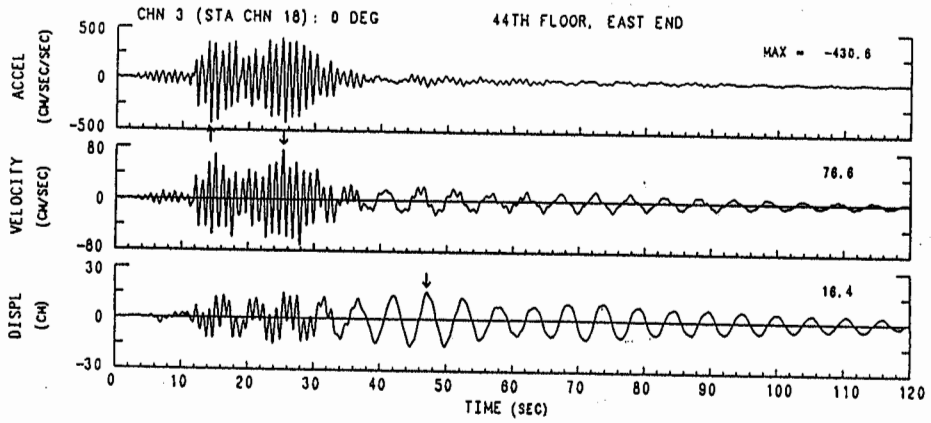

(c) TIME HISTORY AT 44TH FL.

FIGURE 6 RECORDED DATA- S.F. 47-STORY OFFICE BLDG. (FROM OSMS 91-07)

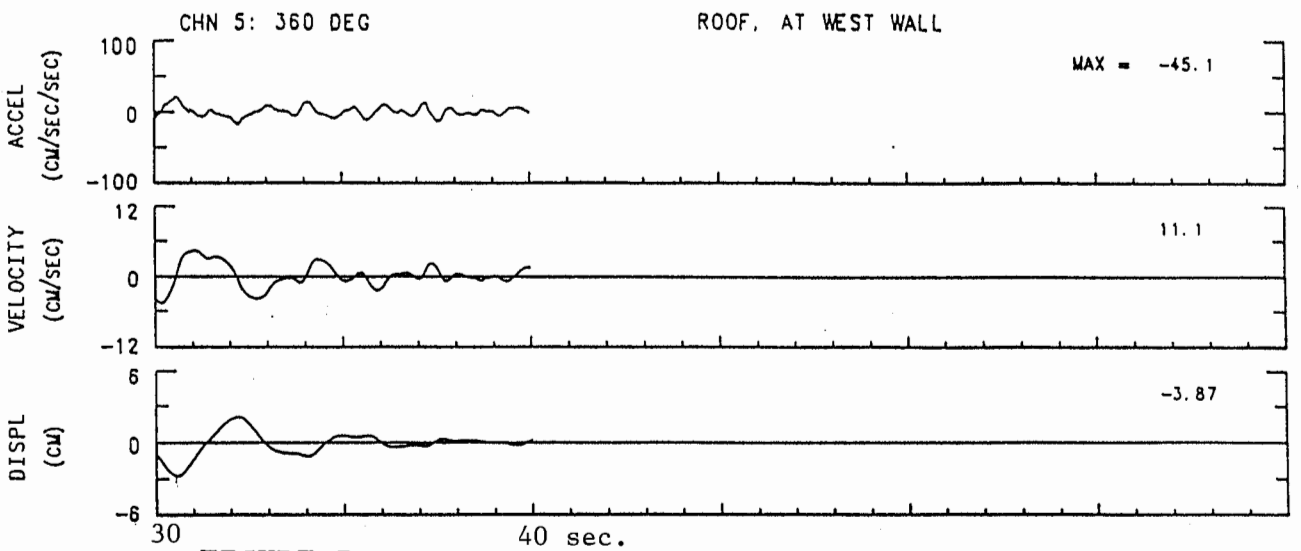

FIGURE 7 RECORDED DATA- LONG BEACH CITY HALL (FROM CSMIP)

EFFECT OF RELATIVE DISPLACEMENTS BETWEEN ADJACENT BRIDGE SEGMENTS

Kazuhiko Kasai[1], Wen D. Liu[2], and Van Jeng[1]

ABSTRACT

This paper presents the results of a study on the responses of the San Juan Bautista 101/156 Separation Bridge instrumented by the California Division of Mines and Geology under its Strong Motion Instrumentation Program (CSMIP). The bridge experienced three significant earthquakes as follows: 1979 Coyote Lake earthquake (before seismic retrofit), 1984 Morgan Hill earthquake (after seismic retrofit), and 1989 Loma Prieta earthquake. The recorded seismic responses during the three earthquakes are analyzed and correlated with theoretically predicted responses. Adjustments of structural parameters and modeling concept to achieve satisfactory correlations are discussed. Important characteristics of relative motions between adjacent bridge segments are explained based on the records and analyses. Comments are also given regarding the performance of cable restrainers for seismic damage mitigation.

INTRODUCTION

During an earthquake, adjacent bridge segments often vibrate out-of-phase due to their different dynamic characteristics as well as their support conditions that allow the relative motions between the segments. The out-of-phase motion of the bridge segments leads to two types of relative displacement problems: First, when the distance between the segments increases and exceeds the range of support provided by either abutment, column, or hinge seat, a falling of bridge deck could occur. Many of the catastrophic loss-of-span type failures of bridges in the past earthquakes have been attributed to this effect. Second, when the distance between the segments decreases, pounding (i.e., collision) of the segments could occur and severe impact force could develop at the contact region. Unlike the case for buildings [2], this typically results in localized damage of the bridge segments.

To prevent the serious loss-of-span failure from occurring in either a new or an existing bridge, one could provide restrainers to limit the increase of distance between the segments. During the period from 1974 to 1985, such practice was performed on all existing California bridges by the California Department of Transportation (CALTRANS) as a part of its Phase 1 seismic retrofit project. The seismic behavior of such a retrofitted bridge appears to be extremely complex due to the participation of the cable restrainers in the relative displacement responses of adjacent bridge segments. Clearly, it is necessary to understand the relative motion between adjacent segments including the effects of cable restrainers and develop a rational relative motion analysis method in order to mitigate the catastrophic collapse of either a new or an existing bridge in a future severe earthquake. The study presented herein performs correlative seismic analyses for a bridge structure that has experienced moderate excitation in 1979 before cable restrainers installation, and in 1984 after cable restrainers installation as well as significant excitation in 1989. The objectives are: (1) to study the degree to which practical computer analysis models can accurately capture actual bridge seismic relative displacement time history response (with and without restrainers); (2) to discuss the complexities involved in bridge relative displacement problems that must be considered to evaluate the seismic performance of a bridge.

DESCRIPTION OF STUDY BRIDGE

Fig. 1 shows the San Juan Bautista 101/156 Separation bridge considered in this study. This multispan, steel plate girder structure is one of the first bridge instrumented (in 1977) by CSMIP. The

[1] Assistant Professor, Dept. of Civil Engineering, Illinois Institute of Technology, Chicago, IL 60616.
[2] Associate, Imbsen and Associates Inc., Sacramento, CA 95827.

bridge is a skewed bridge of total length 326 feet with five bents, and it consists of separated segments. The bent span varies from 33.5 to 68.5 feet. The bridge was constructed in 1958 and was retrofitted with cable restrainers in the early 1980's. The bridge is well instrumented having 12 acceleration recording channels at Bents 3 to 5 (see the layout in Fig. 1). These channels are oriented in two orthogonal directions (i.e., normal to the bent and tangential to the bent), respectively. The structure consists of six simple spans supported on seat-type abutments and five two-column bents (Fig. 1). The abutments and bents are skewed at 34.8 degrees with respect to the bridge centerline. The superstructure is composed of five steel girders composite with a reinforced concrete deck (Fig. 2). Each of the five girders is supported on fixed bearing at one end of the span which provide a pinned connection, and an expansion (rocker) bearing at the other end. The expansion (rocker) bearings are oriented to allow the movement in the longitudinal direction of the bridge. Across the girders, intermediate diaphragms normal to the bridge centerline provide lateral support to the girders. At both ends of each span, end diaphragms are provided along the direction parallel to the bent (i.e., 34.8 degrees skewed from the normal).

The simple supports at the abutments and bents are made of metal bearings. The fixed bearing assembly is used at the northern end of each girder to provide a pinned connection. An expansion bearing assembly provides a roller connection at the southern end of each girder. Fig. 3 shows how these bearings were oriented on the concrete pedestals at abutments and bents to provide for thermal and shrinkage movements along the longitudinal axis of the bridge. The connections of these bearings are vulnerable to seismic damage. Once bearing connections failed, the deck may be unseated from the bent support. During the early 1980's, Caltrans retrofitted the bridge with longitudinal, transverse and vertical restrainers at various bearing locations and also extended the length of concrete pedestal at abutments. Fig. 4 shows the detail of longitudinal restrainers connecting the girder to the bent cap.

ANALYSIS OF RECORDED SUPPORT MOTIONS

The study bridge experienced three significant earthquakes as follows: (1) 1979 Coyote Lake earthquake (before cable restrainers addition); (2) 1984 Morgan Hill earthquake (after cable restrainers addition); and (3) 1989 Loma Prieta earthquake (after cable restrainers addition). The two earlier earthquakes originated from Calaveras fault, while the recent Loma Prieta earthquake originated from the San Andreas fault. The bridge is almost directly on top of the San Andreas fault.

Support Accelerations. - The recorded peak accelerations during the past three earthquakes are summarized in Table 1. The bridge shaking was the most severe during Loma Prieta earthquake, and was the least severe during Morgan Hill earthquake. The frequency contents of the two-directional support accelerations are obtained by calculating the smoothed Fourier amplitude spectra (FAS), and are shown in Fig. 5(a) for the three earthquakes. Loma Prieta earthquake caused extremely low frequency accelerations in both normal and tangential directions. Figs. 5(b) and (c) show the resulting response spectra with damping ratio = 5%. Note the extremely large displacement response of a low frequency system (Fig. 5(c)) subjected to the Loma Prieta motion.

Support Displacements. - Fig. 6(a) compares the displacement histories (integrated by CSMIP) of Bent 5 support due to the three earthquakes. By performing frequency analyses (Fig. 6(b)), it was found that the support motions have about 2.5 to 3.5 sec. period in the two orthogonal directions for both Coyote Lake (see also Ref. 4) and Morgan Hill earthquakes. However, a longer period of about 6 sec. was found (see Figs. 6(a) and (b)) for the support displacement due to Loma Prieta earthquake, which is consistent with the trend discussed earlier for the support acceleration (Fig. 5(a)). Further, the magnitude of the displacement is extremely large as compared with those from the other earthquakes. This striking difference might be attributed to the fact that the bridge is located on and parallel to the San Andreas fault and it is only about 6 miles away from the south end of the rapture of Loma Prieta earthquake. Transforming the recorded motion shown in Fig. 6(a), it was observed that the maximum ground displacement in the direction perpendicular to the earthquake wave moving direction is about 3 times the maximum ground displacement in the other direction. Similar trends were observed in many of the accelerometers located elsewhere during the Loma Prieta event (see Ref. 3).

Relative Support Displacement. - The difference between the displacements of two distant supports (i.e., relative support displacement) has been long interested by engineers due to its importance in designing expansion joint and support length of long span structures such as bridges and pipelines. The recorded acceleration data at Bent 5 (Channels 1 to 3) and Bent 3 (Channels 10 to 12), 107 feet apart from each other, are used to study this. The relative support displacement histories between the two supports plotted in Fig. 6(c) as well as frequency analyses indicate that, due to the effect of travelling seismic wave, their periods are similar to the ones observed above for the single support displacement. Also, the relative support displacements tend to be large when the support displacements are large (compare Figs. 6(a) and (c)). Hall and Newmark [1], as well as Wilson [4] attempted to estimate the maximum relative support displacement by using the concept of simple wave propagation theory. The data obtained from the present study would be useful to verify the accuracy of their methods. Hall and Newmark's method obtains the ground strain averaged over the distance between the supports by dividing the maximum ground velocity due to earthquake divided by the typical ground wave velocity [1]. The maximum relative support displacement is obtained as a product of the strain and the support distance. On the other hand, Wilson's method obtains the displacement by taking the difference of sinusoidal ground motions at the two supports having the vibration phase that is calculated as the distance between the supports divided by the typical ground wave velocity. This method requires the knowledge on the maximum displacement of the support. These two methods are applied to estimate the maximum relative displacement between the respective supports of Bents 3 and 5, assuming the ground wave velocity of 1000 ft/sec. It is found that Wilson's method gives significantly unconservative results, and that Hall and Newmark's method provides very close results. As will be discussed below, the magnitudes of the relative support displacements of the study bridge during the 3 earthquakes are comparable to the maximum displacement of the deck measured with respect to the support. This is mainly due to the very short period and corresponding small deformation of the bridge. Thus, in similar cases, maximum relative support displacement becomes as important as the deformation of the bridge for the relative motion problem of the bridge adjacent segments.

ANALYSIS OF RECORDED SUPERSTRUCTURE MOTIONS

Basic Structural Dynamic Characteristics. - In order to study the vibration frequency contents of the study bridge, transfer functions as well as Fourier amplitude spectra are generated from the records of the channels located at the superstructure. Fig. 7 contrasts the frequency contents of the response of Channels 4 and 5 located at the top of Bent 5 subjected to Coyote Lake earthquake and Loma Prieta earthquake (Fourier amplitude spectrum normalized to its maximum value was used for each earthquake). Fig. 7 essentially indicates the significantly higher fundamental vibration frequencies of the bridge in both normal and tangential directions during Loma Prieta earthquake as compared to the Coyote Lake event. Additional analyses using the Morgan Hill earthquake records were also conducted, and same trend was observed. The dynamic characteristics of the bridge apparently changed prior to Morgan Hill earthquake. The dominant frequency in the direction normal to bent changed from 3.1 Hz to about 4.5 Hz (during Loma Prieta earthquake), and tangential to bent from 5.5 Hz to either 6 or 7 Hz. According to the record, a retrofit work of the bridge with cable restrainers was completed before the Morgan Hill earthquake, and it might be the reason for this significant frequency change. It also should be noted that the bridge response after the retrofit seems to contain a variety of significant frequency contents, suggesting a complex nonlinear response resulting from frequent change of the structure stiffness during the earthquakes.

Impulsive Accelerations. - The significant change in frequency contents observed above for the entire duration of earthquake is further investigated by closely examining the acceleration time history of Channel 8 at the bottom of Span 4 (Fig. 1). The location is sensitive to pounding between the adjacent decks or pulling of the cable restrainers. As seen from Fig. 8(a), during Coyote Lake event the the acceleration had essentially the same frequency contents before (i.e., from 3 to 4 sec.) and during (i.e., from 4 to 5 sec.) it reached the peak, indicating that there was no significant impact in the vicinity of the channel (compare the normalized FAS taken from 3 to 4 sec. and from 4 to 5 sec., respectively). In contrast, Figs. 8(b) and (c) show that significant changes in the frequency contents before and during the

occurrence of the acceleration peak resulted. For example, see the acceleration history in Fig. 8(c) showing significant increase in the frequency of the acceleration during 3 to 4 sec., as well as the corresponding normalized FAS. The above analyses conducted for Channel 8 were repeated for other neighboring channels, and the evidence of impact (somewhat less significant than recorded by Channel 8) was also found. These impulsive accelerations indicate the occurrence of pounding or pulling during Morgan Hill and Loma Prieta earthquakes, as will be illustrated analytically.

Structural Displacement.- It should be noted that the relative displacement between the two structures is the sum of the difference of their support displacements (i.e., relative support displacement) and the difference of their structural displacement measured with respect to the ground (i.e., relative structure displacement). In order to see the contribution of the relative support displacement to the relative displacements between adjacent segments of the bridge, the maximum magnitudes of these responses were compared using Channels 4 and 8 (i.e., relative displacement between the Span 4 and Bent 5). It is found that the relative support displacements are of significant magnitudes for estimating the relative displacements, mainly due to extremely large ground motions developed as well as small deformation of the bridge during the Loma Prieta event. This, however, will not be the case if the structure has larger structural period, and its displacement is large.

ANALYTICAL MODELING OF STUDY BRIDGE

Basic Structural Model and Parameters. - Three-dimensional models of the bridge were developed which accounted for the skewed supports at abutments and bents, expansion joint discontinuities, and foundation flexibility effects. Across the deck-to-deck and deck-to-bent connections, the following features need to be considered: stretching of cable restrainers in the longitudinal direction which tie the deck to the bent cap; and impacting between adjacent spans. The analyses were carried out using the nonlinear time-history dynamic analysis program, IAI-NEABS. Bent columns and cap members are modeled using beam elements. For concrete column members, an effective moment of inertia equal to 40% of the gross-section moment of inertia was used to account for the nonlinear behavior. The composite deck (reinforced concrete deck supported on five steel girders) was modeled using a series of beam elements in a line. At the end of each span, a series of zero-length hinge subelements were used to model the multiple bearing supports and the effect of transverse diaphragm. Each girder bearing is idealized individually as a zero-length hinge element with proper translational stiffness coefficients. At the end of the span, the upper ends of the five subelements are connected to the centroid of the deck superstructure through the master-slave transformation. (This is an approximation typically used in modeling the two-dimensional deck geometry with a single line element and to preserve the primary end restraint, i.e., moment release along the direction of the bent.). If the transverse diaphragms and the composite deck form a rigid constraint, the entire deck will act as a unit and tend to rotate about an axis parallel to the bent. For this case, the above approximation is correct. At the other extreme, assuming no effect of diaphragms, individual girders will tend to bend about an axis normal to the bridge centerline and the concrete deck will experience two-way bending. In reality, the actual behavior is probably between these two extreme cases. For simplicity in practical modeling needs, the rigid-link assumption is usually adopted. Raleigh damping magnitude was used to achieve 5% damping ratio for the principal vibration modes of the bridge.

In seismic response analysis, the important structural responses are typically in the column. The adequacy of the above modeling assumption can be verified by the response measurement at the bent cap. Based on soil boring data, the following foundation stiffness coefficients for bent footing and abutments were calculated by the soil engineer assisting the present study: For footing, the coefficients are 1.84×10^5 k/ft, 1.40×10^5 k/ft, 1.46×10^5 k/ft, 4.95×10^6 k/ft/rad, 2.29×10^6 k/ft/rad, in the order of vertical, tangential to bent, normal to bent, strong axis rotational, and weak axis rotational directions, respectively. Similarly, for abutment stiffness, they are 1.70×10^6 k/ft, 1.26×10^5 k/ft, 1.4×10^5 k/ft, 5.01×10^7 k/ft/rad, and 1.92×10^6 k/ft/rad. In a previous study [4], it was concluded that in order to match the measured response due to the 1979 Coyote earthquake, the abutment longitudinal stiffness has to be reduced to 3000 kip/ft. We will reexamine this assumption. In the nonlinear model, cable restrainers are modeled as

tension-only member (with or without initial cable slack) and the impact between adjacent deck are monitored at the two edges of the deck across the bent cap using gapped and compression-only stiffness properties. A seat gap of 0.3 inch was used.

CORRELATIVE STUDY (COYOTE LAKE EARTHQUAKE)

Linear dynamic analyses by the direct integration method were conducted for this event. The three-component records obtained at the base of Bent 5 (Channels 1, 2, & 3) were used as the uniform support excitation. The spatial variation of ground motion was shown to be small.

Model I. - Initially, rocker bearings at each bent are modeled as roller supports. Horizontal and vertical responses are decoupled. The resulting response correlations were not very good. The FAS of the calculated and measured total acceleration response at the top of Bent 5 is shown in Fig. 9 for the normal direction. As shown in the figure, it overestimated the normal response at 2 Hz, but did not capture the measured frequency at 3 Hz. In addition, the tangential response of the bent at 5 to 6 Hz were not predicted well by this model.

Model II. - Based on measured responses at deck and top of Bent 5, there was no significant difference (Fig. 10). This is an indication that the rocker bearings were "locked." The model was modified to reflect this observation, i.e., each span now is pinned at both ends to the supporting bents. To soften now this continuous system, the abutment stiffness in the direction normal to the bent is reduced to 14,000 kip/ft (from 140,000 kip/ft) which is still much higher than the value used by Wilson [4]. The modal frequencies for modes involving bent 5 are 3 Hz for the normal response and 6 Hz for the tangential response. Comparisons for time history and FAS of total accelerations are shown in Fig. 11 for channels 4, 8, 5, 6 and 9. Very close correlation was obtained at top of the bent for both normal and tangential responses. Both the frequency content and the amplitude are predicted very well. This is a strong indication that the modeling assumptions adopted for the deck superstructure and the skewed support are sufficiently accurate. Furthermore, during this earthquake, there was no evidence of impacting between adjacent decks. Based on the longitudinal shear and vertical reaction calculated at each girder rocker bearing, an equivalent friction of 0.4 can be established which is the resistance required to prevent rocker "rocking".

CORRELATIVE STUDY (LOMA PRIETA EARTHQUAKE)

As discussed earlier, during the Loma Prieta earthquake, there was high acceleration (0.94g) recorded on the deck (uncorrected data) which suggested impacting between adjacent spans might have occurred. Also, after the seismic retrofit, the effect of cable restrainers should be included in the model. To accommodate these aspects, the "locked" rockers on top of each bent were released and modeled with nonlinear elements which include Coulomb friction, cable restrainer (tension only with no slack), and impact. Based on measured responses at the bent, there is an apparent shift in the frequency content of the bent vibration in the normal direction (see Fig. 10). The frequency is now increased to 4 to 5 Hz. Similar observation was made for the Morgan Hill Earthquake. The tangential response of the bent remains essentially the same. Several factors could contribute to this: (1) compaction of bent foundation material; (2) effect of cable restrainers; and (3) impacting of adjacent spans. To assess the effects, nonlinear analyses were carried out.

The impacting between adjacent spans produces very high frequency oscillation of acceleration (up to 30 to 60 Hz) at the point of direct contact. Because of the skewed geometry, impacting occurred at one edge of the deck. The structural elements cannot transmit such high frequency motion. At the point of direct impact, the acceleration response has a very high amplitude and high-frequency oscillation. During earlier part of the time history, impacting also occurred. However, it occurred during the subdivision of the regular time step but bounced back at the end of the regular step. The effect of such impact was accounted for in the analysis. Fig. 12 showed the forces in the cable restrainers. At about 3 seconds, cable restrainers began engaged. However, the forces are generally low which is consistent with the

excitation level. At Bents 5 and 6, there is slight rotation of the deck which may be due to the edge-impact. The measured and calculated acceleration response at top of Bent 5 are shown in Fig. 13 for both normal and tangential directions. The essential features of the response were captured in the analysis. The correlation of calculated responses with measured responses during the Loma Prieta Earthquake was not as good as that obtained for the Coyote Lake Earthquake. This is due to the complex phenomenon of friction, cable stretching, and impacting.

CONCLUSIONS

Seismic response records of the study bridge subjected to the past three earthquakes were analyzed with an emphasis on the relative displacement characteristics of the bridge. The analyses indicate complex nature of the problem. Theoretical models were also developed and the responses of the analytical models were correlated with the recorded responses. Adjustments of structural parameters and modeling concept to achieve satisfactory correlations were discussed. The results indicate the need for further study on the modeling of bridge with cable restrainers subjected to pounding and pulling.

ACKNOWLEDGEMENTS

The study was supported through funding from the California Strong Instrumentation Program, California Division of Mines and Geology. The funding is gratefully acknowledged. The writers also thank Dr. Allaoua Kartoum at Imbsen & Associates, Inc., for his significant assistance in the study reported herein.

REFERENCES

1. Hall, W.J., and Newmark, N.M., "Seismic Design of Bridges -- An Overview of the California Seismic Design Criteria for Bridges", Proc., Earthq. Resist. of Hwy Bridges, ATC, November, 1979.
2. Kasai, K., Patel, D.J., Maison B.F., Jeng, V., and Patel, P., "A Study on Earthquake Pounding Between Adjacent Buildings", 6th Canad. Conf. Earthq. Eng., Toronto, Ontario, June 12-14, 1991.
3. Vidale, J.E., and Bonamassa, O., Strong Shaking Directions from the 18 October 1989 Loma Prieta Earthquake and Aftershocks in San Francisco and Oakland", Proc. SMIP91 Seminar on Seismological and Engrg. Implic.s of Recent Strong Motion Data, Scaramento, CA. May, 1991.
4. Wilson, J., "Analysis of the Observed Earthquake response of A Multiple Span Bridge", Ph.D Thesis, Calif. Inst. Tech., December 1984.

Table 1. Peak Accelerations Recorded at the Bent Supports of San Juan Bautista 101/156 Separation Bridge.

		Prior to Seismic Retrofit	After Seismic Retrofit with Cable Restrainers	
Channel		Coyote Lake 1979	Morgran Hill 1984	Loma Prieta 1989
1 N 2 Up 3 E	Bent 5, Base of Column	.12g .05g .08g	.07g .03g .04g	.15g .10g .14g
10 N 11 Up 12 E	Bent 3, Base of Column	.12g .06g .11g	-- .03g .04g	.12g .08g .14g

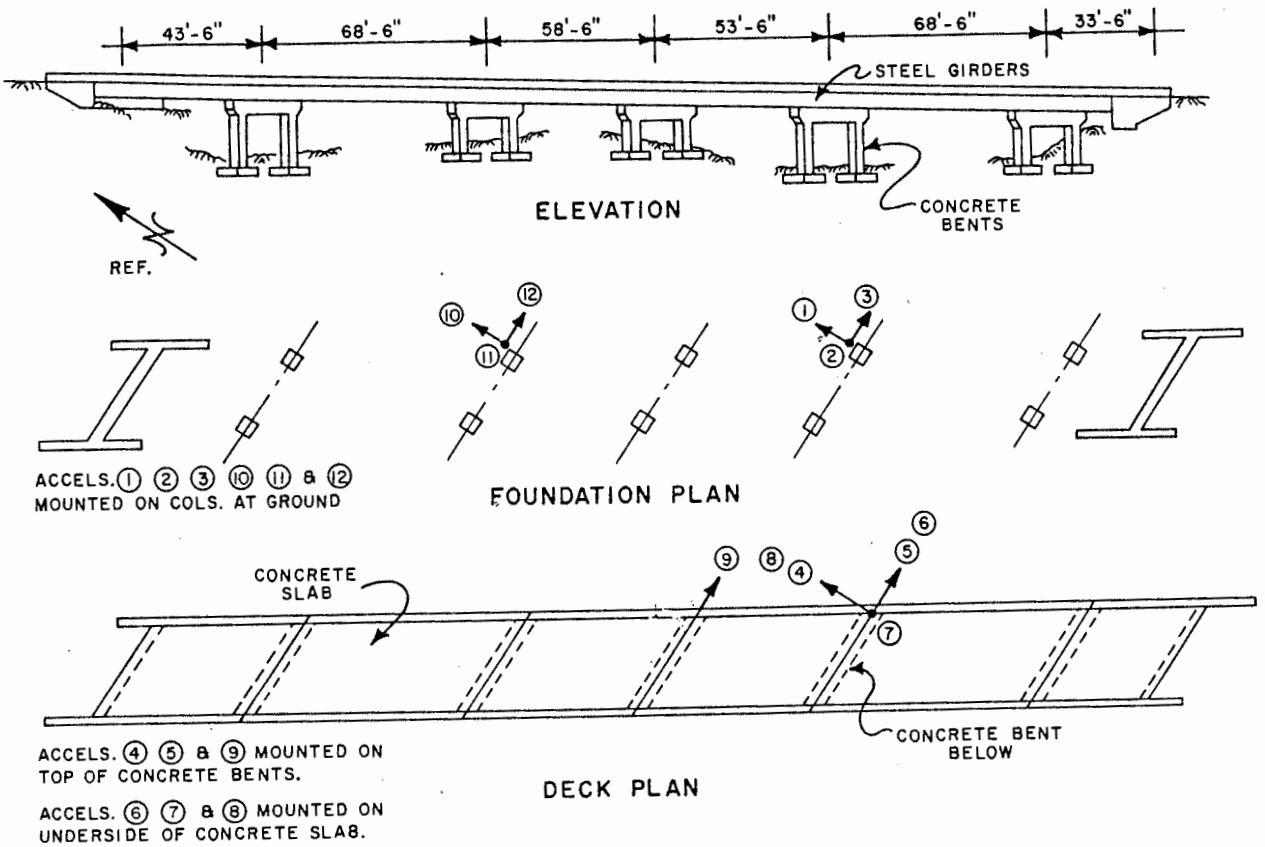

Fig. 1 Location and Orientation of Recording Channels at 101/156 Highway Separation Bridge.

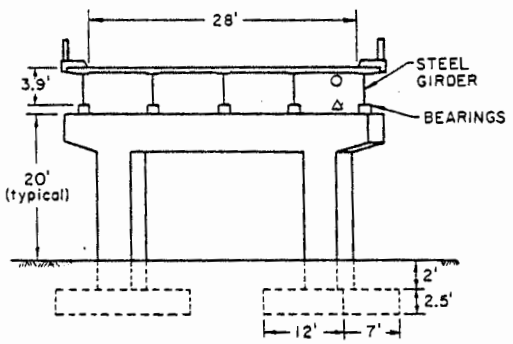

Fig. 2 Typical Bent Elevation.

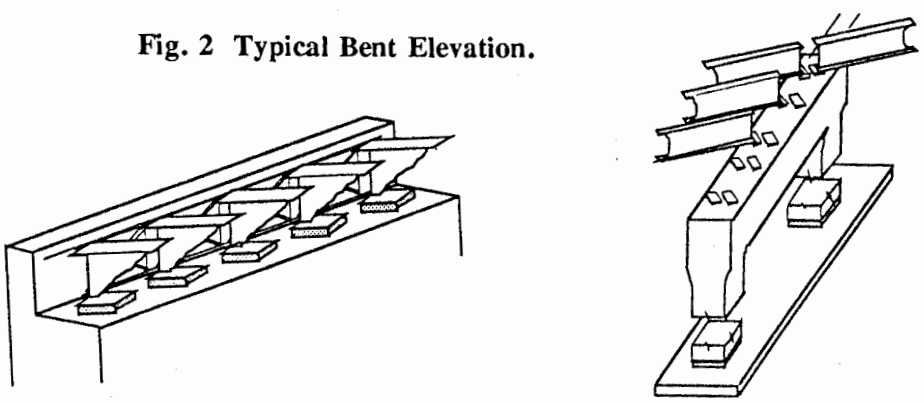

a) Abutment

b) Typical Bent

Fig. 3 Skewed Bearing Supports.

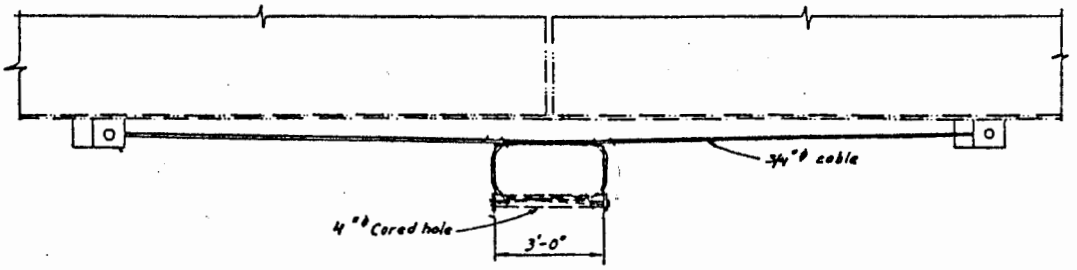

Fig. 4 Elevation View of Longitudinal Cable Restrainer.

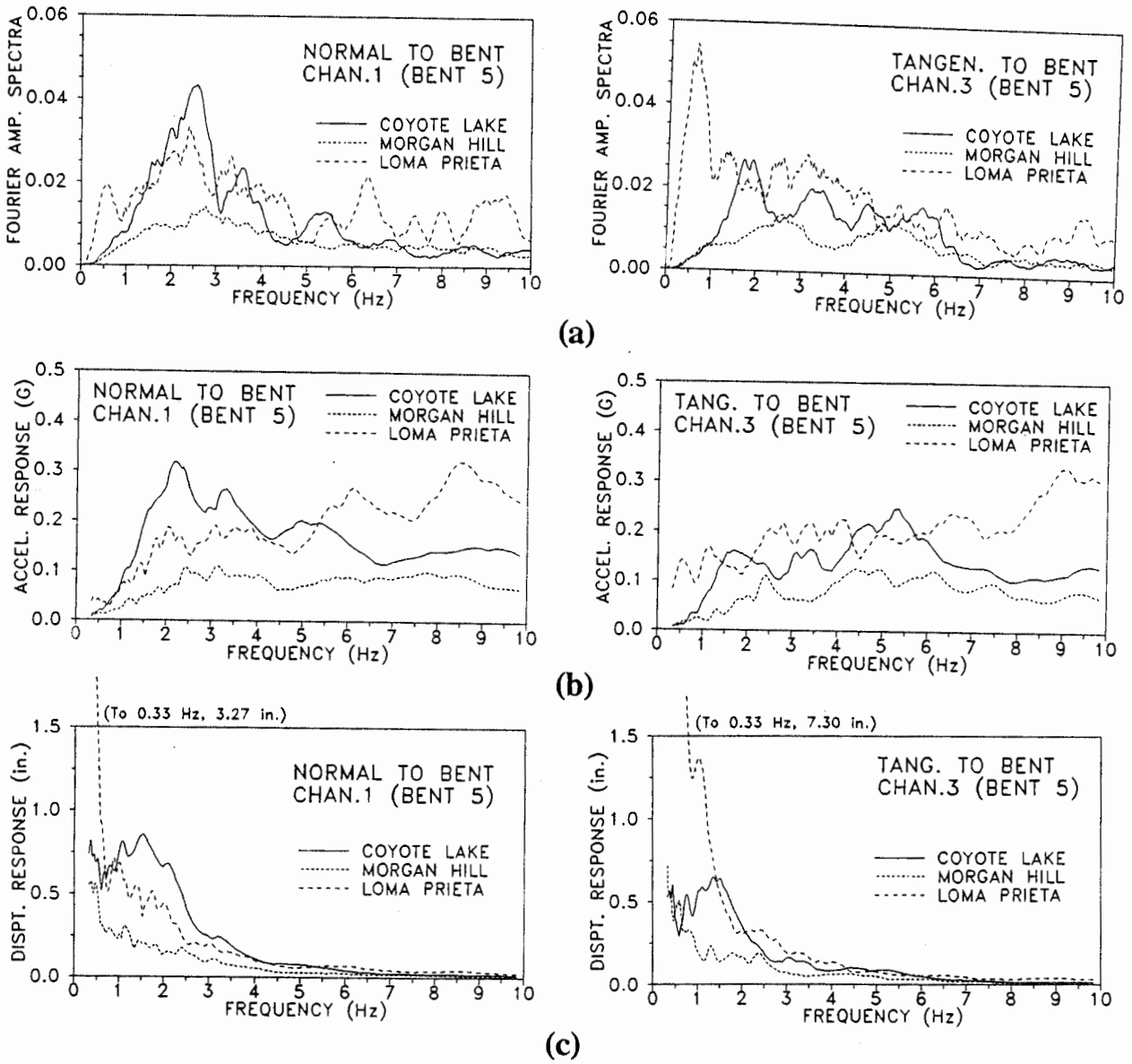

Fig. 5 Support Acceleration Frequency Characteristics : Calculated Magnitude of (a) Fourier Amplitude Spectra, (b) Acceleration Response Spectra, and (c) Displacement Response Spectra.

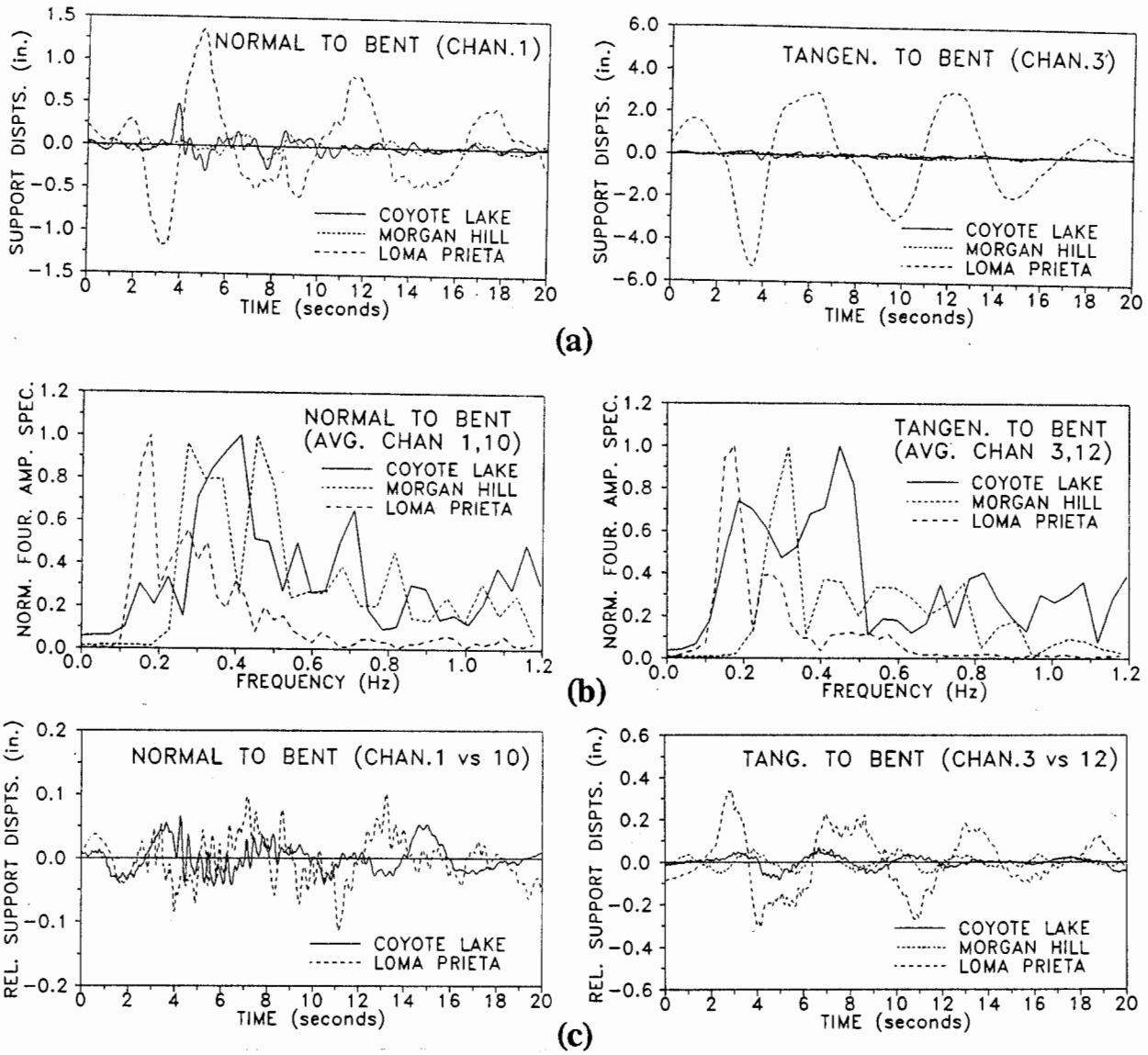

Fig. 6 Support Displacement Characteristics : (a) Support Displacement Histories, (b) Normalized Fourier Amplitude Spectra of Support Displacement, and (c) Relative Support Displacements Histories.

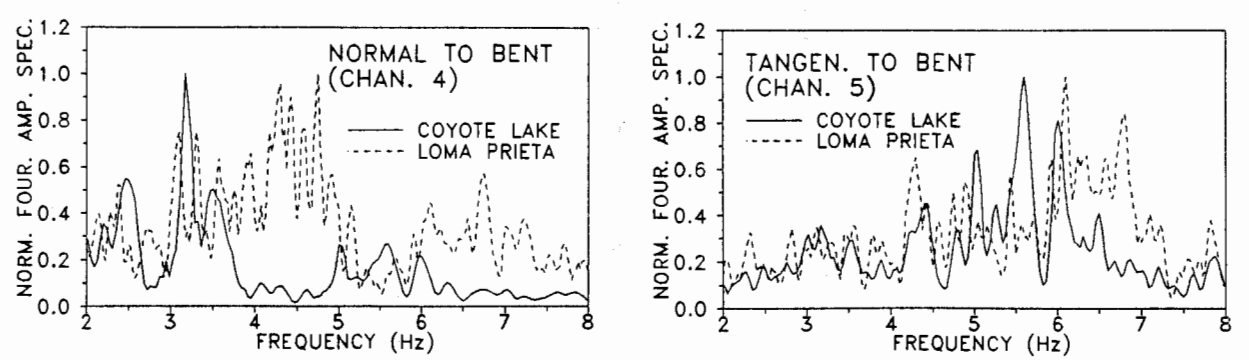

Fig. 7 Comparison of Structure Frequency Characteristics Before and After Retrofit.

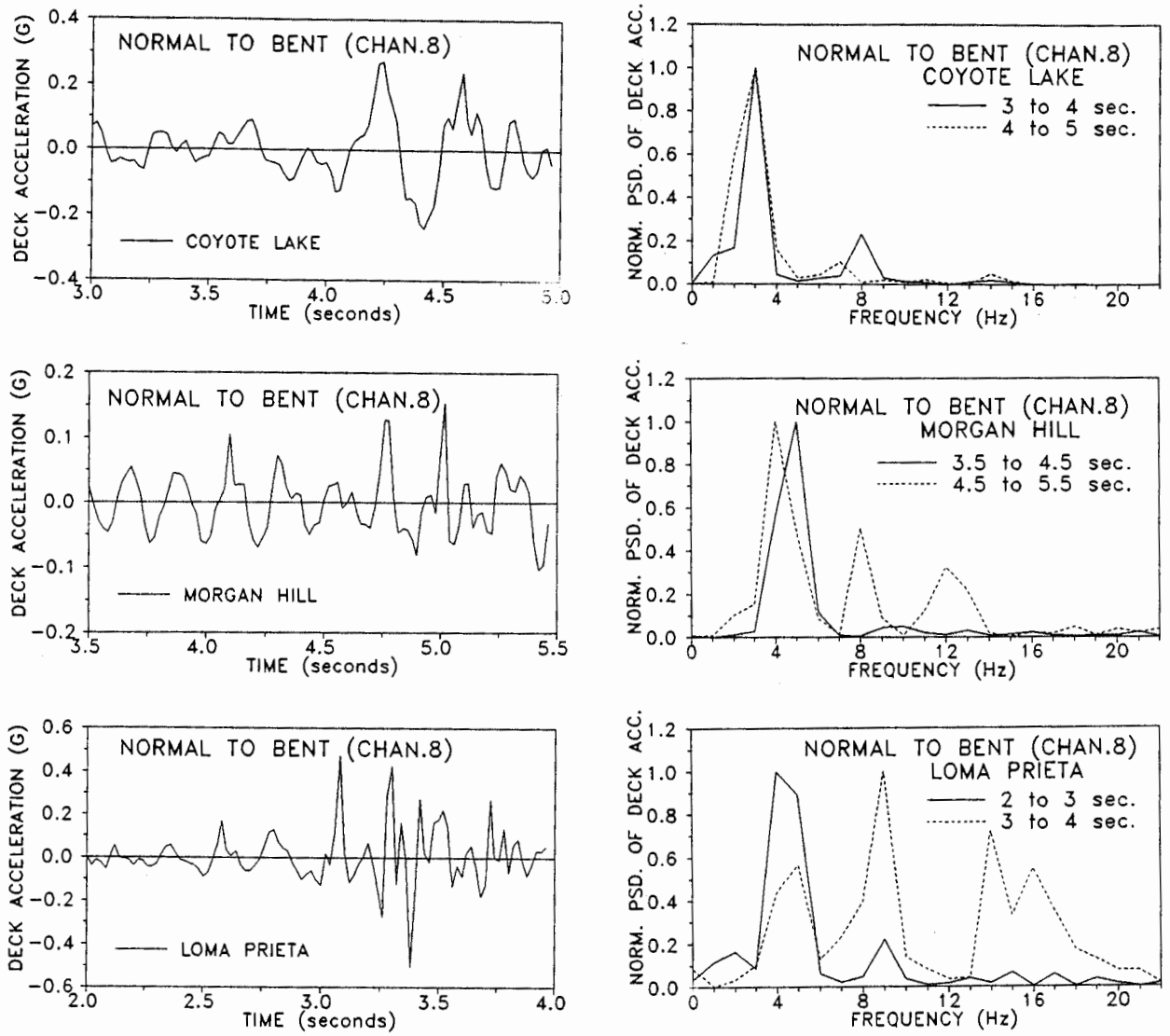

Fig. 8 Changes in Frequency Contents of Study Bridge During Earthquake.

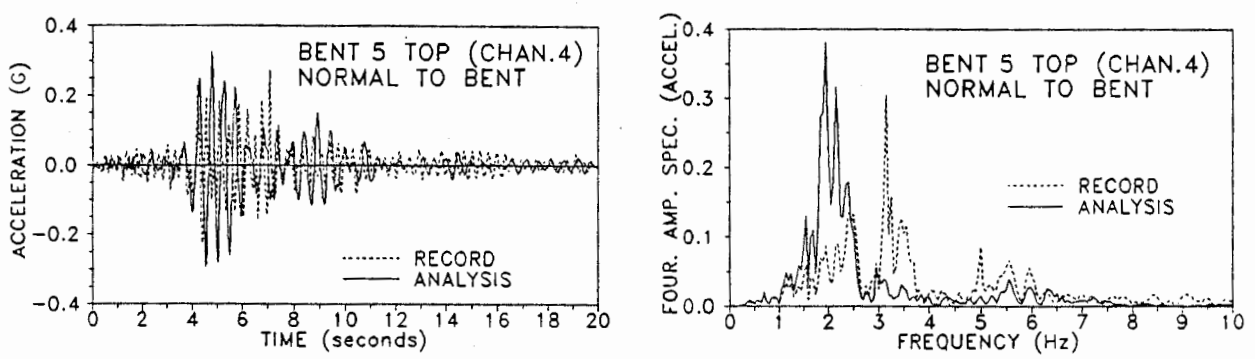

Fig. 9 Recorded and Calculated Acceleration Response (Model I) for Coyote Lake Earthquake.

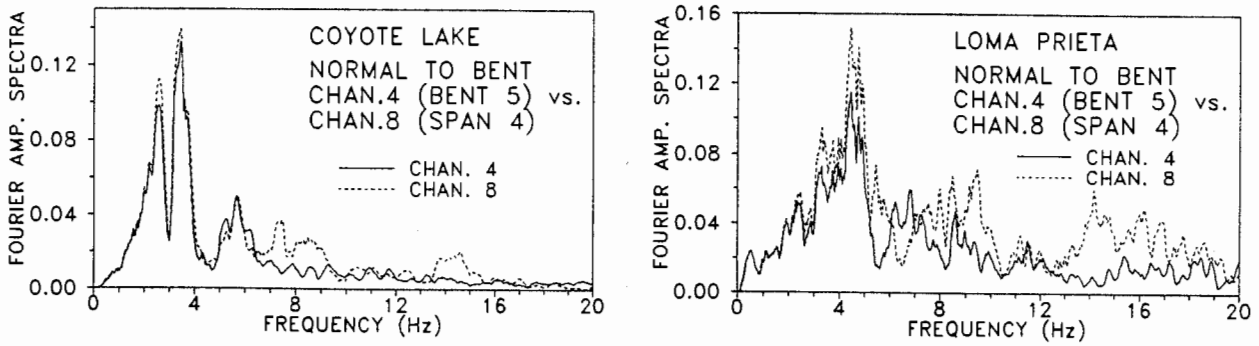

Fig. 10 Frequency Content Recorded for Coyote Lake Earthquake and Loma Prieta Earthquake.

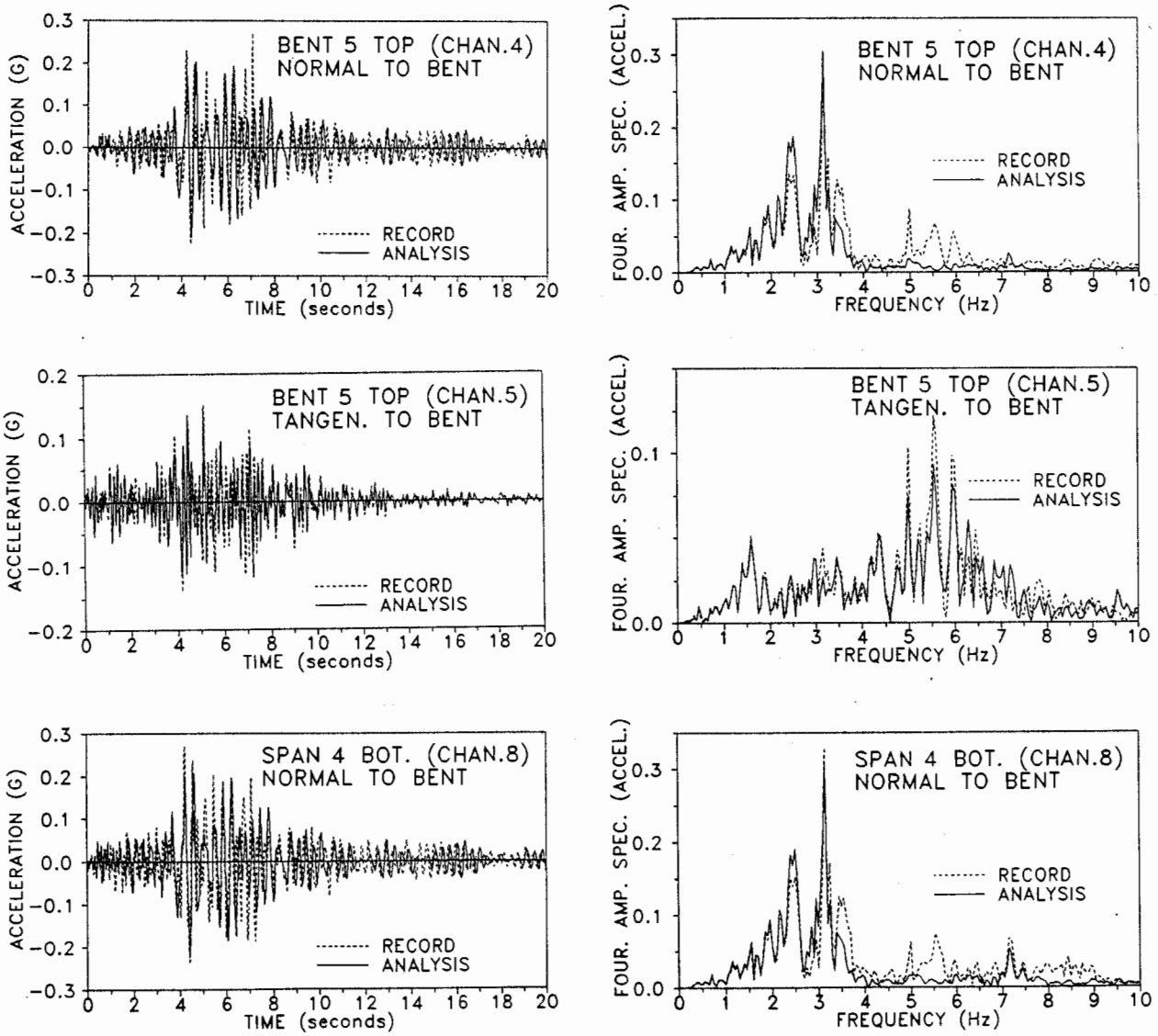

Fig. 11 Recorded and Calculated Acceleration Response (Model II) for Coyote Lake Earthquake.

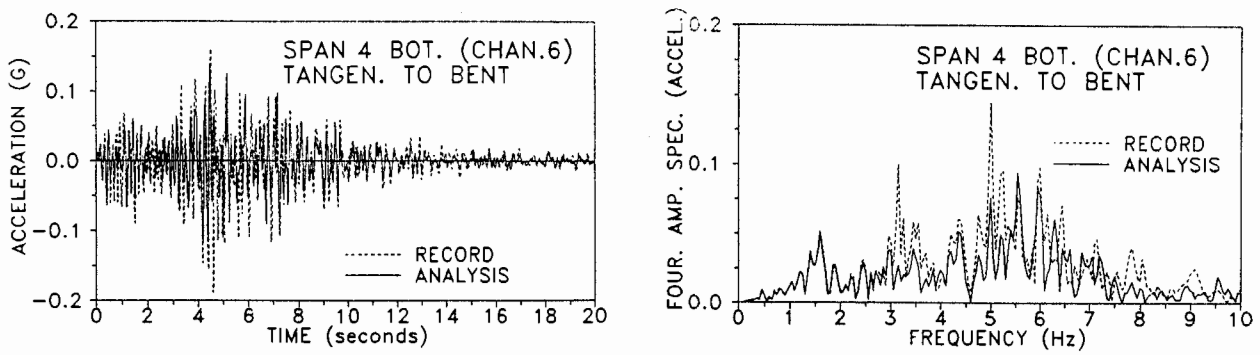

(Fig. 11 Continued)

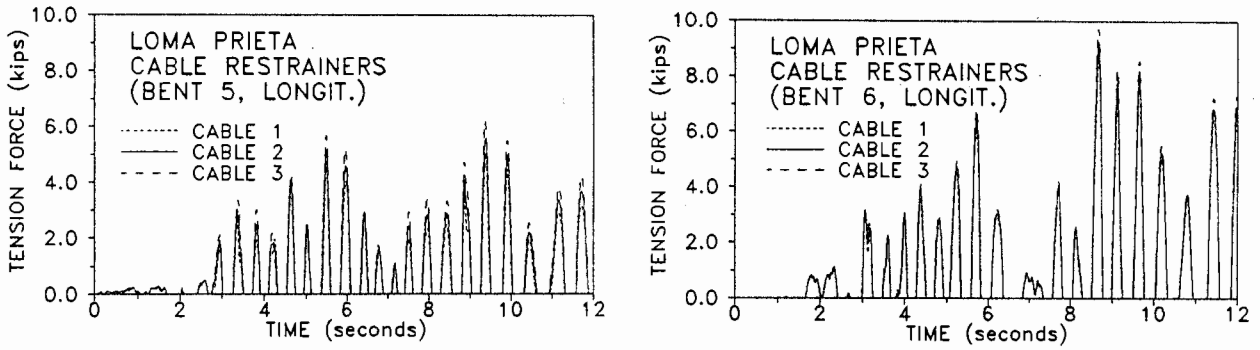

Fig. 12 Analytically Obtained Tension Force Histories of Cable Restrainers.

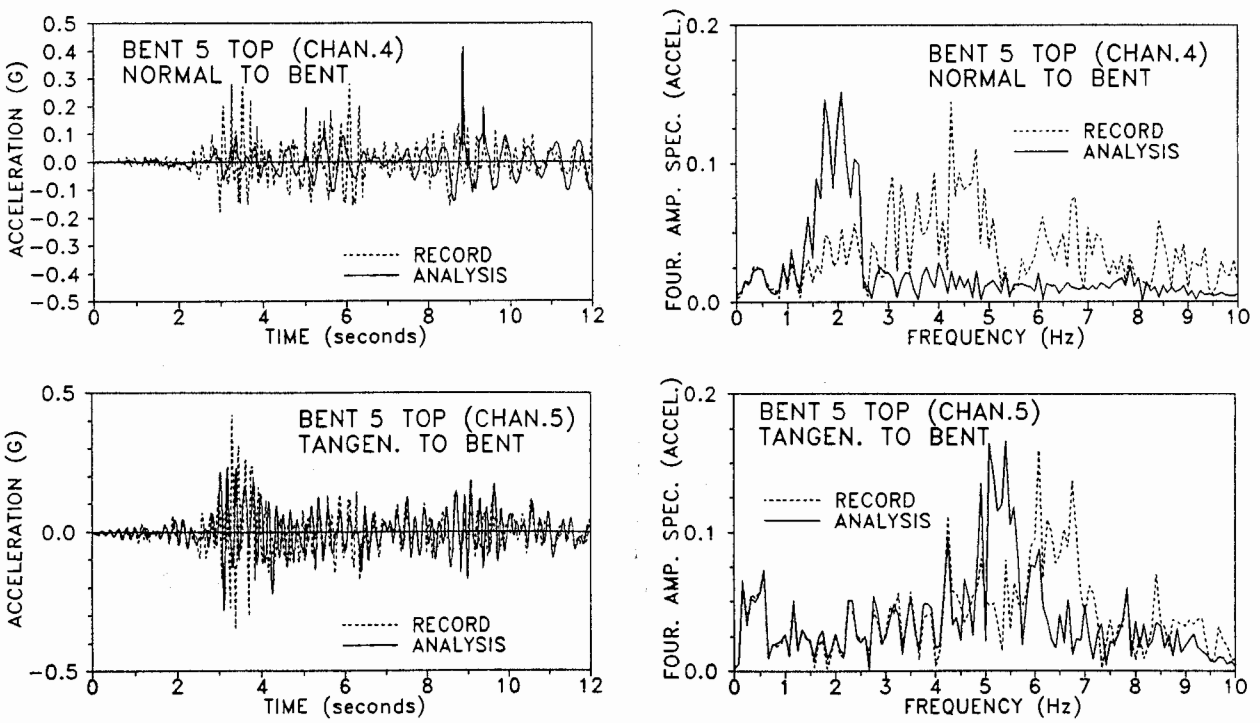

Fig. 13 Recorded and Calculated Acceleration Response for Loma Prieta Earthquake.

NONLINEAR DYNAMIC RESPONSE ANALYSIS OF LEXINGTON DAM

L. H. Mejia, J. I. Sun, S. Salah-mars, Y. Moriwaki, M. Beikae

Woodward-Clyde Consultants
500 12th Street
Oakland, California 94607

ABSTRACT

The dynamic response of Lexington Dam during the October 17, 1989 Loma Prieta earthquake and a smaller earthquake is analyzed using equivalent-linear and nonlinear procedures. The calculated motions at the dam crest are compared to the recorded motions during the earthquakes. The computed response of the dam using nonlinear procedures is in reasonable agreement with the recorded response and the response calculated using equivalent-linear methods.

INTRODUCTION

The seismic stability evaluation of earth dams generally requires an evaluation of their dynamic response to earthquake ground motions. An important requirement of analytical procedures for the dynamic response analysis of earth dams is that they consider the nonlinear stress-strain behavior of soils. Dynamic response analysis procedures which model the nonlinear behavior of soils using the equivalent-linear approach proposed by Idriss and Seed (1967) are now widely used. While these procedures provide an approximate representation of the nonlinear behavior of soils which is adequate for many practical purposes, they do not model the actual nonlinear stress-strain path of soils during seismic loading. For a given seismic loading the analysis is carried out using linear visco-elastic properties corresponding to an average level of strain during the loading. Because equivalent-linear procedures cannot model yielding of soils, they may lead to calculated stresses higher than may actually be possible, and they cannot model permanent deformations resulting from soil yielding.

Fully nonlinear two-dimensional procedures which can model the time-varying stress-strain behavior and yielding of soils are now becoming more widely available. The purpose of this paper is to present the results of equivalent-linear and fully nonlinear analyses of the dynamic response of Lexington Dam during the October 17, 1989 Loma Prieta (M_s 7.1) and August 8, 1989 Lake Elsman (M_L 5.2) earthquakes. The calculated motions at the crest of the dam are compared to the recorded motions during the earthquakes to evaluate the use of these types of analyses for calculating the dam's dynamic response.

DESCRIPTION OF LEXINGTON DAM

Lexington Dam is located in the Santa Cruz mountains of California about 15 miles north of Santa Cruz and about 13 miles and 5 miles northwest of the epicenters of the Loma Prieta and Lake Elsman earthquakes, respectively. The dam is a 207-foot-high zoned earthfill with upstream and downstream slopes of 5½:1 and 3:1, respectively. The crest of the dam is 40 feet wide and about 810 feet long. A plan view and the approximate maximum cross section of the dam are shown in Figures 1 and 2, respectively.

The dam is founded on Franciscan sandstone and shale with minor amounts of greenstone, chert and schist. It was built in 1953 of densely compacted local materials. The downstream shell consists of clayey

sandy gravel with about 15 to 40% fines of low to medium plasticity. The materials in the upstream shell and the upper 80 feet of the core are generally similar and consist of clayey sands with about 15 to 35% gravel and 20 to 50% fines of medium plasticity. The materials in the core below 80 feet are clearly distinct from those above and consist of a clay of medium to high plasticity.

The results of insitu and laboratory tests presented by Wahler and Associates (1982) indicate that the materials are generally very stiff. However, because of the difficulty in sampling gravelly materials, the data on dynamic properties and strength from undisturbed samples is limited. Downhole and crosshole seismic wave velocity measurements indicate that the shear wave velocity of the materials at small strains increases with depth and may be reasonably approximated by the expression:

$$V_s = (k_{2max} \cdot (\sigma_m)^{½} \cdot g / \gamma)^{½}$$

where V_s is the shear wave velocity in ft/sec, k_{2max} is a constant, σ_m is the mean effective stress in psf, g is gravity in ft/sec^2, and γ is the unit weight in kcf. The ranges of shear wave velocities measured in the dam and the corresponding values of k_{2max} for the dam materials are presented in Table 1. Limited data is available regarding shear wave velocities of the foundation rock. The available data indicates that the average shear wave velocity of the foundation immediately beneath the main body of the dam is about 3,000 ft/sec. Towards the upper reaches of the abutments it is somewhat less than 2,000 ft/sec. Compression wave velocities of about 10,000 ft/sec were measured immediately beneath the main body of the shells and core.

The reservoir level at the time of the earthquakes was between 90 and 100 feet below the maximum storage level. The reservoir level at the time of the geophysical measurements was also low. Piezometer readings in the upstream shell and core of the dam indicate that the pore water pressures in the embankment fluctuate little in response to changes in the reservoir level and that they are generally less than hydrostatic. Water level readings in the downstream shell indicate that these materials are unsaturated and that the phreatic surface is near the foundation.

RECORDED RESPONSE

The strong motion instrumentation at the dam site consists of 3 accelerographs located as shown in Figure 1. The instruments are oriented to record motions transverse (0° component) and parallel (90° component) to the longitudinal axis of the dam and in the vertical direction. The instruments have recorded motions during several earthquakes including the October 17, 1989 Loma Prieta and the August 8, 1989 Lake Elsman earthquakes, and a small (M_L 5.0) nearby earthquake on June 27, 1988. The recorded motions from these three earthquakes were digitized and processed by the staff of the California Strong Motion Instrumentation Program (Shakal and others, 1989). Figure 6 shows the acceleration response spectra of the motions recorded in the transverse direction (0° component) at the left abutment and right crest accelerographs during the Loma Prieta and Lake Elsman earthquakes. The motions from the June 27, 1988 earthquake were not used in this study since the instruments appear to have triggered late during this event.

A summary and an analysis of the motions recorded at the dam site during the Loma Prieta and Lake Elsman earthquakes has been presented by Makdisi and others (1991). Evidence of the nonlinear behavior of the dam during the Loma Prieta earthquake can be directly observed in the earthquake records (Mejia and others, 1992).

Other instrumentation at the dam includes survey monuments along the crest, pneumatic piezometers in the upstream shell and core, and open standpipe piezometers in the downstream shell. Measured deformations at the survey monuments presented by Volpe and Associates (1990) indicate that crest settlements during the Loma Prieta earthquake varied from a maximum of 10 inches near the crest midpoint to about 1 inch near the left abutment and 4 inches near the right abutment. Horizontal deformations transverse to the dam axis varied from less than 1 inch (downstream) near the left abutment, to 3 inches (downstream) near the crest midpoint, to about 2 inches (upstream) near the right abutment. Deformations during the Lake Elsman earthquake were very small.

An apparent water level rise of about 6 feet was measured in two piezometers in the core and one piezometer in the upstream shell after the Loma Prieta earthquake. The piezometer readings decreased slightly during the following several months. A relatively large seep developed on the downstream face six weeks after the earthquake and lasted for a few months. The seep appears to coincide with an increase in water levels in one of the three observation wells in the downstream shell. No significant water level changes were measured after the Lake Elsman earthquake.

SOIL MODELS

Three stress-strain soil models are used to analyze the dynamic response of Lexington Dam: the equivalent-linear model proposed by Idriss and Seed (1967), a multiple-nested yield surface plasticity model presented by Salah-mars and Kavazanjian (1992), and a model based on the failure-seeking model proposed by Cundall (1979) and the bounding surface plasticity model proposed by Dafalias and Hermann (1982). This latter model is generally similar to the multiple yield surface model and will not be presented herein.

Equivalent-Linear Model

The equivalent-linear model is schematically illustrated in Figure 3. In this model the hysteretic stress-strain behavior of soils under symmetrical cyclic loading is represented by an equivalent modulus G corresponding to the secant modulus through the end points of the hysteresis loop and an equivalent damping ratio λ corresponding to the hysteretic damping (see Figure 3(a)). The equivalent modulus and damping typically vary with strain as shown in Figure 3(b). For a given seismic loading these relationships, usually known as the modulus reduction and damping curves, are used iteratively to select modulus and damping values which are compatible with the average strain induced by the loading. In the analyses presented herein the average strain was calculated as 0.65 times the peak maximum shear strain.

Multiple-Nested Yield Surface Model

In this model the stress-strain behavior of soils is represented by a family of circular yield surfaces which are nested in stress space as shown in Figure 4(a). The yield surfaces can be made to follow kinematic hardening rules which result in hysteretic stress-strain behavior under symmetrical cyclic loading as shown in Figure 4(b). The stress-strain relationship connecting the end points of the hysteresis loops at different strains, shown by the dashed line in Figure 3(a), is usually referred to as the backbone curve. Any backbone curve can be modeled by selecting an appropriate number of yield surfaces. The resulting amount of hysteretic damping will depend on the backbone curve selected and will correspond to Masing-type behavior. In the analyses presented herein a small amount of viscous damping was used so that the total damping at small strains would be similar to that used in the equivalent-linear analyses.

For a given seismic loading the model will track the stress-strain path of the soil with time and will accumulate permanent strains under sustained yielding. A tension stress cut-off can be modeled to prevent excessive tension stresses from developing in the soil. The analysis is conducted in terms of total stresses which seems reasonable for Lexington Dam in view of the dense and clayey nature of its materials. Degradation in soil stiffness and strength during the earthquakes was assumed to be small based on the high densities of the materials, the results of laboratory tests by Wahler and Associates (1982), and the moderate duration of the earthquakes. While the soil model can appropriately treat permanent volumetric strains under isotropic stress loading (i.e. volumetric plasticity) this option was not used in the present study and the bulk modulus of the materials was assumed to be elastic and equal to the bulk modulus used at small strains in the equivalent-linear analyses.

EQUIVALENT-LINEAR ANALYSES

The equivalent-linear analyses of Lexington Dam were performed using the computer programs FLUSH (Lysmer and others, 1975) and SUPERFLUSH (Udaka, 1989). FLUSH is a two-dimensional plane strain finite element code for the dynamic analysis of soil structures and the analysis of dynamic soil-structure interaction. The program assumes that the base of the finite element model is rigid. SUPERFLUSH is an enhanced version of FLUSH which allows use of a compliant boundary at the base of the model.

The finite element mesh used in the equivalent-linear analyses is shown in Figure 5. This mesh corresponds approximately to the maximum section of the dam and is near the location of the right crest accelerograph. The motions recorded at the abutment in the direction transverse to the axis of the dam (0° component) were used as input motions in the analyses. The acceleration response spectra of these motions together with the spectra for the recorded motions at the right crest accelerograph are shown in Figure 6.

The dynamic material properties required for the equivalent-linear analyses are the total unit weight, the shear modulus at small strains (G_{max}), Poisson's ratio, and the modulus reduction and damping curves. The values of G_{max} were calculated using the k_{2max} values estimated from the measured shear wave velocities. The values of Poisson's ratio and total unit weight were estimated from the measured shear and compression wave velocities and laboratory test results. A summary of these values is presented in Table 1.

Parametric dynamic response analyses performed by Makdisi and others (1991) using various modulus reduction and damping curves indicate that the average modulus reduction and the lower-bound damping curves proposed by Seed and Idriss (1970) for sands result in a calculated dynamic response of the dam which is in good agreement with the recorded response during the Loma Prieta and Lake Elsman earthquakes. Additional parametric analyses were performed in this study to supplement those presented by Makdisi and others (Mejia and others, 1992).

Figure 7 shows a comparison between the recorded and calculated response spectra at the dam crest using FLUSH for two assumptions of the modulus reduction and damping curves. In one analysis (labeled "clay curves" in Figure 7) the modulus reduction and damping curves proposed by Vucetic and Dobry (1991) for clays with a PI of 30 were used for the medium to high plasticity clays in the core below 80 feet. The average modulus reduction and lower-bound damping curves proposed by Seed and Idriss for sands were used in all other zones of the dam. In the second analysis (labeled "sand curves" in Figure 7) the Seed and Idriss curves were used in all zones of the dam. As shown in Figure 7, use of the Seed and Idriss curves in all zones of the dam leads to calculated response spectra which are in very good agreement with the recorded spectra at the right crest accelerograph. The spectra calculated using the

Vucetic and Dobry curves in the core below 80 feet are significantly higher than the recorded spectra and the spectra calculated using the Seed and Idriss curves.

Parametric analyses were performed with SUPERFLUSH to evaluate the effects of foundation flexibility on the computed dynamic response of the dam. Based on the geophysical measurements at the site a shear wave velocity of 3000 ft/sec and a Poisson's ratio of 0.4 were used for the foundation rock in the analyses. The motions recorded at the left abutment were input at an assumed rock outcrop with the same shear wave velocity as the foundation. Figure 8 shows a comparison between the recorded and calculated response spectra at the dam crest using a rigid base model and a compliant base model and the Seed and Idriss curves. It may be seen that for the Loma Prieta earthquake the spectra calculated with the two models are in good agreement. For the Lake Elsman earthquake the spectrum calculated with the compliant base model is slightly lower than that calculated with the rigid base model. Nonetheless, it appears that for the assumed rock characteristics and input motions the effects of foundation flexibility on the calculated dynamic response of the dam are relatively small.

NONLINEAR ANALYSES

The nonlinear analyses using the multiple-nested yield surface model were performed using the computer program DYSLAND (Salah-mars, 1989). The bounding surface model is incorporated into the program DYNARD (Moriwaki and others, 1988). The results of analyses using the multiple-yield surface model are presented herein. A description of all analyses performed and additional results are presented by Mejia and others (1992).

The nonlinear analyses were performed using the same finite element mesh used for the equivalent-linear analyses (Figure 5). The recorded motions at the left abutment were input at the base of the model which was assumed to be rigid. Analyses were performed for the recorded polarity of the motions and for a reverse polarity (i.e. motions of opposite sign). Analyses were conducted with and without initial static stresses in the dam. The initial stresses were obtained from an analysis of the dam under gravity loads. The analyses without initial stresses simulate the equivalent-linear analyses since these do not consider the effects of initial stresses directly. Reversing the polarity of the motions had little effect on the calculated dam response in the absence of initial stresses.

Parametric analyses were performed for several backbone curve models. The parameters of these models were selected based on the available data regarding the dynamic stress-strain and strength characteristics of the dam materials. Analyses results for the backbone curves selected to be compatible with the modulus reduction curves used in the equivalent-linear analyses are presented herein. The backbone curves were developed from the estimated values of G_{max} and the modulus reduction curves assumed for the main zones of the dam. The resulting backbone curves are generally consistent with the available laboratory data regarding the stress-strain and strength characteristics of the materials.

Figure 9 shows a comparison between the recorded and calculated response spectra at the dam crest from the nonlinear analyses without initial stresses. In general, the spectra calculated for the Lake Elsman earthquake are in relatively good agreement with the recorded spectrum. For the Loma Prieta earthquake, the spectrum calculated using backbone curves in the lower core corresponding to the Vucetic and Dobry modulus curve is significantly higher than the recorded spectrum for periods less than about 0.5 seconds. The calculated spectrum for the backbone curves corresponding to the Seed and Idriss curve is in good agreement with the recorded spectrum. Figure 10 shows a comparison between the calculated response spectra from the equivalent-linear and the nonlinear analyses (for the backbone curves in the lower core

corresponding to the Seed and Idriss modulus curve). It may be seen that the spectra calculated with these two types of analyses are in good agreement.

Figure 11 shows a comparison between the recorded and the calculated response spectra from the nonlinear analyses with and without initial stresses (for the backbone curves in the lower core corresponding to the Seed and Idriss modulus curve). It may be seen that the acceleration response spectra calculated at the dam crest are not very sensitive to the initial static stresses in the dam. This, however, is not the case for the calculated crest displacements.

Figure 12 shows the acceleration and relative displacement time histories calculated at the dam crest for the Loma Prieta earthquake using the lower-core backbone curves corresponding to the Seed and Idriss modulus curve. The calculated residual vertical and horizontal displacements at the crest are about 5½ and 2 inches, respectively. These displacements are somewhat smaller than the observed permanent displacements during the earthquake but are roughly in the same proportion and have the same relative sense. The calculated residual displacements for the Lake Elsman earthquake are less than ½ inch, in good agreement with the observed displacements. Further discussion of the calculated displacements is presented by Mejia and others (1992).

CONCLUSIONS

The dynamic response of Lexington Dam during the October 17, 1989 Loma Prieta earthquake and the August 8, 1989 Lake Elsman earthquake was analyzed using equivalent-linear and nonlinear procedures. The computed response of the dam using equivalent-linear procedures together with the average modulus reduction curve and the lower-bound damping curve proposed by Seed and Idriss (1970) for sands is in good agreement with the recorded response during the earthquakes. For the assumed rock characteristics the effects of foundation flexibility on the calculated response of the dam were found to be relatively small. The computed acceleration response spectra using fully nonlinear procedures are in reasonable agreement with the spectra recorded at the dam crest and the spectra calculated using equivalent-linear procedures. In addition, nonlinear procedures predict permanent deformations of the same order of magnitude as those observed at the dam crest after the earthquakes.

ACKNOWLEDGEMENTS

The studies summarized in this paper were funded by the Strong Motion Instrumentation Program of the California Division of Mines and Geology. Additional co-funding was provided by the professional development program of Woodward-Clyde Consultants. This support is gratefully acknowledged. Special thanks are due to Mr. Robert Tepel and the Santa Clara Water District for providing data regarding Lexington Dam and its earthquake performance.

REFERENCES

Cundall, P., (1979), The Failure Seeking Model for Cyclic Behavior in Soil: an Initial Formulation for Two-Dimensions, Peter Cundall Associates, Technical Note PCAN-1, July.

Dafalias, Y.F., and Hermann, L.R., (1982), Bounding Surface Formulation of Soil Plasticity, Soil Mechanics-Transient and Cyclic Loads, Edited by G.N. Pande and C. Zienkiewicz, John Wiley & Sons Ltd.

Idriss, I.M., and Seed, H.B., (1967), Response of Horizontal Soil Layers During Earthquakes, Internal Report, Department of Civil Engineering, University of California, Berkeley, August.

Lysmer, J., Udaka, T., Tsai, C.F., and Seed, H.B., (1975), FLUSH - A Computer Program for Approximate 3-D Analysis of Soil-structure Interaction Problems: Earthquake Engineering Research Center, Report No. EERC 75-30, University of California, Berkeley, November.

Makdisi, F.I., Chang, C.Y., Wang, Z.L., and Mok, C.M., (1991), Analysis of the Recorded Response of Lexington Dam During Various Levels of Ground Shaking, Proceedings of the Seminar on Seismological and Engineering Implications of Recent Strong-Motion Data, Strong Motion Instrumentation Program, California Division of Mines and Geology, May.

Mejia, L.H., Salah-mars, S., Sun, J.H., Moriwaki, Y., and Beikae, M., (1992), Non-Linear Dynamic Response Analysis of Lexington Dam: Report in preparation for the California Division of Mines and Geology, Strong Motion Instrumentation Program (SMIP). Woodward-Clyde Consultants, Oakland, California.

Moriwaki, Y., Beikae, M., and Idriss, I.M., (1988), Nonlinear Seismic Analysis of the Upper San Fernando Dam Under the 1971 San Fernando Earthquake, International Conference on Earthquake Engineering, Tokyo.

Salah-mars, S., (1989), A Multiple Yield Surface Plasticity Model For Response of Dry Soil to Impact Loading, Ph.D. Dissertation, Civil Engineering Department, Stanford University, California, June.

Salah-mars, S., and Kavazanjian, E. Jr., (1992), A Virtual Surface Concept for Nested Yield Surface Plasticity, to be published in: International Journal for Numerical and Analytical Methods in Geomechanics.

Seed, H.B., and Idriss, I.M., (1970), Soil Moduli and Damping Factors for Dynamic Response Analyses, Report No. EERC 70-10, University of California, Berkeley, California, December.

Shakal, A., Huang, M. Reichle, M., Ventura, C., Cao, T., Sherburne, R., Savage, M., Darragh, R., and Peterson, C., (1989), CSMIP Strong-motion Records from the Santa Cruz Mountains (Loma Prieta), California earthquake of 17 October 1989: California Strong Motion Instrumentation Program Report No. OSMS 89-06, 195 p.

Udaka, T., (1989), Super FLUSH Users Guide: Earthquake Engineering Technology, San Ramon, California.

Volpe, R.L. & Associates, (1990), Investigation of SCVWD Dams Affected by the Loma Prieta Earthquake of October 17, 1989, March.

Vucetic, M., and Dobry, R., (1991), Effect of Soil Plasticity on Cyclic Response, ASCE, Journal of Geotechnical Engineering, Vol. 117, No. 1, January, pp. 89-107.

Wahler Associates, (1982), Seismic Safety Evaluation of Lexington Dam: final report submitted to Santa Clara Valley Water District, May.

TABLE 1

SUMMARY OF MATERIAL PROPERTIES FOR ANALYSIS

Zone of Dam	Measured Shear Wave Velocity (ft/sec)	Estimated k_{2max}	Total Unit Weight (pcf)	Poisson's Ratio
Upstream shell	600-1800	130	138	0.45
Core above 80 feet	900-1600	130	138	0.40
Core below 80 feet	900-1000	45	122	0.45
Downstream shell	1100-2200	235	138	0.35

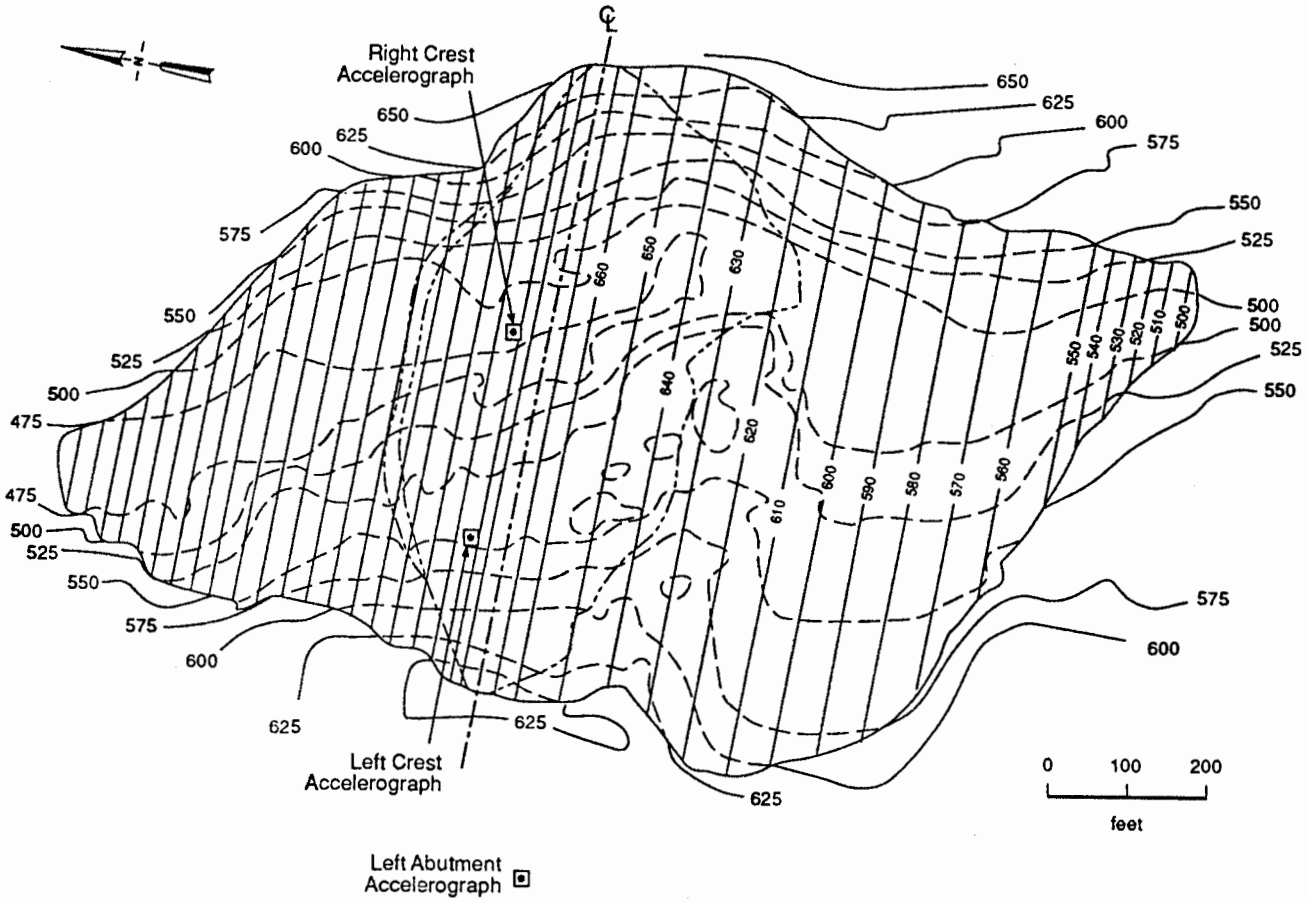

Figure 1. Plan view of Lexington Dam

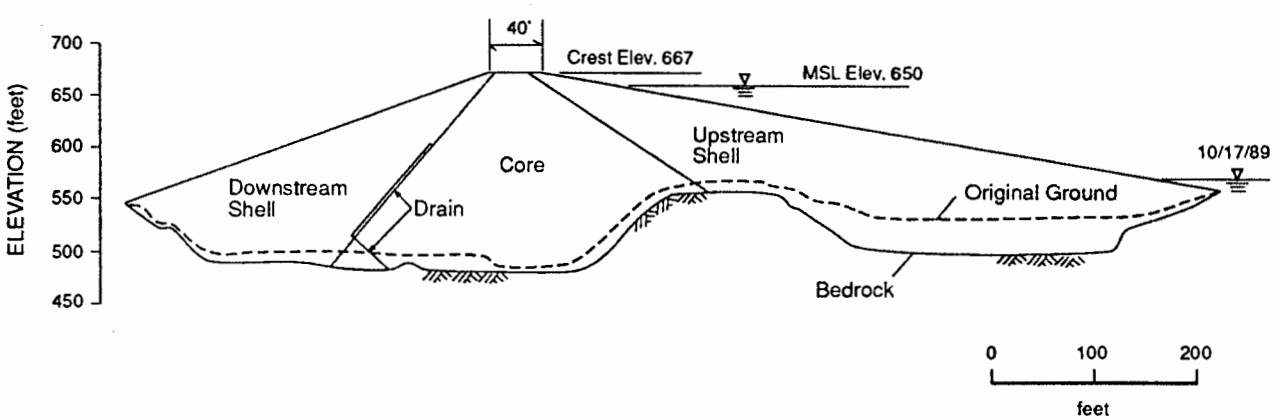

Figure 2. Maximum section of Lexington Dam

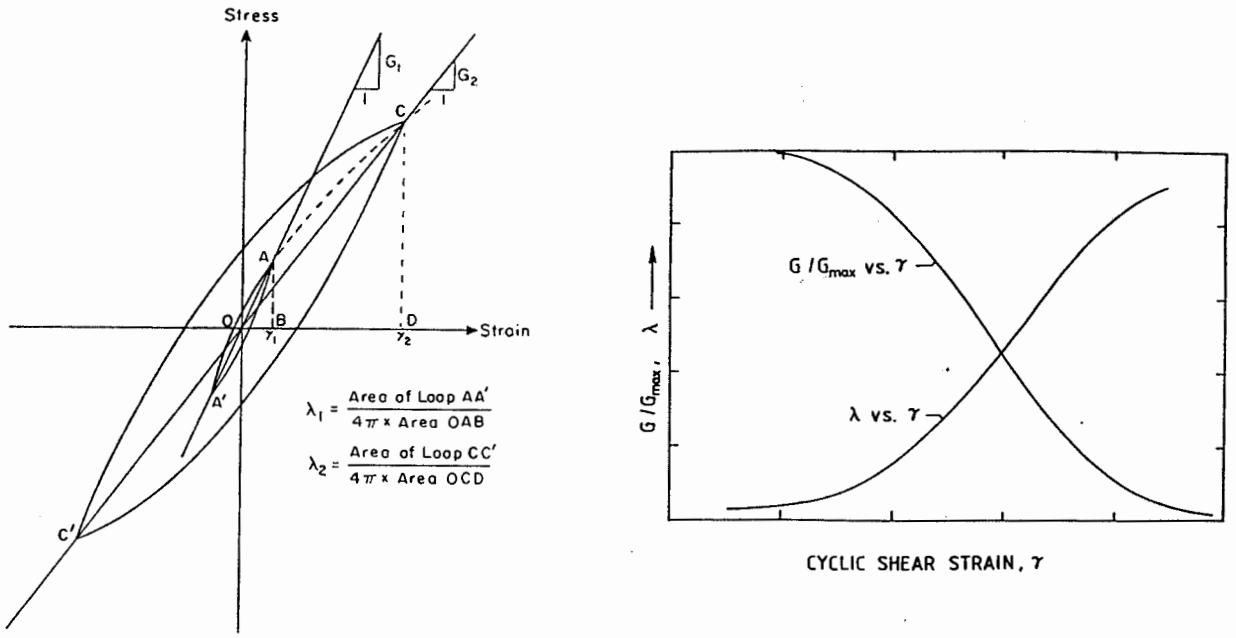

(a) Equivalent modulus and damping

(b) Modulus reduction and damping relationships with strain

Figure 3. Equivalent-linear model

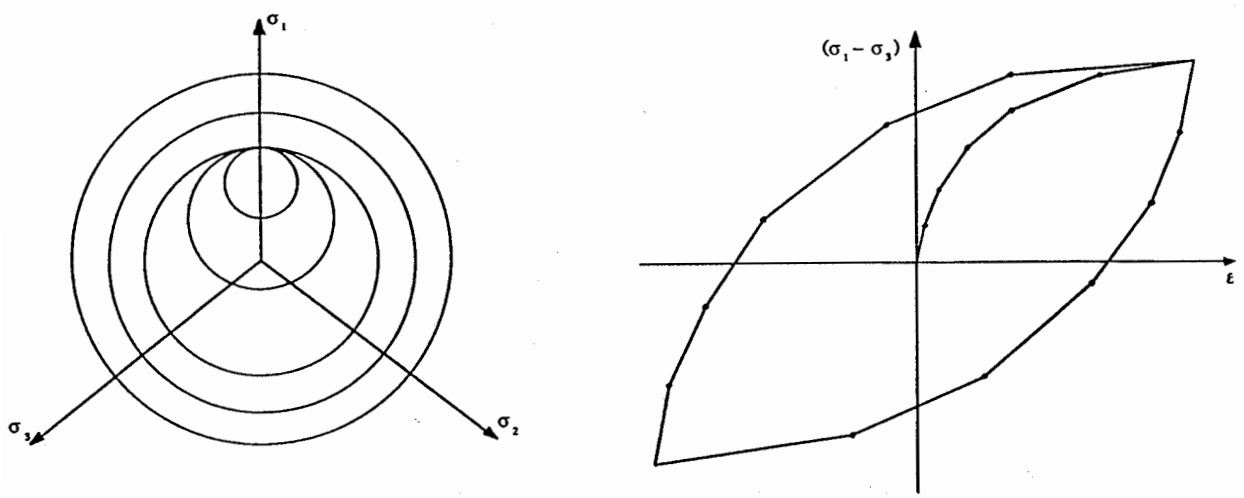

(a) Yield surfaces

(b) Example hysteretic loop

Figure 4. Multiple-nested yield surface model

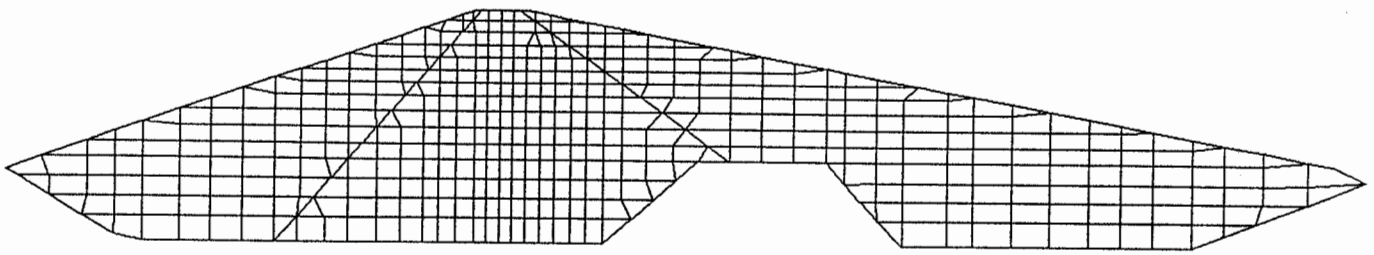

Figure 5. Finite element mesh used in analyses

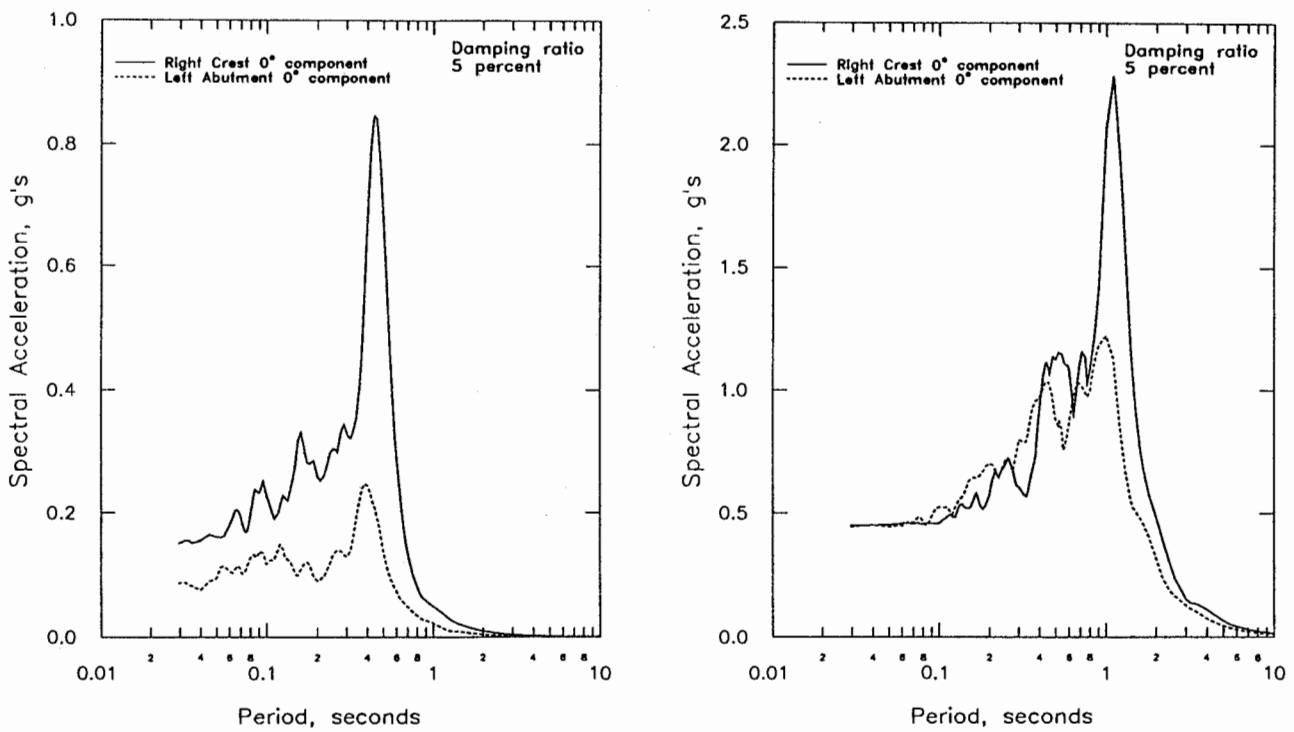

(a) Lake Elsman earthquake (8/8/89)

(b) Loma Prieta earthquake (10/17/89)

Figure 6. Acceleration response spectra of motions recorded at Lexington Dam

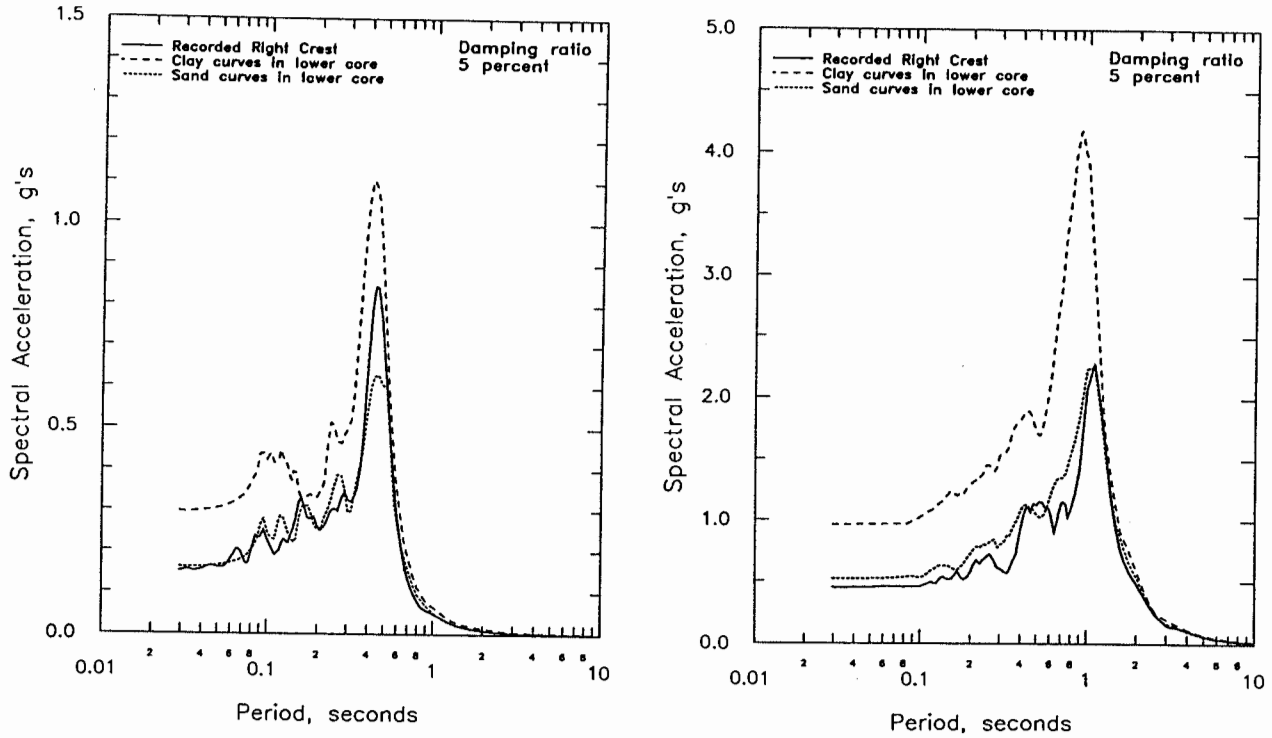

(a) Lake Elsman earthquake (8/8/89)

(b) Loma Prieta earthquake (10/17/89)

Figure 7. Comparison between recorded and calculated response spectra at the dam crest using FLUSH

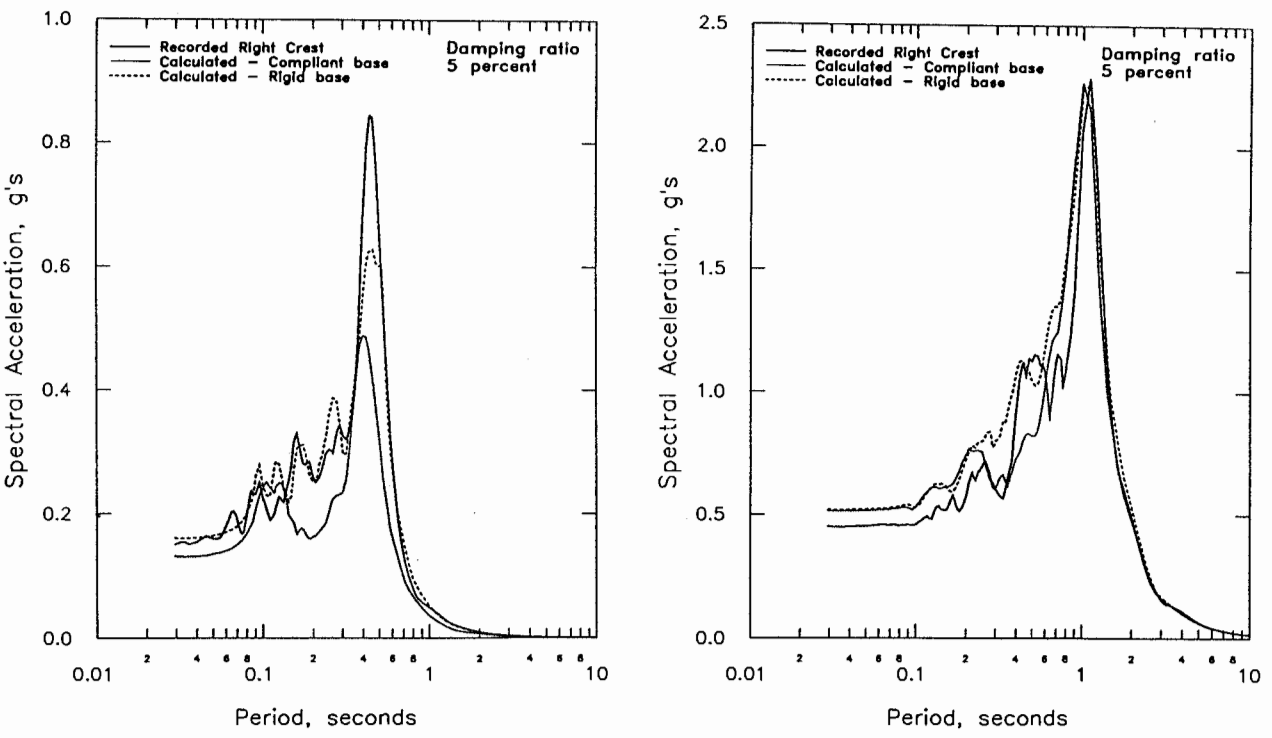

(a) Lake Elsman earthquake (8/8/89)

(b) Loma Prieta earthquake (10/17/89)

Figure 8. Comparison between recorded and calculated response spectra at the dam crest using rigid base and compliant base models

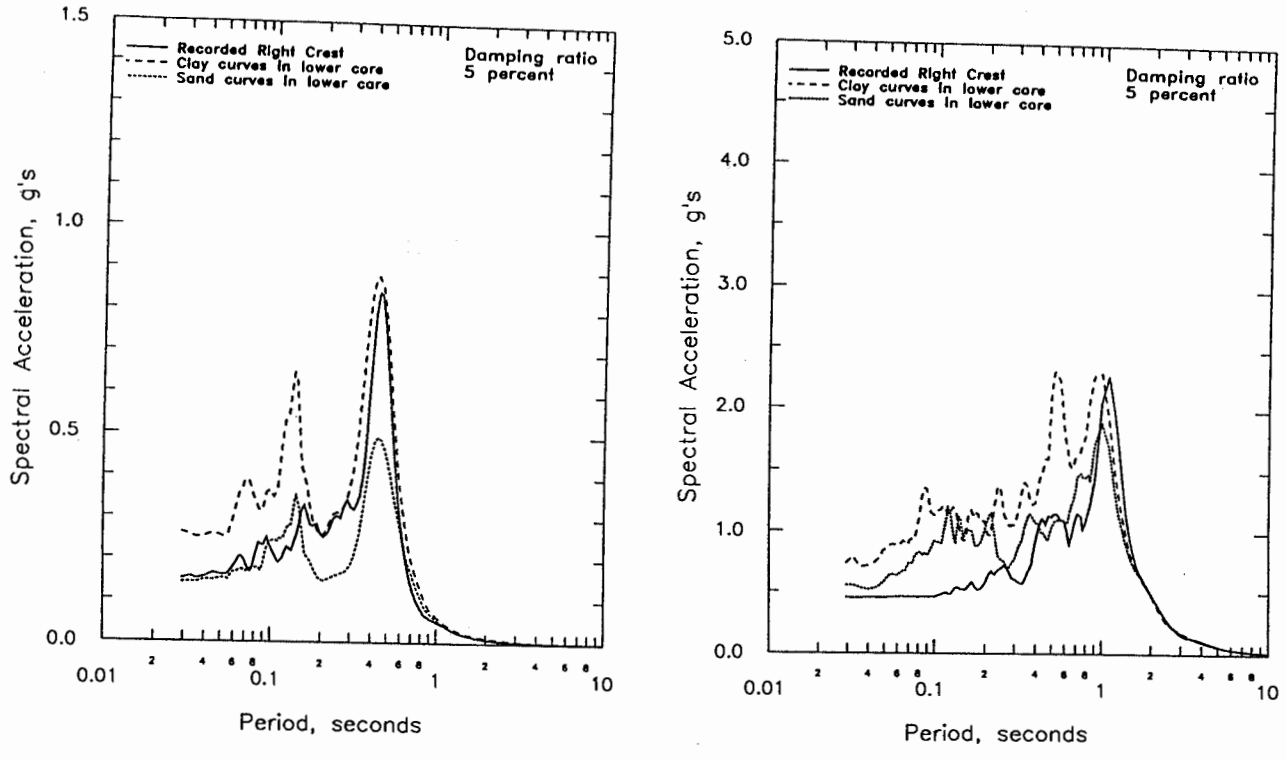

(a) Lake Elsman earthquake (8/8/89)

(b) Loma Prieta earthquake (10/17/89)

Figure 9. Comparison between recorded and calculated response spectra at the dam crest using DYSLAND without initial stresses

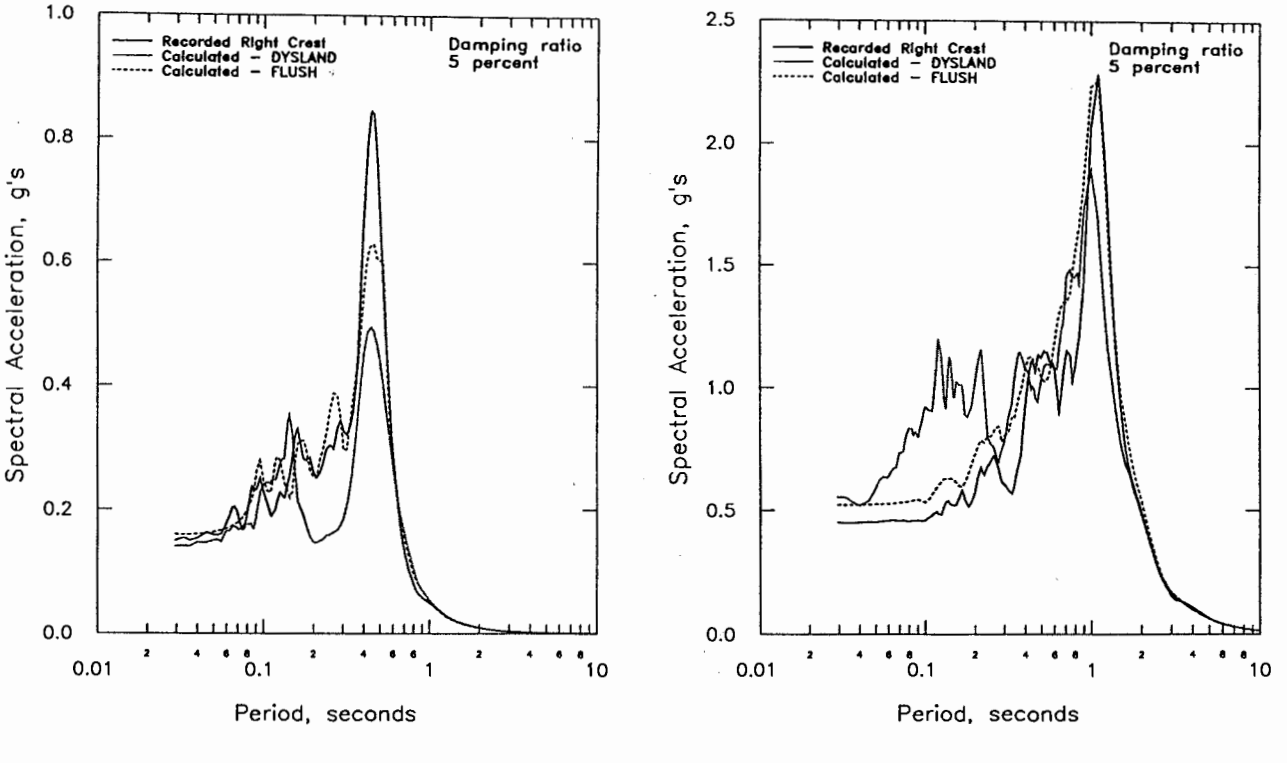

(a) Lake Elsman earthquake (8/8/89)

(b) Loma Prieta earthquake (10/17/89)

Figure 10. Comparison between recorded and calculated response spectra at the dam crest using FLUSH and DYSLAND without initial stresses

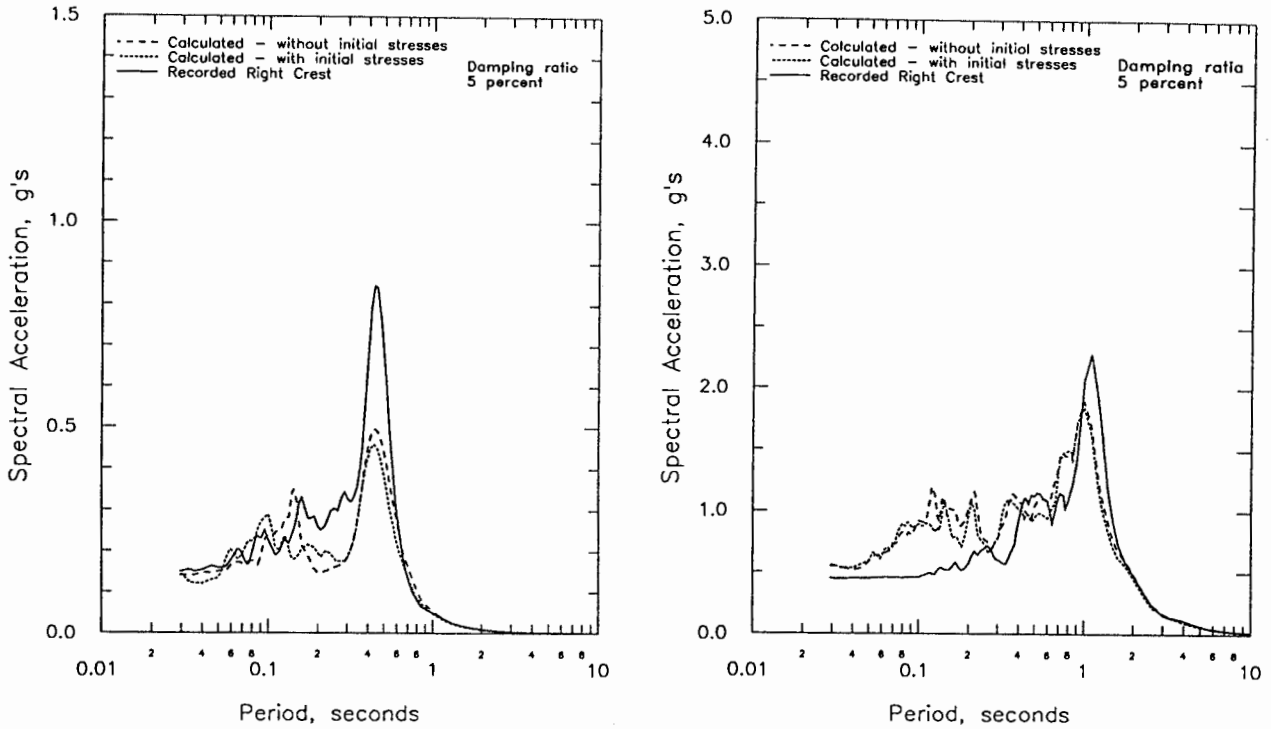

(a) Lake Elsman earthquake (8/8/89) (b) Loma Prieta earthquake (10/17/89)

Figure 11. Comparison between recorded and calculated response spectra with and without initial stresses

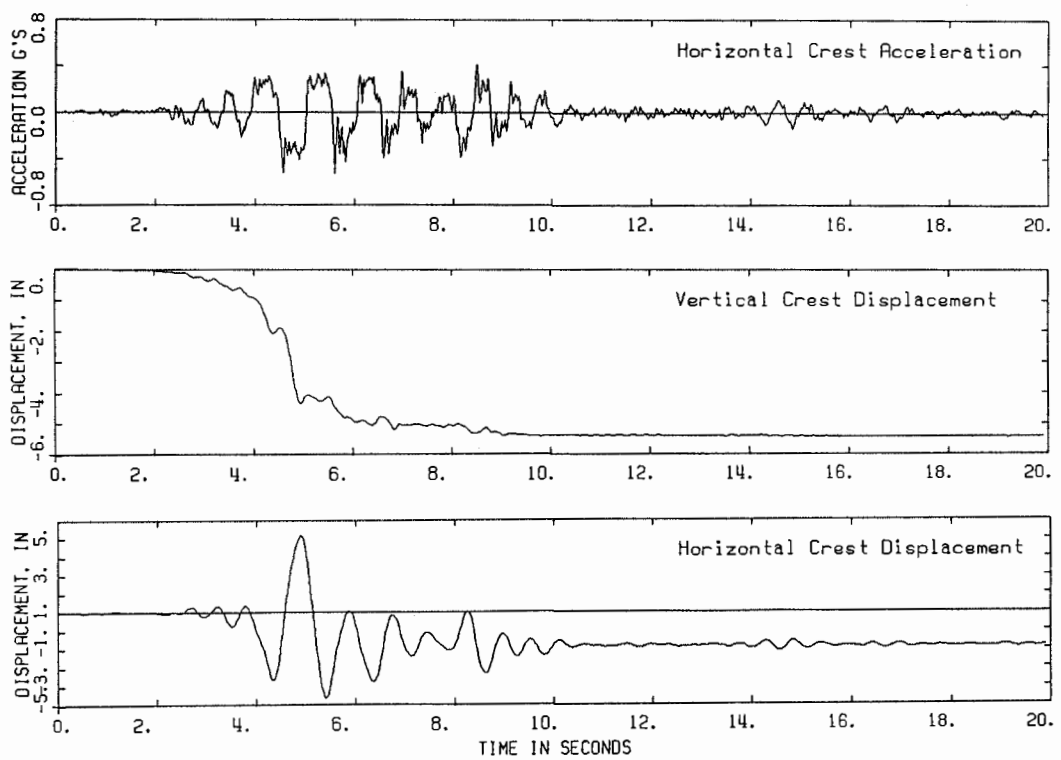

Figure 12. Calculated acceleration and relative displacement time histories for Loma Prieta earthquake